Bárbara Cassiana Rodrigues Camacho

Licenciada em Ciências da Engenharia Química e Bioquímica

Experimental Gravimetric Adsorption Equilibrium of n-Alkanes and Alkenes, Carbon Dioxide and Nitrogen in MIL-53(Al) and Zeolite 5A

Dissertação para obtenção do Grau de Mestre em
Engenharia Química e Bioquímica

Orientador: Isabel A. A. C. Esteves, Investigadora Auxiliar, FCT/UNL Requimte

Co-orientadores: José Paulo Barbosa Mota, Professor Catedrático, FCT/UNL

Mário Fernando José Eusébio, Professor Auxiliar, FCT/UNL

Júri:

Presidente: Prof. Doutora Maria Madalena Alves Campos de Sousa Dionísio Andrade

Arguente: Doutora Ana Mafalda Almeida Peixoto Ribeiro

Vogal: Doutora Isabel Alexandra de Almeida Canento Esteves Esperança

FACULDADE DE CIÊNCIAS E TECNOLOGIA
UNIVERSIDADE NOVA DE LISBOA

Março, 2014

Bárbara Cassiana Rodrigues Camacho

Licenciada em Ciências da Engenharia Química e Bioquímica

Experimental Gravimetric Adsorption Equilibrium of n-Alkanes and Alkenes, Carbon Dioxide and Nitrogen in MIL-53(Al) and Zeolite 5A

Dissertação para obtenção do Grau de Mestre em
Engenharia Química e Bioquímica

Orientador: Doutora Isabel Alexandra de Almeida Canento Esteves

Co-orientadores: Professor Doutor José Paulo Barbosa Mota

Professor Doutor Mário Fernando José Eusébio

Monte da Caparica, Faculdade de Ciências e Tecnologia, Universidade de Lisboa

Março 2014

Experimental Gravimetric Adsorption Equilibrium of n-Alkanes and Alkenes, Carbon Dioxide and Nitrogen in MIL-53(Al) and Zeolite 5A

Dedico esta conquista, com todo o carinho aos meus Pais,

Rita Camacho e Alberto Camacho.

Agradecimentos

A elaboração da tese, pela sua finalidade académica, consiste em um trabalho individual, contudo há vários contributos que não podem nem devem deixar de ser realçados, uma vez que sem eles a realização desta não seria possível. Como tal sinto-me grata pelo apoio, pelo carinho demonstrado, pelas críticas construtivas, sempre fundamentadas por bases fortes e extremamente impulsionadoras para a realização de uma tarefa como esta, em que se pretende rigor máximo e que representa o culminar de cinco anos de aprendizagem.

Neste contexto, dedico um especial agradecimento à Doutora Isabel Esteves, pelo profissionalismo com que me orientou em uma área tão delicada como a adsorção. Agradeço a forma como abraçou esta causa, partilhando experiências, apoiando e motivando em todos os momentos, assim como, de um modo mais pessoal, a sua amizade.

Ao Professor Doutor José Paulo Mota, pelo exemplo de competência científica, pelas inúmeras trocas de impressões, correcções e comentários, que representaram uma mais-valia na realização deste trabalho.

Ao Professor Doutor Mário Eusébio, por me ter trazido até este grupo, que se distingue pelo trabalho de excelência que realiza e do qual muito me orgulho de ter feito parte.

Ao Doutor Rui Ribeiro, pela motivação, boa disposição com que sempre me auxiliou nas mais diversas tarefas que surgiram e claro pela companhia nas extensas horas de trabalho laboratorial. Ao Doutor Ricardo Silva, pelo interesse e preocupação que permanentemente demonstrou em me ajudar, até mesmo nos conhecimentos mais básicos.

Aos meus colegas de laboratório Eliana Órfão, João Gomes e Inês Valente, que sempre se apresentaram dispostos a contribuir, pela convivência diária e a entreajuda que constantemente existiu entre nós.

Á Dona Maria José Carapinha, pela sua simpatia e forma carinhosa com que continuamente me ajudou a resolver os mais variados problemas e questões que surgiram ao longo destes tempos.

Não posso deixar de agradecer á Faculdade de Ciências e Tecnologia – Universidade Nova de Lisboa pelas condições de trabalho que ao longo destes anos proporcionou, e sem as quais não seria possível a concretização deste Mestrado.

Á Joana Afonso, pela enorme amizade que criamos ao longo deste período académico e que de certo levo comigo, agradeço a partilha dos desabafos, as conversas e risos intermináveis. Um agradecimento muito especial a ti e á tua família por várias vezes me ajudarem a sentir em “casa”.

Á Sofia Messias, Rafaela Santos, Nádia Carmo, pela vossa amizade, companheirismo e maneira como sempre me estimularam não só na concretização da tese, mas também na realização de todo o curso. Ao Alexander Fernandes e Igor Fernandes, pelas conversas e por toda a compreensão ao longo destes anos, um muito obrigado pelos momentos mais descontraídos, que inúmeras vezes faziam falta.

Aos meus amigos, Sara, Isabel, Érica, Catarina, João Tiago, Gonçalo, Hugo, Tiago António, Pedro, Diogo a todos vocês que não menciono, mas que sabem bem quem são, agradeço pela maneira como me apoiaram e encorajaram ao longo deste processo, aceitando constantemente as minhas ausências.

Ao meu irmão, Décio Camacho, pelo incentivo, pelo que representa para mim e por ser sempre a melhor companhia que podia ter durante esta caminhada. Ao meu sobrinho Santiago Camacho, por me premiar com a alegria de uma criança e um amor incondicional. A vocês fico grata pela força, ainda que inconsciente, me transmitiram e por pertencerem á família de que tanto me orgulho. Um obrigado em particular, para ti avó Maria da Conceição, que te tornas-te na minha estrela guia.

A ti, Cristiano de Jesus, que em todos os momentos te sinto ao meu lado, um agradecimento muito especial pelo amparo e carinho diários. Por me fazeres acreditar que chegaria ao fim desta difícil, porém gratificante etapa. A tua transmissão de confiança, apoio e paciência em todos momentos foram insubstituíveis. Obrigada por olhares sempre por mim, por me ajudares a compreender que a distância não passa de uma mera medida e por tornares todos estes dias, mais simples. E porque um puro obrigado, nunca será suficiente para mostrar a minha desmedida gratidão, só me resta desejar que estejas sempre presente e puder retribuir tudo o que tens sido para mim. Um obrigado muito sentido, para toda a tua família, que nunca me faltou com uma palavra de afecto e coragem.

Finalmente, aos mais importantes, os meus pais, aos quais dedico esta tese e que embora nunca tenha maneira suficiente de lhes mostrar o quanto estou agradecida, aqui fica o meu mais sincero obrigada! Obrigada pela maneira como me incutiram a alegria de viver e a confiança necessária para realizar os meus sonhos, por terem sonhado e percorrido estes caminhos comigo, afinal sem vocês nada disto seria possível. Ao longo destes anos vencemos várias batalhas e vivemos momentos inesquecíveis, uns mais positivos, outros nem tanto, mas que só me trouxeram certezas e uma delas, é que são sem dúvida os melhores Pais, o meu verdadeiro tesouro. Obrigada Mãe por seres o pilar da minha vida, obrigada Pai por seres o meu herói. Obrigada por fazerem de mim, aquilo que hoje sou. Não posso por fim, deixar de vos felicitar, porque esta conquista não é só minha, é também vossa, é da nossa família.

Por fim, a todos os familiares e amigos, que embora não citados, de uma maneira ou de outra tiveram um papel fundamental no desenvolvimento deste trabalho e para os quais sou uma esperança, resta-me afincadamente não vos desiludir.

A todos, sem excepções, um autêntico e enorme obrigado.

Bárbara Camacho.

Abstract

The objective of this work was the measuring of adsorption equilibrium, by the gravimetric method. Experimental results are presented for the adsorption equilibrium of the series of n-alkanes, ethylene, nitrogen and carbon dioxide in two microporous materials, the metal-organic framework, MIL-53(Al) and zeolite 5A. Both of them have desirable characteristics for adsorption processes, such as the capture and storage of carbon dioxide, natural gas storage, separation of components of biogas, and separation of olefin/paraffin. The determination of the equilibrium of the pure components (ethane, propane, butane, ethylene, carbon dioxide and nitrogen) covers a wide range of thermodynamic conditions; temperatures between 303.15K and 373.15K, as well as pressure values between 0 and 50 bar. The adsorption equilibrium data were analyzed through the global adjustment for each adsorbate/adsorbent system, using the Sips and Toth models. The isosteric heat was also determined. The experimental data of methane, carbon dioxide and nitrogen were correlated successfully by the potential theory of adsorption collapsing into a single characteristic curve, independent of temperature. This analysis allows the extrapolation of adsorption data for other gases, for which no experimental data is still known. The adsorption capacity is generally higher in MIL-53(Al) than in zeolite 5A, and in the two adsorbents, the preferred adsorption capacity for carbon dioxide is a good indication that these materials have a strong potential in the capture and storage of carbon dioxide, in the purification of biogas or purification of methane from natural gas.

Keywords: Equilibrium Adsorption, Adsorption Isotherms, Adsorbent Materials; Adsorbates; Gravimetric Method.

Resumo

Este trabalho, tem por objectivo a medição de equilíbrios de adsorção, através do método gravimétrico. Os resultados experimentais são apresentados para o equilíbrio de adsorção da série de alcanos, etileno, dióxido de carbono e azoto em dois materiais microporosos, a estrutura metálica-orgânica, MIL-53(Al) e o zeólito 5A. Ambos com características desejáveis em processos de adsorção, como sejam, a captura e armazenamento de dióxido de carbono, armazenamento de gás natural, separação de componentes do biogás, e separação de olefinas/parafinas. A determinação dos equilíbrios dos componentes puros (etano, propano, butano, etileno, dióxido de carbono e azoto) cobre uma vasta gama de condições termodinâmicas; temperaturas entre 303.15K e 373.15K, assim como valores de pressão entre 0 e 50 bar. Os dados de equilíbrio de adsorção, foram analisados, através do ajuste global por adsorbato para cada um dos adsorventes, recorrendo aos modelos de Sips e Toth. O calor isostérico também foi determinado. Os dados experimentais de metano, dióxido de carbono e azoto, foram correlacionados com sucesso pela teoria do potencial de adsorção, colapsando em uma única curva característica, independente da temperatura. Esta análise permite a extrapolação de dados de adsorção para outros gases, para os quais ainda não são conhecidos dados experimentais. A capacidade de adsorção é, em geral, superior no MIL-53(Al) do que no zeólito 5A, sendo que em ambos os adsorventes, a capacidade de adsorção preferencial para o dióxido de carbono é um bom indicador de que estes materiais, apresentam um forte potencial na captura e armazenamento de dióxido de carbono, na purificação de biogás ou na purificação de metano proveniente do gás natural.

Palavras-chave: Equilíbrio de Adsorção; Isotérmicas de Adsorção; Materiais Adsorventes; Adsorbatos; Método Gravimétrico.

List of Contents

List of Figures

List of Tables

List of Symbols

$A, B, C\ e\ D$ – Adsorbate specific constants

ARE% - Average relative error

b - Affinity constant (bar^{-1})

b_0 - Affinity constant at a reference temperature, T_0 (bar^{-1})

c_1, c_2, c_3 - Constants characteristic of the adsorbent

$\overline{D_p}$ - Average pore diameter of the adsorbents (μm)

f - Fugacity (bar)

f_s - Saturated Fugacity (bar)

m - Weight read from the balance at any time (g)

m_h - Mass of the sample holder (g)

m_s - Mass of the sample adsorbent (g)

n - Parameter of the Sips isotherm model

n_0 - Parameter of the Sips isotherm model at the reference temperature, T_0

n' - Parameter related to the characteristic energy for the pore size distribution

N_{exp} - Number of data points

P - Pressure (bar)

P_c - Critical pressure (bar)

P_s - Saturated vapor pressure (bar)

q_{ex} - Specific excess adsorbed (mol/kg)

q_{exp} - Experimental values of amount adsorbed (mol/kg)

q_i - Adsorbed quantity of the more adsorbed specie (mol/kg)

q_j - Adsorbed quantity of the less adsorbed specie (mol/kg)

q_{mod} - Predicted values by the model of amount adsorbed (mol/kg)

q_{net} - Net amount adsorbed (mol/kg)

q_t - Total amount adsorbed (mol/kg)

q_{ts} - Maximum amount adsorbed (mol/kg)

Q - Heat of adsorption (kJ/mol)

Q_{st} - Isosteric heat of adsorption (kJ/mol)

R_g - Ideal gas constant (J/mol.K)

t - Parameter of the Toth isotherm model

t_0 - Parameter of the Toth isotherm model at the reference temperature, T_0

T - Temperature (K)

T_0 - Reference temperature (K)

T_b - Temperature of the liquid adsorbate at normal boiling point (K)

T_c - Critical temperature (K)

V_b - Molar volume of the liquid adsorbate at normal boiling point (cm^3/mol)

V_c - Critical volume (cm^3/mol)

V_h - Volume of all moving parts present in the measuring cell (cm^3/g)

V_m - Molar volume of the adsorbed phase (cm^3/mol)

V_p - Accessible pore volume of the adsorbent (cm^3/g)

V_S - Specific volume impenetrable to the adsorbate (cm^3/g)

W - Volume of the adsorbed phase (cm^3/g)

W_S - Specific micropore volume of the sample (cm^3/g)

Z_{Ra} - Rackett compressibility factor

Greek Letters

α - Constant parameter of the Sips/Toth isotherm model

$\alpha_{i/j}$ - Selectivity

β - Affinity coefficient

γ - Parameter related to the characteristic energy for the system

θ - Fractional loading

ρ_a - Density of the adsorbed phase (g/m^3)

ρ_g - Density of the bulk (g/m^3)

ρ_h - Density of the sample holder (g/m^3)

ρ_s - Density of the sample adsorbent (g/m^3)

ϕ - Adsorption Potential (J/mol)

Ω - Adsorbate estimated thermal expansion coefficient

Chapter I

1. Introduction

1.1. Motivation

Energy and its sources have been playing a fundamental role in the activities of mankind, such that energy consumption has experienced an explosive growth. In order to respond to this huge demand, it is necessary to find resources for energy production. An obvious choice rests on fossil fuels as a primary resource, since their cost are not high, are available in large quantities and have a high calorific value [1, 2].

Fossil fuels ensure about 75% of the energy produced worldwide, and as such there is a need to find other alternatives, since they are a non-renewable source and their burning is responsible for the harmful release of various gases to the atmosphere. The emission of gases such as carbon dioxide (CO_2) and methane (CH_4) among others represents a problem for environmental protection, since they are both gases with greenhouse effects [1, 3].

The environmental effects of carbon dioxide (CO_2) are of significant interest. The increased concentration of CO_2 in the atmosphere has contributed to the aggravation of the rate of global warming thus making this gas, the main culprit in anthropogenic climate change. As such, the capture and storage of CO_2 continue to be topics of great research [4]. On the other hand, methane (CH_4), a gas of powerful greenhouse effect and probably the most abundant organic compound on Earth, has attracted some interest as it is the main component of natural gas. Similarly, other hydrocarbons such as ethane (C_2H_6), propane (C_3H_8), butane (C_4H_{10}), ethylene (C_2H_4) and propylene (C_3H_6) are also sources of energy for civilizations. Given their environmental concerns, research in the area of better and sustainable use of hydrocarbon processing has been held.

One alternative that has been much studied and represents a growth of 50% for the next 20 years is natural gas. Currently natural gas is already responsible for providing a

quarter of the energy needed to population worldwide. Besides being an effective alternative to fossil fuels, burning natural gas produces less carbon dioxide (CO_2) and more water vapor per unit of energy, relatively to the burning of other fuels, thus demonstrating to have a better performance to the environment. Natural gas mainly consists of methane (CH_4) 80-95 mol%, the remainder being small amounts of carbon dioxide (CO_2), nitrogen (N_2) and higher molecular weight hydrocarbons such as ethane (C_2H_6), propane (C_3H_8) and butane (C_4H_{10}). In order to respect the quality of natural gas, this should not exceed the amount of 2% and 4% (v/v) in carbon dioxide (CO_2) and nitrogen (N_2), respectively. However, there are some sources where contamination of carbon dioxide (CO_2) is greater than 10%, which means that there is a need to reduce carbon dioxide (CO_2) in excess in order to obtain a gas with suitable properties [5, 6].

Additionally, biogas is also an alternative energy source which is renewable. It is typically produced by fermentation or anaerobic digestion of organic matter under anaerobic conditions and it is composed mainly of methane (CH_4) and carbon dioxide (CO_2). Moreover, if biogas is sufficiently "clean" it has the same characteristics as natural gas [6, 7].

The separation and purification of gas mixtures are processes increasingly used industrially. The main applications of these processes are connected to the purification of raw materials, purification and recovery of primary products, and the removal of polluting gaseous effluents. There are several methods for the separation of gases, but in recent years adsorption has been presenting a considerable growth, because it has the ability to separate gas mixtures with optimum efficiency. This major operation unit in chemical engineering is currently a growing area of research with the development of new low-carbon processes.

Adsorption has revealed to be a great alternative for capture and storage of CO_2 from combustion gas streams, increasing the target of analysis concerning the options available to reduce gas emissions with impact on global climate change. Simultaneously, the materials field of research has evolved such that there are now several solids that have been synthetized and studied as potential adsorbents of carbon dioxide (CO_2), from activated carbons, to zeolites, and especially metal-organic frameworks (MOF's), in order to evaluate its effectiveness in adsorption processes. It is therefore important to perform an exhaustive characterization of these adsorbents in terms of CO_2 balance, along with the study of other relevant parameters, such as adsorption-desorption kinetics, stability, regeneration, etc [8].

The interest of studying the equilibrium of adsorption of nitrogen (N_2), carbon dioxide (CO_2) and methane (CH_4) over potential adsorbents is increasing due to the many environmental and energetic problems disclosed. Since the major constituents of flue gases emitted by fossil fueled power plants are CO_2 and N_2 it is vital to study the adsorption equilibrium properties of such gases on the potential adsorbents to be used in separation processes [9, 10, 11]. Also, biogas, which is a promising a renewable source of energy, consists mainly of methane (CH_4) and carbon dioxide (CO_2). In order to be used as fuel,

biogas must be upgraded to bio-methane which, can be injected in the natural gas grid, for domestic consumption or be directly used as vehicle fuel [7, 6, 12]. Adsorption processes can only be employed in biogas upgrading if the adsorption equilibrium of CO_2 and CH_4 on the adsorbent material is known.

Olefins such as ethylene (C_2H_4) and propylene (C_3H_6) have proved possess high economic value because they are commonly used in polymer production and other applications [13]. They are typically used in oil refineries, a large number of physical and chemical processes for converting oil into gasoline, fuel oil and hundreds of other commercial products. The catalytic cracking is a process used to increase gasoline production from oil. The purge of this process contain large amounts of olefins that should be recovered. One of the most popular and used methods for the separation of olefins from their respective paraffins is the traditional distillation. However this process is extremely difficult and has high energy costs. Adsorption-based processes have been explored as an alternative to distillation processes. One mixture of interest is propane (C_3H_8) / propylene (C_3H_6) has been the subject of extensive study, since it is a relevant separation in the petrochemical industry [14].

Likewise, the search for a suitable adsorbent is crucial for the success of any adsorption process, and thus its field of reseach has been the subject of extensive research [15].

The motivation of this Master's thesis arises from the current society concerns on the environmental impact of several gases with greenhouse effects, along with the search for new sustainable and low-carbon technologies based on adsorption, as described above. The main objective of the work proposed comprises the characterization of the selected adsorbents for the referred gases of interest, since this is essential for the development and design of gas separation processes such as Pressure Swing Adsorption (PSA), Simulated Moving-Bed (SMB) and their new hybrid schemes, which lately have gained great interest due to their lower energy requirements and associated costs. The equilibrium of adsorption of pure components in two different materials, zeolite 5A and metal-organic framework (MOF) MIL-53(Al) was extensively analyzed. This study covers a wide range of thermodynamic conditions (0 - 50bar and 303.15 - 373.15K) for the series of n-alkanes (C_2H_6, C_3H_8 and C_4H_{10}), ethylene (C_2H_4), carbon dioxide (CO_2) and nitrogen (N_2), which will add to the published literature an heavy amount of adsorption data that was found to be scarce for the wide range of conditions experienced, especially for the MIL-53(Al) solid**.**

1.2. Structure of the Thesis

The structure of this thesis comprise with the following content:

- **Chapter 1:** Introduction

- **Chapter 2:** Background

This chapter discusses the theory and experimental methods related to the adsorption phenomenon and analyze the latest developments that have been made in this research field. A brief approach is done concerning the gases studied in this work, i.e. the series of light alkanes and alkenes, carbon dioxide and nitrogen. Moreover, a short reference to the chosen adsorbent materials, zeolites and metal-organic frameworks (MOF's) is also made.

- **Chapter 3:** Experimental Work on Adsorption

In this chapter it is possible to find all the experimental work. It encloses the characterization of the adsorbent materials used, a brief reference to the method used in the experimental determination of the adsorption isotherms, as well as the description of the entire gravimetric unit used for the purpose of this work. Lastly, the complete experimental methodology employed is included in this chapter.

- **Chapter 4:** Experimental Results and Data Analysis

This chapter presents the experimental results obtained in this work, along with their data analysis. In order to obtain broader models to describe the adsorption isotherms, global data fittings were performed by using the Toth and Sips model equations. A second approach adopted was the potential theory of adsorption that has proved to be quite interesting. Very little information using this theory is available in open literature, especially for the selected adsorbents. An error determination accompanied the experimental analysis.

- **Chapter 5:** Conclusions and Future Work

Chapter 5 presents the work conclusions and reports several suggestions for possible future work to be developed.

Chapter II

2. Background

This chapter provides an introduction to the adsorption phenomena, its importance and principles, thus proving some developments that have been made in this area.

2.1. Adsorption Phenomena

The Adsorption Phenomenon has been recognized by humanity throughout the ages, and is increasingly used in performing separations and purifications.

Adsorption occurs whenever a porous solid surface (adsorbent) is exposed to a gas or a liquid (adsorbate). This exothermic phenomenon is defined as enrichment of the material or increase in the density of the fluid in the vicinity of an interface. Therefore, the porous solid surface is considered as the "heart of adsorption", providing a very high surface area or high micropore volume, and consequently a high adsorptive capacity [16]. The inverse endothermic process is called desorption where the molecules adsorbed at the solid surface of the adsorbent are released [17].

The adsorption occurs due to the effect of the various types of linkages between the adsorbate-adsorbent pair: van der Waals interactions, covalent bonding, acid-base, hydrogen bonding, among others. The strength of binding is extremely important, because if the interactions are fairly weak, small adsorbate amounts are adsorbed; if the interactions are strong, the regeneration of the adsorbent will be difficult to achieve [18].

It is also important to realize that depending on the strength of the bonds between the molecules being adsorbed and the adsorbent material, two types of adsorption can be distinguished: physical adsorption (physisorption) and chemical adsorption (chemisorption).

Physisorption occurs when adsorption interaction forces between molecules are weak, with links based on intermolecular forces of van der Waals and/or electrostatic interactions. The heat of adsorption is relatively low compared to chemical adsorption, and presents a reversible character. This adsorption is invariably exothermic, a fact which can be verified by studying their thermodynamics [19, 20].

Chemisorption occurs when the adsorption process takes place through chemical interactions between the molecules of the adsorbent and adsorbate at the surface of the solid. In this case, the bond strengths are mainly of covalent nature or ionic, restricted at the first surface layer of the adsorbent [19, 20]. This type of adsorption is usually irreversible with a much higher adsorption heat than in the case of physisorption.

Table (2.1) shows the main differences between the physisorption and chemisorption.

Table 2.1: Distinction between Physisorption and Chemisorption. Adapted from [11, 13].

Physisorption	Chemisorption
Low heat of adsorption	Heat of adsorption on the order of enthalpy reaction
Mono or multilayer	Only monolayers
Adsorbed molecules do not suffer dissociation	Can occur dissociation of molecules
Occurs at low temperatures	Occurs at high temperatures
Reversible	May be irreversible
Low degree of specificity	High degree of specificity

The adsorption process at an industrial level is extremely important, as such, some adsorbents are already used on a large scale as desiccants, catalysts or catalyst supports and others are used for the separation, purification and/or storage of gases, pollution control, among others. In addition, this process plays a vital role in biological mechanisms. Adsorption-based separation processes have been the subject of considerable research for CO_2 capture from flue gases, capture and recovery of VOC's, air drying, biogas upgrading, hydrogen purification, and removal of light hydrocarbons from various gas streams [12, 21, 22, 23, 24, 25].

Adsorption in porous materials is currently the subject of academic and industrial research. In particular, gas adsorption has become one of the most widely used procedures for

determining the surface area and pore size distribution of a diverse range of porous materials. Such materials (adsorbents) will be extremely important in any adsorption process.

The older types of known industrial adsorbents are activated carbon and silica gel, but there is a great interest in developing new materials having pores of well-defined shape and size, as are the cases of metal-organic structures that have recently presented an increasing applicability as adsorbents [26, 27, 5, 28, 29].

2.2. Adsorption Equilibria

With the advancement of research conducted in the field of adsorption became necessary to quantify the amount adsorbed, retained by the adsorbent, which was named by adsorption capacity. The adsorption capacity depends then on the temperature and the pressure or the concentration, in the case of the adsorbate in question being a gas or a liquid, respectively.

The amount adsorbed retained by the adsorbent after reaching the equilibrium is named adsorption capacity. The adsorption capacity of the solid depends both on the temperature and the pressure or the concentration, being the adsorbate in question a gas or a liquid.

For the study of the adsorption equilibria and adsorption capacity of an adsorbent, it is normally considered one of the three constant variables, that is, the adsorption data is considered as isosteres if the amount adsorbed is constant; isobars for constant pressure values, or isothermal if the temperature is kept constant.

Adsorption isotherms are the most frequently used procedure in data collection and, depending on the properties of the adsorbate and the adsorbent in question, they may acquire different shapes [2]. Adsorption isotherms are then used to compare the adsorption capacity of the adsorbents for specific substances. In literature there are numerous records of experimental isotherms data, measured in several solid-gas systems, with a wide variety of forms. The shape of the adsorption isotherms present inflections, and therefore concave and convex configurations may be obtained [30]. Most of these isotherms, resulting in physical adsorption, may be conveniently grouped into six distinct categories according to the IUPAC classification. Originally the first five types (I to V) of isotherms were proposed by Brunauer and his colleagues in 1940 [26].

Figure (2.1) shows the classification system of adsorption isotherms adopted by IUPAC.

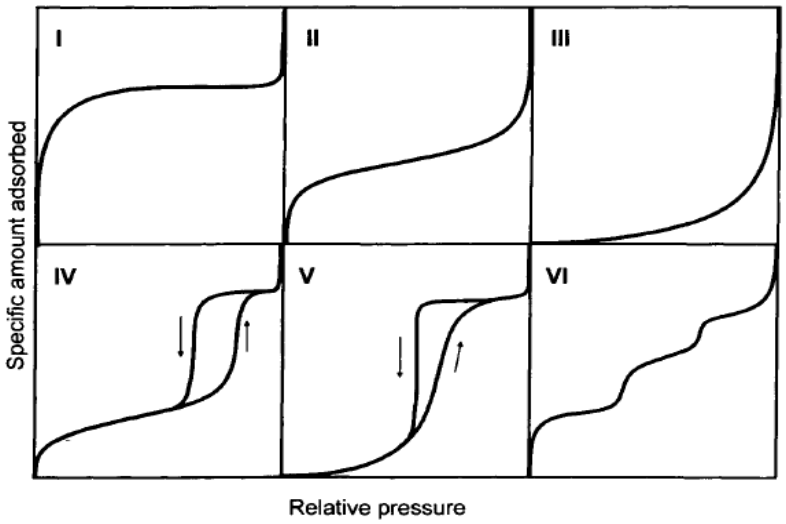

Figure 2.1: The six types of adsorption isotherms, as classified by IUPAC [26]. Specific amount adsorbed versus relative pressure P/P_0, where P_0 is the saturation vapor pressure.

The isotherms of the type I are reversible and have a concave shape in relation to the axis of relative pressure, since the specific amount adsorbed increases significantly at low pressures, ultimately reaching a plateau. Such isotherms are normally given for microporous solids and a pore size not much larger than the adsorbate molecules [26, 31].

As for the type II, these isotherms are also reversible and they are obtained with non-porous or macroporous adsorbents, then having a monolayer formation followed by adsorption of multiple layers [26, 31].

Type III isotherms show a convex shape along the whole axis relative pressure. These isotherms are reversible, but are not very common the systems that have this type of curvature. In such cases, the adsorbent-adsorbate interactions play a very important role [26, 31].

The type IV isotherms whose initial region is closely related to type II isotherm, tend to stabilize at high relative pressures. It has a characteristic appearance, the hysteresis loops, which are associated with capillary condensation that occurs in the mesopores. The lower branch represents the measurements obtained by progressive addition of adsorbate, and the upper branch of the phasing. Such isotherms are common and are provided by various industrial mesoporous adsorbents, but the exact shape of the hysteresis loop varies from system to system [26, 31].

The isotherms of type V are rare, they are related to the type III isotherms, also presenting a convex shape along the axis of relative pressure. As in the case of type III, this is indicative of frank interactions between porous adsorbent and adsorbate. However, these type

V isotherms exhibit a hysteresis loop which is related with the mechanism for filling and emptying the pores [26, 31].

Finally, the VI type of adsorption isotherms, also commonly known as isothermal steps is also relatively rare and in which the sharpness of steps depends on the system and temperature. This shows the various steps that occur in multiple layers of adsorption on uniform surfaces and non-porous. The height of each step is related to the ability of each layer [26, 31].

This classification is a simplification, since many experimental isotherms have a composite nature, and some are more complex than expected. It is obvious that this kind of classification is only applicable for the adsorption of a single component. Such experimental measurements are extremely useful to characterize porous materials [26].

The theoretical modeling of adsorption isotherms is extremely important for the practical processes of scale-up of adsorption.

2.2.1. Adsorption Hysteresis

Although the adsorbed amount gives an idea of the pore form, another way of evaluate the behavior of the pore is to investigate the shape of the hysteresis loop when present [16].

The terms of adsorption and desorption are commonly used to indicate the direction by which the equilibrium states were discussed. The adsorption hysteresis occurs when the amount adsorbed is not brought to the same level by the adsorption and desorption at a given pressure balance [26]. The hysteresis is a phenomenon which arises essentially in the area of multilayer physical adsorption isotherms, is usually associated with mesoporous structures and can exhibit a variety of shapes [31].

Although the effect of various factors on adsorption hysteresis are not yet fully understood and remain the subject of considerable study, there is a classification made by the IUPAC which that classifies 4 types of hysteresis designated of H1 - H4 [31, 32].

Figure (2.2) shows the classification system of hysteresis loops adopted by IUPAC [32].

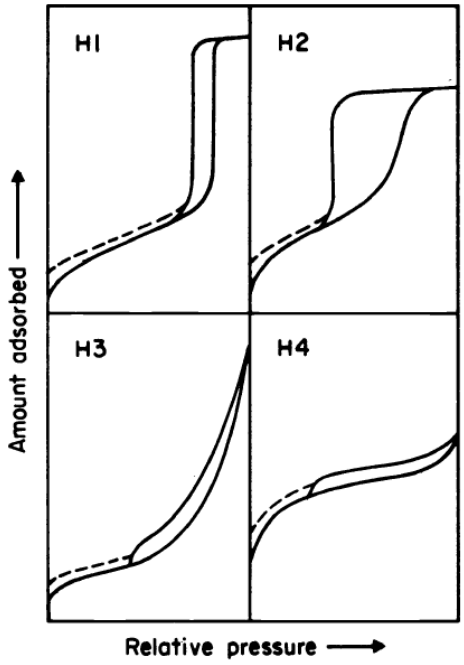

Figure 2.2: The four types of adsorption hysteresis as classified by IUPAC [31]. Amount adsorbed versus relative pressure P/P0, where P0 is the saturation vapor pressure.

As it can be seen in Figure (2.2), there are two kinds of extremes, H1 and H4. In the first case, H1, the branch of the adsorption and desorption are almost vertical and parallel along a range of appreciable gas adsorption. In the case of H4 it appears that the two branches are almost horizontal and parallel along the axis of relative pressure. The types of hysteresis H2 and H3 are then considered intermediate between these two extremes [31].

For systems mainly microporous, hysteresis at low pressures (shown in Figure (2.2) by dashed lines) can also appear. In these cases the removal of adsorbed material is only possible if the adsorbent is degassed at higher temperatures. This phenomenon may be associated with swelling of the non-rigid porous structure or with an irreversible adsorption of molecules in pores with approximately the same size as the adsorbed molecule, or in some cases with irreversible chemical interaction between the adsorbed and the adsorbent [31].

2.3. Experimental Methods for Measuring the Adsorption Isotherms

The measurements of gas adsorption are not difficult to perform, as long as they are carried out carefully, with the appropriate equipment and process design. Additionally, prior to any measurements of adsorption equilibria several considerations should be accounted for:

a) What is the purpose of the work?

b) What are the operating conditions?

c) What is the desired data accuracy?

Obviously, the selection of the methodology and experimental conditions always depend on the purpose it is intended, being still necessary always ensure a controlled and well-defined measurement procedure [26].

Gas adsorption equilibrium can be measured by several different methods. In this section the more classical methods are addressed, namely the gravimetric and volumetric/manometric ones. A brief reference to the calorimetric method is made.

Both gravimetric and volumetric/manometric techniques have the same objective, that is, to measure the amount of gas adsorbed on an adsorbent surface as a function of the pressure of the gas, thus obtaining an adsorption isotherm after reaching the equilibrium at each point of the curve. These techniques have their advantages and disadvantages, so it is important to have the knowledge about both of them, especially to decide which method use [32]. The major distinctions between these two methods are:

a) Cost.

Normally the gravimetric method is more expensive than the volumetric one. Although both methods require an accurate pressure reading, the gravimetric equipment usually entailed higher investment costs.

b) Capacity.

Normally, the gravimetric method is more precise than the volumetric one, since the latter technique has cumulative errors on the adsorption measuring points of the isotherm. Therefore, due to its limitations this method is used in routine work, but the gravimetric technique is commonly preferred [32].

2.3.1. The Gravimetric Method

The gravimetric method is a method that has great potential in research on phenomena of gas adsorption in porous solids. The main characteristic of the gravimetric method is its ability to measure small changes regarding the weight of an adsorbent sample. The most accurate and reliable measurement of adsorption isotherms can be carried out by weighing the mass of adsorbent which is in contact with the adsorbate using a very sensitive microbalance; preferably a magnetic suspension balance (MSB).

The principle of the gravimetric method is simpler than the volumetric method. Typically, physical adsorption isotherms are represented by the adsorbed amount depending on the pressure.

The gravimetric adsorption measurements have shown to have a great use, from characterizing porous means, measuring gas adsorption equilibriums to investigating the adsorption kinetics [17]. Finally, is relevant to give some attention to the advantages and disadvantages of this method of measurement of adsorption equilibrium.

The main advantage of the gravimetric method is undoubtedly its high precision and accuracy, made possible by the commercially available microbalances. The amount of adsorbent material is also a positive aspect, since smaller amounts can be used when are only available small quantities of newly developed material; or a considerable solid quantity can be employed allowing results with a higher reproducibility. Unlike the volumetric/manometric method, extremes of pressure (too high or too low pressures) do not represent a problem in gravimetric adsorption measurements, since in these measurements the adsorbed mass is determined by its weight. Another advantage is that using this type of isothermal measurements, it is possible to determine the kinetics of the process.

Regarding the disadvantages of gravimetric adsorption, the main one is undoubtedly the expensive equipment's associated. Its complexity can also become a negative aspect, since a magnetic suspension balance (MSB) is usually quite sensitive to electromagnetic fields. Another disadvantage lies on the measurement techniques, since the adsorption equilibrium measurements using this technique is laborious and, although it is possible the automation of the system, it is recommended to supervise it regularly [17, 32].

2.3.2. The Volumetric Method

The oldest method and still widely used to measure adsorption equilibrium is the volumetric (or manometric) method. This is based on measuring the pressure of a gas in a calibrated volume, at a constant volume and at a known temperature. Typically, physical adsorption isotherms are presented as volume of gas adsorbed depending on the relative pressure.

Today it is known that it is inappropriate to use the term volumetric since the amount adsorbed is measured by the change in gas pressure, rather than volume [26, 17]. It is important then to discuss some of the advantages and disadvantages of this method.

One of the great advantages as mentioned above is that the volumetric method is much less expensive; the only associated cost is related with the pressure transducers investment, which depends on the accuracy required. Their simplicity is another positive side, since this technique does not require sophisticated equipment, and furthermore the experiment itself is simple and can even be automated.

On the other hand, the main drawback of this technique is that it is not very suitable for research, especially for low pressure ranges. Another negative aspect of this process is also the amount of adsorbent material; if only a few milligrams of adsorbent is available, the gravimetric method is strongly recommended due to the cumulative errors present on the volumetric adsorption measurements. Another disadvantage of this technique is that it does not provide information on the kinetics of the adsorption process [17, 32].

2.3.3. The Calorimetric Method

Calorimetric measurements are less common when compared to the techniques listed above. In fact, to be effective this method must be combined with a volumetric or gravimetric technique.

The calorimetry evaluates a physical quantity different than the gas adsorption amount obtained by the other two methods. In detail, the calorimetry measures the temperature variation to which adsorption occurs as a function of pressure. Calorimetric measurements are less accurate and extremely difficult to perform, requiring a great deal of time and effort, thus it is rarely used in determining experimental isotherms [32].

2.4. Adsorbent Materials

In an adsorption process, the adsorbate molecules aggregate onto the surface of the adsorbent and/or in the pores of it. The adsorbent is normally porous in nature with a high surface area capable of adsorbing a particular fluid, which can be liquid or gaseous. Therefore, the adsorbent material plays an important role in adsorption, since the effectiveness of both kinetics and equilibrium of adsorption is directly determined by the quality of the solid. Note however that this fact then generates a dilemma, since an adsorbent with a high capacity, but with slow kinetics is not a good choice, because the time that the adsorbate molecules take to reach the interior of the adsorbent is too long. On the other hand, adsorbents with a low capacity and rapid kinetics are also not a good choice, because a large amount of solid is needed to perform the adsorption process. Hence, a good adsorbent is the one that provides a good kinetics and has a good adsorption capacity, but simultaneously is easily regenerated. In order to meet these two requirements, it is necessary to take into account two aspects [16]:

a) The solid must have a relatively high surface area or a considerable microporous volume;

b) The solid must have a sufficiently large pore network so as to achieve transport of the adsorbate molecules to his inside.

In order to satisfy the requirements described above, a good adsorbent should arise from a combination of two characteristics: i) a small size pore; and ii) a reasonable porosity [16]. In this context, it is convenient to classify the pores according to their sizes. The classification recommended by IUPAC to delineate the pore size was developed based on nitrogen adsorption at 77K for a wide range of porous solids, giving then the following distribution:

a) Widths of exceeding 50nm pores are called macropores;

b) Pores with widths between 2nm and 50nm are called mesopores;

c) Widths of pores with less than 2nm, are designated micropores.

There is then a concern about the study of the limits of the pores, since the mechanisms of filling of these pores are dependent on their shape, the properties of the adsorbent and the interactions between the adsorbent and the adsorbate [31].

The R&D on new adsorbents is presently booming. The development of better adsorbents can improve the performance of current processes of adsorption, from the petrochemical, chemical, biochemical, biological, biomedical and others [33]. It is noticeable that there are numerous materials used as adsorbents in adsorption phenomenon, from activated carbon, silica gel, zeolites to metal organic frameworks (MOF's), among others.

The present work employed zeolite 5A and the metal-organic framework (MOF) MIL-53(Al) as adsorbents; the former is a common solid whereas the latter one is a newly developed porous material. Due to their high porosity, high adsorption capacity, and thermal stability, the MOF's materials have shown great potential for applications in gas storage, gas separation, catalysis, and allied fields [34, 35, 36, 37, 38, 39].

2.4.1. 5A Zeolite

A class of porous solids, as widely used as the activated carbons, are zeolites. These materials can be natural or have a synthetic origin, although the latter source is preferred. There are many types of synthetic zeolites such as type A, X, Y, ZSM among others.

Although zeolites have been known for over 200 years, its recognition as a highly selective adsorbent was held just 50 years ago. Since then several hundred of new porous zeolites have been synthesized. This class of adsorbents can be considered as one of the most important and well established class of microporous adsorbents, wherein the porosity is intra-crystalline [16]. It is unquestionable, the importance that zeolites have shown in the development of adsorption technology. Three major areas of application of this material are:

a) Removal of trace impurities, or diluted from a gas;
b) Bulk separation of gas mixtures;
c) Gas analysis

Category I refers to the traditional use of zeolitic adsorbents, are examples of this drying gas, desulfurization and removal of corrosive and toxic organic compounds through a contaminated gas. There are several industrial gases containing various kinds of impurities that are treated by adsorption in zeolites. It is due to this application that zeolites are commonly known as "molecular sieves".

Category II is the latest application in development for this type of adsorbent. The trend is then to separate gas mixtures, recovering and increasing the degree of purity of them so that they can be reused.

Finally, the most important example in category III, is gas chromatography, which is widely used as an analytical tool in research and process control [15, 40].

Zeolites are the most widely reported physical adsorbents for CO_2 capture in literature. In addition, these adsorbents are responsible for the first production of commercial hydrogen (H_2) from the H_2/CO_2 separation. An advantage on the use of zeolites is that they are typically used at high pressures; on the other hand, the regeneration of the adsorbent is presented as a

disadvantage, since it implies costs by the need to be performed at very high temperatures [8, 41].

Once known some general characteristics of the various types of zeolites, it is convenient to devote some attention to one of the materials used in this work, namely the zeolite 5A.

The basic unit of a zeolite structure is TO_4 tetrahedron, where T is typically silicon or aluminium (or a phosphorus on aluminophosphate). In the case of type A zeolites, the typical composition of the unit cell is $[Na_{12}\{Al_{12}Si_{12}O_{48}\}.27H_2O]_8$ and the ratio of Si:Al, always close to 1.0. There are several variants of type A zeolites (3A, 4A, 5A), these arise when the cation Na^+ is exchanged for cations K^+, Ca^{2+} or Mg^{2+}, causing a significant effect on the adsorptive properties of the zeolite A. In Figure (2.3), it is possible to see the typical structure of a zeolite of type A, as well as a sample of zeolite used in this experimental work.

In the case of zeolite 5A, this occurs when the Na^+ cations are exchanged for Ca^{2+}, whereas the number of cations required is further reduced, thus leading to an increase of porous volume. It is then possible to conclude that the 5A zeolite is crystalline and highly porous, having a network of internal pores with approximately $4.3E^{-04}\ \mu m$ in size and with molecules dimensions relatively small [26, 42].

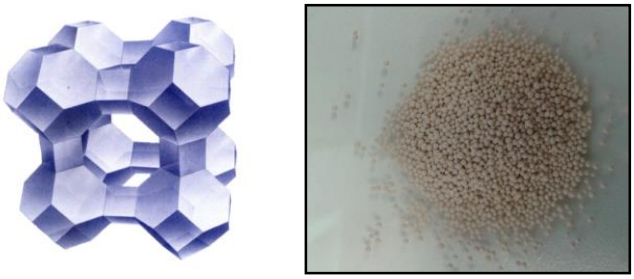

Figure 2.3: Typical Structure of zeolite type A (left) and image of the sample of zeolite 5A, used in the experimental work (right) [91].

2.4.2. Metal Organic Framework MIL-53(Al)

In addition to the need to improve the traditional materials such as activated carbon and zeolites, it is vital to develop new potential adsorbents. The progress of this area then results in a wide variety of materials with different characteristics (pore size, surface area, etc.) and therefore quite different adsorption properties (selectivity, adsorption capacity, etc.), thus increasing the specificity of each adsorbent [43].

It has been over the past 10 years, that a large number of hybrid organic - inorganic porous solids, which belong to a new class of nanoporous structured materials, to which are denominate as organic metal structures (MOF's), have become the subject of considerable study. These have emerged as promising candidates for various applications including in the area of adsorption [44]. To date, the number of synthesized MOF's is already extremely large, as such, the need to characterize and experimentally test these materials is growing [45, 46].

The high porosity, high adsorption capacity and thermal stability of MOF's makes them large enhancers for applications in the storing area, purification and separation of gases, in catalysis, among others. Therefore, some MOF's materials are already produced on an industrial scale, since they are economically viable and of easy regeneration [47, 48, 49].

The organic metal structures (MOF's) are materials made from metal-oxygen polyhedral containing either divalent (Zn^{2+}, Cu^{2+}) or trivalent (Al^{3+}, Cr^{3+}) cations interconnected by various organic compounds such as carboxylates or phosphonates. As in the case of systems of zeolites, the pore size and composition of the surface can be easily adjusted by changing the nature of the organic binder or metal center. MOF's are geometrically and crystallographic ally structures well defined, and in most cases are strong enough to allow removal of guest species, resulting in a permanent porosity. The large number of different structures of these materials and the unusual characteristic of some MOF's of being selectively flexible during the adsorption of different gases make these solids very interesting for adsorption [50, 51].

Metal organic frameworks (MOF's) can be classified into two main classes, rigid and flexible/dynamic. The rigid MOF's usually have relatively stable and resistant porous structures with a constant porosity, similar to zeolites. On the other hand, the flexible MOF's are dynamic structures that respond to external stimuli, such as pressure, temperature and adsorbate molecules. This extraordinary sensitivity to external stimuli makes the MOF's unique adsorbents, and with properties that are not within the reach of traditional adsorbents, such as zeolites and activated carbons [1, 52].

The series of MIL-n (*Materials of the Institute of Lavoisier*), hybrid porous materials, synthesized by the group of Férey, are promising candidates on the adsorption of some gases, such as CO_2 and series of alkanes [50, 51].From the several isotypes (for example, chromium,

aluminum and vanadium) porous terephthalates (MIL-53), the aluminum analog - MIL-53(Al) - has revealed to be a very interesting MOF's material and was one of the main focus of this work. The structure of MIL-53(Al) is formed by the interconnection of infinite trans chains of corner-sharing (via OH groups) AlO_4-$(OH)_2$ octahedron by 1,4-benzenedicarboxylate acid (BCD) ligands. Its chemical formula is then $Al(OH)(O_2C - C_6H_4 - CO_2)$ [47, 53]. MIL-53(Al) not only adsorbs large quantities of gas, but also present an exceptional flexibility undergoing a reversible structural transformation between two distinct conformations of a large pore (lp) and a narrow pore (np), which share the same chemical composition but differ in volume of the unit cell, up to 40%. At room temperature and in the absence of the adsorbate molecules, the lp phase is the most stable form. However, during gas adsorption, the lp phase becomes np at low pressures and inverse transformation occurs at higher pressures [47, 51, 53].

In Figure (2.4), we can see the structure of the two conformations (lp) and (np) as well as a sample of the MOF used in this work.

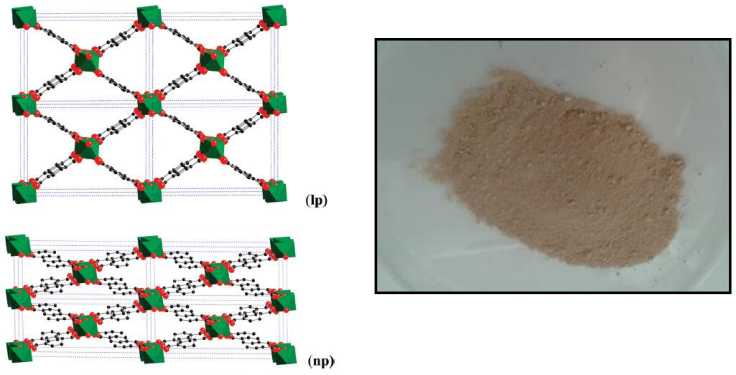

Figure 2.4: Structure of the MIL-53(Al) in two conformations (lp) and (np) (left) [53]. And image of the sample of MIL-53(Al) used in the experimental work.

2.5. Adsorbates

Throughout this chapter one have come to realize the importance of adsorption. It has been so noticeable that adsorption is the term used to describe the phenomenon in which molecules of a given fluid (liquid or gas), are concentrated on a solid surface spontaneously. As such, the phase which one call commonly by fluid is also worthy of some study. Therefore, one can say that this kind of molecular gas or liquid that adheres or is adsorbed on the solid surface is then called adsorbate.

In the case of the development of this work, the adsorbates used were found in the gaseous phase, and the adsorption equilibrium studies were performed for pure components, such as carbon dioxide (CO_2), nitrogen (N_2), the series of n-alkanes and alkenes.

Note that the research conducted for these gases is of extreme importance, since we want to achieve ranges of temperature (303.15K - 373.15K) and pressure (0bar - 50bar) of very considerable interest and of great importance in research.

2.5.1. Carbon Dioxide

Carbon dioxide presents a linear geometry and nonpolar character, so the intermolecular attractions are weak. This at room temperature presents itself in the form of a colorless gas [54].

The study of carbon dioxide is of great importance since the environmental effects have caused severe impacts. The excess of carbon dioxide that is currently released into the atmosphere results from the burning of fossil fuels, mainly by the industry and automotive sector. Since this is an important greenhouse gas, its increase has led to global warming causing climate change [1]. As such, the capture and storage of carbon dioxide (CO_2) are increasingly topics for investigation.

2.5.2. Nitrogen

The nitrogen in ambient conditions is found in the gaseous state under the bimolecular form (N_2). This inert, colorless, odorless and tasteless gas represents 4/5 of the composition of atmospheric air. Nitrogen (N_2) is the major constituent of the Earth's atmosphere and the most abundant in the Universe. This is somewhat reactive element, so that under normal conditions does not combine with any other chemical element [54].

The study of this gas is also important, since, although in low percentages, nitrogen is present in the mixtures of gases that are released into the atmosphere by the industry, as such, knowledge about data such as the adsorption equilibrium of this gas is also important.

The nitrogen has a variety of applications, such as, its use for preserving the freshness of the packaged food or in bulk. It is used, for example, in some systems of aviation fuels to reduce the risk of fire, or to inflate high performance tires.

2.5.3. N-Alkanes and Alkenes

Hydrocarbons are organic compounds constituted essentially by carbon and hydrogen atoms linked by weaker intermolecular forces. Normally hydrocarbons are in a gaseous or liquid state because of its low melting point and boiling point, respectively. These are formed at high pressures inside the Earth and are brought to areas of lower pressure through geological processes, which can form commercial accumulations of great value, such as coal, oil, natural gas, among others [54].

The hydrocarbons can be divided into saturated and unsaturated hydrocarbons. The saturated ones do not form double or triple bonds, such as the series of n-alkanes. In contrast, the unsaturated ones have one or more double or triple bonds between carbon atoms, as the case of alkenes. From the series of alkanes available, this work studied the gases: ethane (C_2H_6), propane (C_3H_8) and butane (C_4H_{10}), while in the series of alkenes is addressed only for the ethylene (C_2H_4) [54].

The simplest alkane is methane (CH_4), this is the main component of natural gas and probably the most abundant organic compound on Earth, which makes it quite attractive. However, it is also a greenhouse gas relatively powerful, leading to a greater concern for environmental protection. Likewise, hydrocarbons are currently the main source of energy for civilizations and their impact on the environment causes some concern. Therefore, it is easily understood why the study of the series of n-alkanes and alkenes are in constant development.

In summary, it should be noticed that the referred gases are generally not found as pure gases. On the other hand, the gases are generally found as mixtures, or contaminated streams. Therefore, the interest in the knowledge of the properties of the pure gases is strictly linked to the objective of performing their purification of separation from different gas streams. Among the typical effluent streams to be treated the separation of CO_2/N_2, CO_2/CH_4, C_2H_6/C_2H_4, and C_3H_8/C_3H_6 are considered of great interest [9, 12, 6].

Chapter III

3. Experimental Work on Adsorption

This chapter comprises the main component of this thesis. It includes the characterization of the adsorbent materials used, the description of the experimental method and equipment used to determine the adsorption isotherms, and the experimental protocol followed during the work.

3.1. Characterization of Adsorbents

The two adsorbents, target of study in conducting this work, belong to a class of microporous adsorbents with a high surface area. Zeolite 5A and MIL-53(Al) were selected since they have shown great potential in the field of adsorption [42, 35].

The adsorbents characterization is then a key issue, since it allows us to identify the properties that influence their performance. It is driven by the need for quantitative and qualitative information that serve as a basis for comparison and selection of the best adsorbent for a specific application [55].

3.1.1. Characterization Techniques

There are several adsorbent properties, such as density, surface area, the average pore size, distribution of pore size, shape and pore volume, among others, which are determined from specific characterization techniques. Only the most relevant ones are discussed here.

The characterization of both zeolite 5A and MIL-53(Al) was performed using techniques such as Mercury Porosimetry, Thermogravimetric Analysis and Nitrogen

Adsorption at 77K. All the supporting information provided by these techniques is available in Appendix A.

Note that before any of these characterization analyses, the two samples were subjected to a pretreatment. In the case of 5A zeolite, the sample was degassed and activated at 623.15K in a muffle (Nabertherm GmbH B170); in the case of the MIL-53(Al) the procedure was the same, but its activation temperature was of 473.15K.

3.1.2. Mercury Porosimetry

The mercury porosimetry is a technique that, for applying various levels of pressure to a sample immersed in mercury, characterizes the porosity of the material. The pressure required to intrude mercury into the pores of the sample is inversely proportional to pore size [56].

The samples of zeolite 5A and MIL-53(Al) were then subjected, separately, to an experimental cycle of intrusion-extrusion of mercury, using a porosimeter, Autopore IV 9500 (Micromeritics Instrument Corporation, Norcross, Georgia). The experimental data are shown in Appendix (A.1), Figure (A.1) and (A.2).

By the analysis of mercury porosimetry is then possible to notice that in the case of zeolite 5A, this shows an average value of pore diameter of $\overline{D_p} = 5E^{-05}\ \mu m$ and a porosity of 56%. In the case of the MIL-53(Al), it announces an average pore diameter of $\overline{D_p} = 30\ \mu m$ and a porosity of 68%. We can then conclude that in this case the MOF represents a more porous material than the zeolite, as would be already foreseen.

3.1.3. Thermogravimetric Analysis (TGA)

Thermogravimetric analysis (TGA) allows us to evaluate the temperature range over which the sample decomposes. This procedure is performed by recording the weight loss as a function of the increasing temperature. Through this analysis, it is possible to observe the physical and chemical properties of the adsorbent material.

Typically, the results are presented graphically in a curve of weight percent as function of temperature. This way, it is possible to know until what temperature it is safe to heat the adsorbent, without occurring changes, in properties of the material.

The samples were analyzed by TGA (model Q50 V6.7 Build 203, Universal V4.4, TA Instruments) under a nitrogen atmosphere at a heating rate of 5 deg/min. It is possible to find the experimental profiles in Appendix (A.2), Figure (A.3) and (A.4).

It is easily possible to conclude that in the case of zeolite 5A, the structure can reach up to 823.15K without any decomposition of it. MIL-53(Al) shows no deformation in its structure until a temperature of 773.15K is reached [47, 57].

3.1.4. Nitrogen Adsorption at 77K

The first systematics measurements of physical adsorption of nitrogen 77K were undertaken by Brunauer and Emmett (1935). Since then, the low-temperature nitrogen adsorption at 77K has become a general procedure for the determination of the surface area and pore size distribution for various porous materials. The use of nitrogen represents an advantage since this probe molecule is inexpensive, readily obtained and well-studied in the adsorption literature [26].

The measurement of the isotherm of nitrogen (N_2) for the adsorbents in question was carried out at 77K, using a static volumetric apparatus (Micromeritics Adsorption Analyzer, Model ASAP 2010). In Appendix (A.3), Figure (A.5) and (A.6) presents the adsorption isotherm.

It is then possible to conclude that for zeolite 5A, the total surface area of the sample, determined by BET surface area method, is 502 m^2/g, of which 448 m^2/g corresponds to the microporous area and the total pore volume is 0.394 cm^3/g, of which 0.233 cm^3/g is the volume of the microporous pores. In the case of the MIL-53(Al) the total surface area of the sample, determined by BET surface area method, is 831 m^2/g, of which 608 m^2/g represent the microporous area, and relatively to the total pore volume, this is of 0.597 cm^3/g, of which 0.332 cm^3/g corresponds to the volume of microporous pores [47, 57].

In Table (3.1) are the main characteristics of the two adsorbents.

Table 3.1: Main characteristics of the MIL-53(Al) and zeolite 5A samples used in this work.

	MIL-53(Al)	5A
BET surface area (m^2/g)	831	502
Microporearea (m^2/g)	608	448
Total pore volume (cm^3/g)	0.597	0.394
Micropore volume (cm^3/g)	0.332	0.233
Porosity (%)	68%	56%

3.2. Adsorption Equilibrium Measurements

The extensive adsorption equilibrium data measured experimentally were obtained by a static gravimetric method, using a high-pressure magnetic suspension balance (MSB) ISOSORP 2000 from Rubotherm GmbH.

Briefly, this method consists in the progressive addition of gas to both measuring cells, which contain samples of zeolite 5A and MOF MIL-53(Al) separately, followed by the equilibration under isothermal conditions, in order to generate the data points throughout the adsorption isotherm. Pressure and weight changes are continuously monitored until the equilibrium, which occurs when it is assumed that the value of pressure and temperature are constant and there are no changes in the mass measured. The procedure is repeated until enough data points are collected to generate a complete isotherm. The cells are then gradually depressurized and equilibrated, to generate other points along the downward path of the isotherm, and check for possible hysteresis effects.

3.2.1. Materials

The 5A zeolite used in this study is in the form of spheres with a mesh between 60 and 80, synthesized by Supelco - Analytical (Bellefonte, USA) (lot.12193 - 50g). This material is intended solely to the area of investigation.

For the second adsorbent material used in this work, the metal organic framework (MOF) MIL-53(Al) is presented in the form of crystals synthesized by BASF (Somerset, NJ) under the trademark Basolite A100 and was purchased through Sigma-Aldrich (product no.688738 - 10g). According to the manufacturer, this material has an average pore diameter of $\overline{D_p} = 32\ \mu m$.

In the case of zeolite 5A were used between 0.50 to 0.55 g of material, whereas for the MOF, MIL-53(Al), a mass of 0.30 to 0.35 g was employed, for the experimental measures of adsorption equilibrium.

All gases used (He (99.999%), N_2 (99.995%), CO_2 (99.998%), CH_4 (99.95%), C_2H_6 (99.95%), C_3H_8 (99.95%), C_4H_{10} (99.95%), C_2H_4 (99.5%)) had the purity needed for research and were supplied by Air Liquide Portugal and by Praxair Portugal Gases.

3.2.2. Experimental Description

Adsorption equilibrium of the series of n-alkanes, ethylene, carbon dioxide and nitrogen in MIL-53(Al) and zeolite 5A were obtained gravimetrically using the high-pressure magnetic suspension balance (MSB) model ISOSORP 2000 by Rubotherm GmbH (Germany), with the acquisition of pressure, through an internally developed software (BioCTR) and temperature controlled by a thermostatic bath (JULABO).

Magnetic suspension balances (MSB) allow the determination, with high accuracy, of the changes in mass of one or two samples simultaneously, which are under a controlled environment (pressure, temperature, etc.). Through these measurements, it is then possible to determine the adsorption equilibrium, as is required in this task. The gravimetric method measures excess adsorption as the apparent increase in weight of the sample corrected for the buoyancy force exerted by the bulk fluid.

The main difficulty when using conventional gravimetric instruments is the direct contact between the measuring cell (sample atmosphere) and the weighing instrument. The balance can be damaged or disturbed by the measuring atmosphere and the measuring atmosphere can be adversely affected by flushing gases and pollution. These limitations considerably reduce the field of application of conventional measuring devices.

The advantage of the high-precision MSB consists in the possibility to weigh samples contactlessly under nearly all environments at high accuracy. Instead of hanging directly at the balance, the sample to be investigated is linked to a so-called suspension magnet which consists of a permanent magnet, a sensor core and a device for decoupling the measuring load (sample). The suspension magnet and the connected sample achieve a constant vertical position in the measuring cell. An electromagnet, which is attached to the underfloor weighing hook of a balance, maintains a freely suspended state of the suspension magnet via an electronic control unit. Using this magnetic suspension coupling the measured force is transmitted contactlessly from the measuring chamber to a microbalance SARTORIUS Model BP211, which is located outside the chamber under ambient atmospheric conditions. Consequently, this arrangement eliminates almost all restrictions which are inherent to conventional gravimetric measuring instruments. Figure (3.1) shows a comparison between the conventional method and the magnetic suspension balance [58, 59].

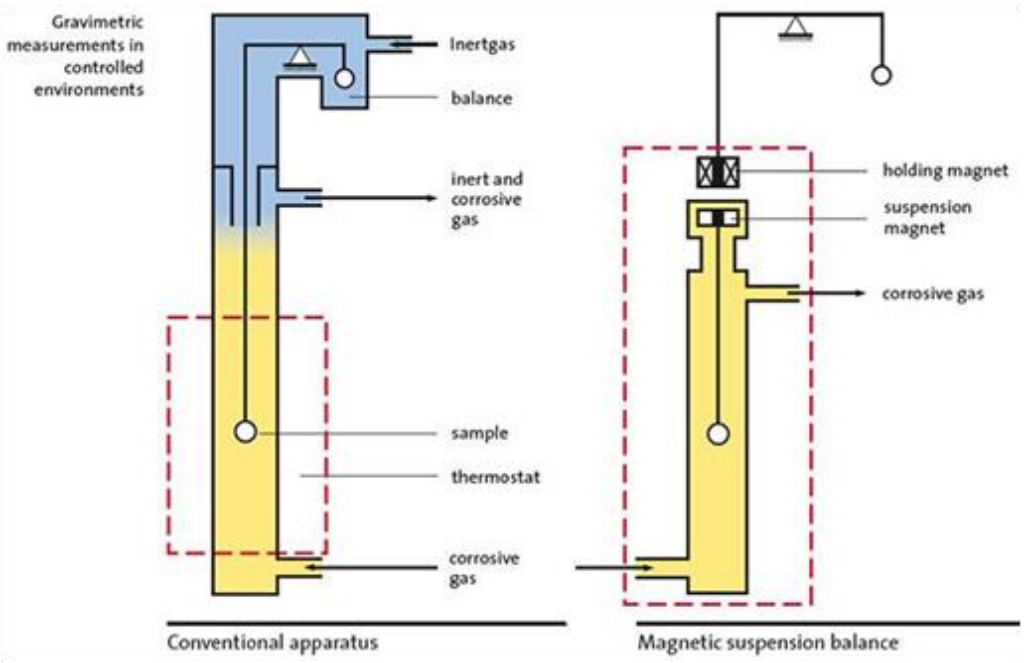

Figure 3.1: Gravimetric measurements in controlled environments. Comparison of conventional instrument (left) and magnetic suspension balance (right) [58].

A controlled suspended state is achieved by means of a direct analogous control circle (PID controller and position transducer). This modulates the voltage on the electromagnet in such a way that the suspension magnet is held constantly in a vertical position. A microcontroller driven digital set point controller superimposed to the direct PID controller allows various positions of the suspension magnet to be set up.

The balance can be tared and calibrated automatically. The magnetic suspension balance offers the possibility of lowering the suspension magnet in a controlled way to a second stationary position, a few millimeters below the measuring position. Then, a small carrier to which the sample is connected is set down on a support. Now the sample is decoupled from the balance. The suspension magnet alone is in a freely suspended state and only its weigh is now transmitted to the balance. This so-called zero point position (ZP), which corresponds to an empty balance pan in a normal weighing procedure, allows a taring and calibration of the balance at all times, Figure (3.2). This feature enhances the accuracy of the measurements considerably, particularly in the case of long term measurements [58, 59].

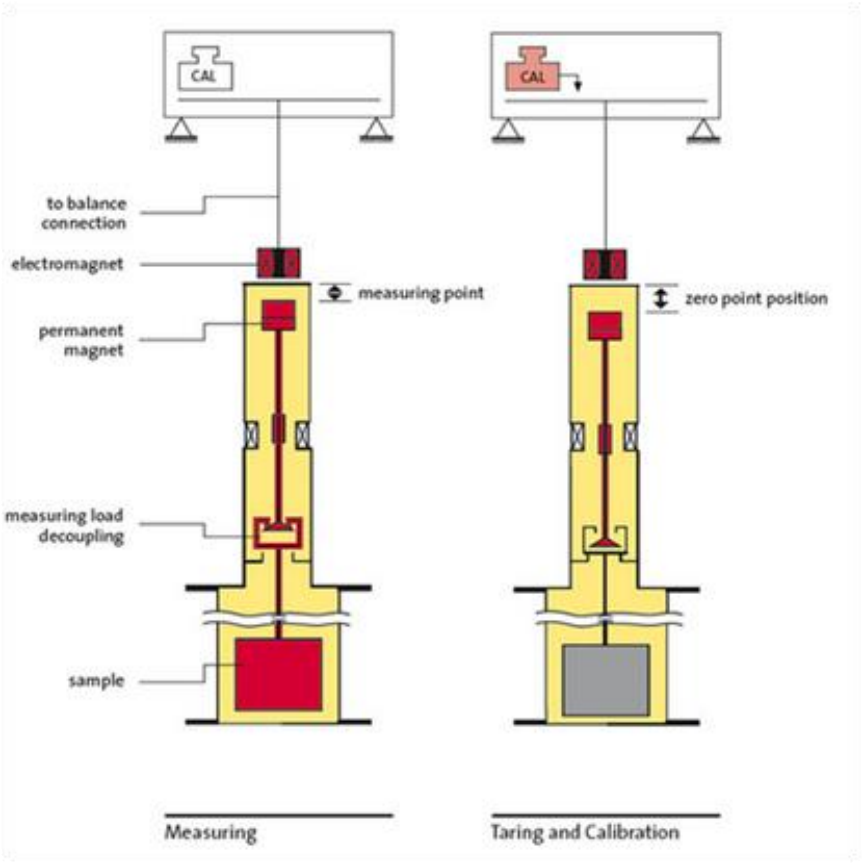

Figure 3.2: Measuring position with sample connected to the balance (left) and automatic decoupling [Zero Point position (ZP)] of the measuring load in order to tare and calibrate the balance (right) [58].

An upgrade of the MSB was performed and tested recently during this thesis, opening two possibilities: i) to measure the mass change of one sample with direct determination of the gas-phase density inside the measuring chamber; or ii) to measure simultaneously two samples with only one magnetic suspension balance. In addition to the first measuring load decoupling a second is arranged in the magnetic suspension coupling. The three different vertical positions of the suspension magnet, which can be arrived at in a controlled way, correspond to three different measuring positions, which double the measuring adsorption data for the same period of working time and under exactly the same conditions [58, 59]:

- **Zero Point:**

The permanent magnet alone is in a freely suspended state, allowing the balance to be tared and calibrated. The drift resulted from the electronics of the MSB is nullified in this ZP position.

- **Measuring Point 1 (MP1):**

The first sample is lifted up and its mass is weighed.

- **Measuring Point 2 (MP2):**

The second sample is raised with the first one and both masses are weighed together. By subtracting the first measuring point (MP1) from the second one (MP2) the mass of the second sample is determined.

In summary, the main advantages of this unique MSB, brought together and implemented during this thesis, is the simultaneous:

✓ Weight measurement of one or two adsorbent samples placed inside the measuring cell and;

✓ Possibility of measurement of the density of the fluid phase inside the cell by using an inert sinker with known volume as second sample. The density of the fluid phase is then measured highly accurate using Archimede's principle of buoyancy.

Figure (3.3) then compares the three different measurement positions. The zeolite 5A and for MIL-53(Al) correspond to the adsorbent samples measured simultaneously inside the MSB described above.

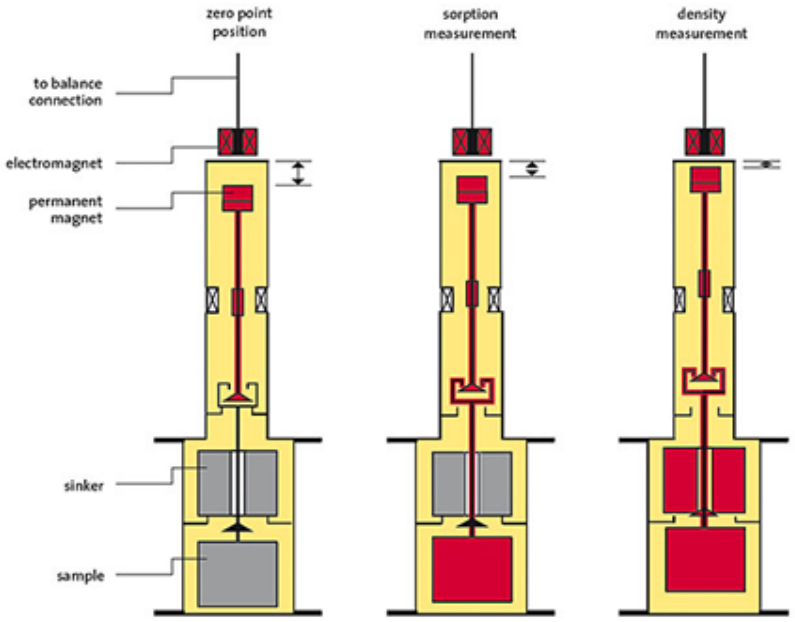

Figure 3.3: Simultaneous measurement of adsorption and density. Comparison of Zero Point (ZP), Measuring Point 1 (MP1) and Measuring Point 2 (MP2) positions [58].

After understanding some of the operational principles of this equipment, Figure (3.4) shows the magnetic suspension balance (MSB) and its components. The device has a resolution of 0.01mg, an uncertainty less than 0.002% of measured value, and a reproducibility of less than 0.03mg to a maximum load of 25g. The conditions that may be imposed to the measuring chamber are limited to 373.15K and 150 bar [58, 59].

Figure 3.4: Magnetic Suspension Balance (MSB) components [58, 59].

3.2.3. Adsorbent Sample Pre-Treatment

Before the measurement of each adsorption isotherm, it is necessary to pre-treat the adsorbent sample so as to ensure that this solid under study is as "clean" as possible, that is, it does not contain any moisture or other adsorbed impurities. This is performed by heating the sample/s at high temperature, according to the type of solid under study. However, the temperature limitation of (373.15K) inside the MSB does not allow activation of samples such as zeolites or MOF's *in situ*, as would be desirable. The activation temperature of the zeolite 5A is 623.15K and of MOF MIL-53(Al) is 473.15K. Therefore, there was a need then to find a reliable way to activate the samples.

The adsorbents activation where performed with the help of external muffles. Thus, whenever necessary, before the adsorption runs, each sample was placed in a small desiccator inside a nearby muffle (Nabertherm GmbH), with an heating ramp of 50 to 60 minutes and the threshold temperature of 623.15K and 473.15K for the 5A zeolite and for MIL-53(Al), respectively, for a period of time of 2 to 4 hours. Consequently, each heated sample was placed inside the MSB under an inert atmosphere of helium. Finally, the samples are degassed *in situ* under vacuum at ca. 353.15K for at least 8 hours. After the procedure described above, and the stabilization of the system at the operating temperature required, the initial masses of the two materials are measured. Generally, at the start of each experiment, the initial sample weight of 5A zeolite is between 0.50 to 0.55g, while for the MIL-53(Al) is between 0.30 to 0.35g.

3.2.4. Experimental Apparatus

The adsorption equilibrium measurements were carried out with the apparatus shown in Figure (3.5). Figure (3.6) presents the schematic diagram of the experimental setup employed.

Figure 3.5: Pictures of the experimental apparatus used in the equilibrium measurements.

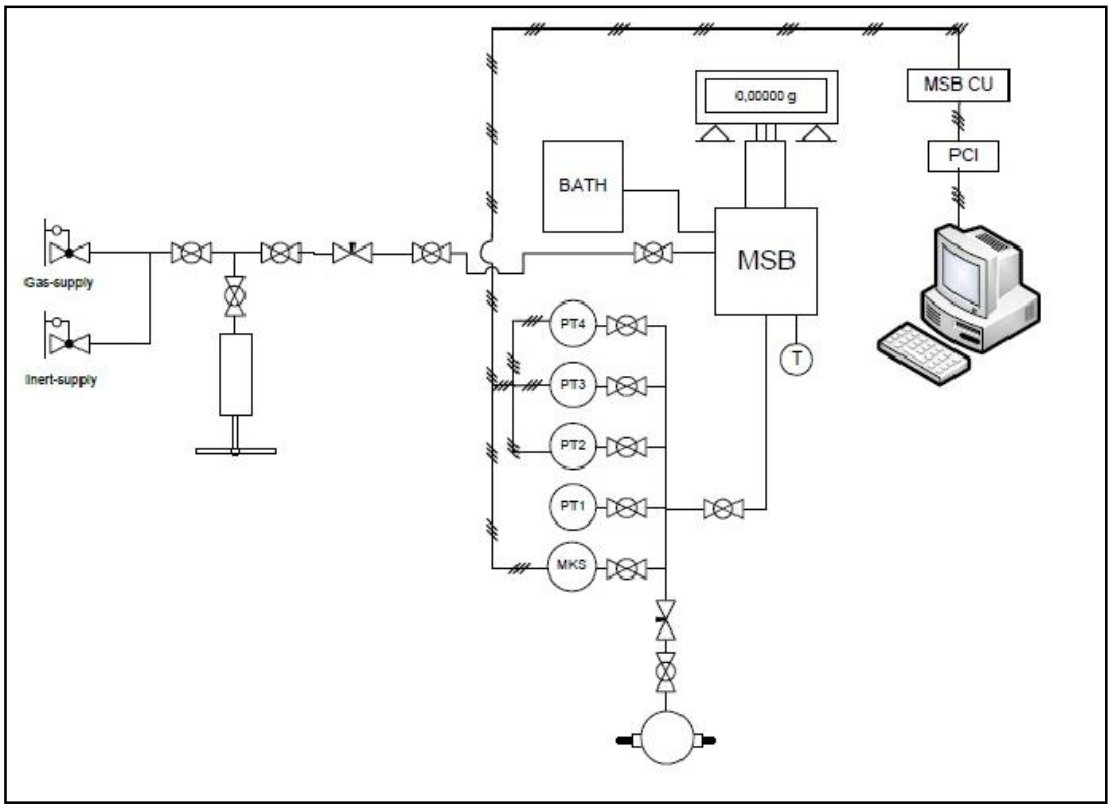

Figure 3.6: Schematic diagram of the experimental apparatus used in the equilibrium.

The adsorbate enters the sealed chamber of the MSB and the pressure is recorded in the output line of the apparatus by four pressure sensors of high precision, each for a given range of pressures. The temperature is measured and controlled within the MSB chamber by a in situ temperature sensor and a thermostatic bath by JULABO. In the experimental unit, all the fittings, stainless steel (*SS*) tubing, valves and instrumentation are 1/8" OD Swagelok type. It is still possible to find a vacuum pump (*EDWARDS*), a compressor (HiP) and a valve assembly coupled to the system. A full description of the equipment used in the facility is in Appendix B.

The temperature variable is the first point of reference on the measurement of an adsorption isotherm, and should be stable throughout the entire experiment. Therefore, the adsorption chamber is kept at the desired temperature by means of a double jacket connected to a thermostatic bath by JULABO with a circulating fluid that has a wide operating range of temperature. Through the signal of a four-wire Pt100 probe, which is inserted directly into the adsorption chamber, it is possible to control the temperature externally to the bath an inside the MSB. It is possible to maintain the temperature of the adsorption chamber within ± 0.01 K of the desired value.

Regarding the pressure, always that the desired pressure was higher to the pressure available by the feed, a manual HiP pressure generator was used.

All the instruments were voltage supplied using typical power suppliers Velleman with variable voltage that covered the range of supply needed for the equipment operation.

The adsorption laboratory apparatus is composed by four main units:

I. - Feed system unit

II. - Gravimetric unit

III. - Temperature measuring and control unit

IV. - Pressure measuring and control system.

I. Feed system unit

This feed unit is composed by a 1/8'' OD *SS* tubing system. It is possible to verify the existence of two feeding lines, one to the inert material and the other for the component in study. It is connected to the feeding line a manual HiP pressure generator, to be used whenever the desired pressure is higher than the pressure available at the feed stream. This system also has a vacuum line connected to a vacuum pump BOC Edwards 5C, that is used whenever it is necessary. Figure (3.7) presents the unit here described as the feed system.

Figure 3.7: Inert, component and vacuum feed streams of the feed system unit.

II. Gravimetric unit

Figure (3.8) shows the gravimetric unit, composed by the magnetic suspension (MSB) with acquisition of weight values in a external SARTORIUS microbalance. Simultaneously, it is held the acquisition of the pressure data with a National Instruments PCI-6023E Board. This acquisition is made through a LabVIEW software (BioCTR) developed internally, where measurements are monitored in order to verify when equilibrium conditions were reached. This is done by means of an equilibrium criteria (mass, pressure and temperature changes).

Figure 3.8: Pictures of the gravimetric unit.

III. Temperature measuring and control unit

With regard to the unit of measurement and control of temperature, this is composed of a thermostatic bath of JULABO, with a circulating fluid, R134a as known as 1,1,1,2-Tetrafluoroethane, that has an operating range between 238.15K and 473.15K [60]. An external temperature four-wire Pt100 probe was used, which is inserted directly into the adsorption chamber and is controlled by the bath, so that it is possible to measure and control temperature with very high accuracy. Figure (3.9) shows the thermostatic bath, as well as the

temperature probe which is in direct contact with the interior of the adsorption chamber, as mentioned above.

Figure 3.9: Pictures of the measuring unit and temperature control.

IV. Pressure measuring and control system

Depending on the system pressure range to be measured, several transducers (PT) were used (see Appendix B), as shown in Figure (3.10). The pressure measurements were performed with the following four sensors:

✓ PT MKS Baratron Type 627D from MKS Instruments Corporation (USA), used in the pressure range of 0-1 bar,

✓ PT PX01C1-150A5T from Omegadyne Inc. (USA), used to measure in the pressure range of 0-10 bar,

✓ PT PX01C1-500A5T from Omegadyne Inc. (USA), used in the pressure range of 0-35 bar,

✓ PT PX03C1-3KA5T from Omegadyne Inc. (USA), used to measure in the pressure range for 0-69/138/207 bar.

The fact that there are four pressure sensors which operate in different pressure ranges, is an asset, since the values obtained for each pressure range has a higher precision.

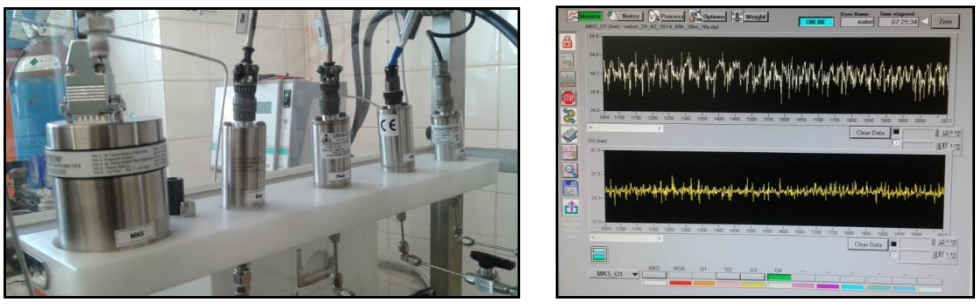

Figure 3.10: Pictures of the measurement and pressure control system.

3.2.5. Experimental Procedure

As mentioned above, the adsorption isotherms were measured using a static gravimetric method. The adsorption equilibrium data, from the series of alkanes, alkenes, CO_2, N_2 and He, on zeolite 5A and on metal organic framework MIL-53(Al) for the temperature range of 303.15 - 373.15K have been measured according to the standard procedures described below:

I. After the pre-treatment of samples, the initial masses of both materials were acquired at 0 bar and constant temperature.

II. After defining the points desired for the single-component adsorption/desorption isotherm to measure, it is then performed a first pressurizing of the adsorption chamber, containing both samples of zeolite 5A and MIL-53(Al), to the desired pressure.

Since there is the opportunity to perform very accurate measurements at very low pressure ranges, a special care was taken in controlling the output pressure of the bottle and the entry of pressure in the adsorption chamber of the MSB.

III. The measurement of the pressure, temperature and weight of the samples are followed, until thermodynamic equilibrium is reached. In order to ensure maximum accuracy, it is assumed that the adsorption equilibrium occurs when the pressure and temperature are constant, and the rate of change in mass of each sample approaches zero usually over 1 hour period.

IV. The values of pressure, temperature, and mass values of the samples are acquired at adsorption equilibrium conditions. The gas pressure in the adsorption chamber is then raised, and the samples are allowed to reach the new equilibrium point of the adsorption isotherm.

V. Once we have determined the low pressure zone of the isotherm with the maximum accuracy possible, the process is repeated in order to determine the remaining required values and obtain a full isotherm adsorption.

Regarding the acquired data, is then important to note that the pressure values are acquired via BioCTR (internally developed software). It should be taken into account, the amount of pressure that is being measured in order to use to the sensor with the most accurate range for the measure in question. Since the acquisition is done continuously, the recorded value corresponds to an average of values which have a rate of change near zero. As to the value of temperature that is measured and controlled using four-wire Pt100 probes and the thermostatic bath by JULABO.

Finally, the weight values of sample masses are registered, performing the taring at the ZP position, in order to make the transition to the MP1 position and then to MP2.

VI. Reached the desired maximum pressure value, the following procedure is the reverse, in other words, depressurization of the adsorption chamber. The determination of each stage of depressurization is followed by equilibrium under isothermal conditions, so as to generate points along the downward path of the isotherm, thus verifying the possible effects of hysteresis. Again, the pressure, temperature and the measured masses are continuously monitored until equilibrium is reached, which is assumed when these three greatnesses present variation rates close to zero.

This procedure is then repeated as many times as necessary until we reach again the pressure value of 0 bar, thus ending the measurement of the points of the intended isotherm.

Chapter IV

4. Experimental Results and Data Analysis

The experimental results obtained with the present study, as well as the analysis of results are presented in this chapter. A detailed study of the adsorption isotherms measured was performed, with the aim of obtaining global adjustments by adsorbate, using the Sips and Toth models [6, 16]

The information provided by the adsorption equilibrium data is fundamental to understand the adsorption processes. The adsorption equilibrium of pure components is essential to understand how those components are adsorbed by the adsorbent phase.

The adsorption isotherms of helium (H_e), nitrogen (N_2), carbon dioxide (CO_2), n-alkanes C_2 to C_4, and ethylene (C_2H_4) were measured for temperatures of 303.15K, 323.15K, 353.15K, and 373.15K, in a pressure range from 0 to 50 bar. Note that, in all cases, points of desorption and adsorption were measured in order to properly define the isothermal under study. Reproducibility of the measurements was checked to ensure data accuracy and feasibility.

4.1. Amount of Gas adsorbed and Buoyancy Forces Account

The gravimetric method, as well as all other conventional methods of adsorption, measures excess adsorption (q_{ex}) as the apparent increase in weight of the sample, corrected for the buoyancy force exerted by the fluid mass [55, 57]. Therefore, in order to determine the absolute adsorption, the corrections of buoyancy forces must be determined.

The buoyancy forces are taken into account to correct the influence of gas density on the measured apparent weight of the sample. The displacements of gas by the sample holder, solid adsorbent, and adsorbed phase, are taken into consideration. The correction due to the

sample holder is obtained with blank experiments performed at different pressures with the empty holder. The buoyancy due to the solid matrix of the adsorbent, which results in an apparent weight loss, is estimated as the product of the skeletal volume of the adsorbent and the gas density. Finally, the buoyancy effect exerted on the adsorbed phase is corrected in order to obtain the absolute adsorption isotherm $q(P,T)$ [6, 57].

The weight m, shown by the balance, results from net force exerted on the sample, and at any time can be described by the following Eq. (4.1) :

$$m = m_h \left(1 - \frac{\rho_g}{\rho_h}\right) + m_s \left(1 - \frac{\rho_g}{\rho_s} + q_{ex}\right) \qquad \textit{Equation (4.1)}$$

where, ρ_h and m_h are the density and mass of the sample holder, respectively, and ρ_s and m_s, in turn, are the mass and density of the sample of adsorbent, respectively, measured after pretreatment of the solid, ρ_g is the density of the bulk gas to the pressure and temperature equilibrium, obtained by the *NIST* database [61], and q_{ex} corresponds to the excess of specific adsorption, expressed by the following expression:

$$q_{ex} = q \left(1 - \frac{\rho_g}{\rho_a}\right) \qquad \textit{Equation (4.2)}$$

q_{ex} gives the amount of gas adsorbed in excess of equilibrium gas that occupies the same volume at the same pressure and temperature, if the gas did not adsorbed in the solid [57], and it is the well-defined thermodynamic quantity, known as the excess adsorption [6]. The ρ_a represents the density of the adsorbed phase.

The blank experiments with an empty holder give the mass and density of the holder from the intercept and slope of the linear decrease of apparent weight with gas density:

$$m = m_h - \frac{m_h}{\rho_h} \rho_g \qquad \textit{Equation (4.3)}$$

The values of m_h and ρ_h, were estimated at 293.78K, and re-checked, using helium (H_e), thus verifying the validity of the measurements. Figure (4.1) and (4.2) show the blank experiments carried out for the two cells used in the present study. Table (4.1) summarizes the blank parameters obtained. It possible to find in Appendix (C.1), Table (C.1), the respective experimental data for these measurements.

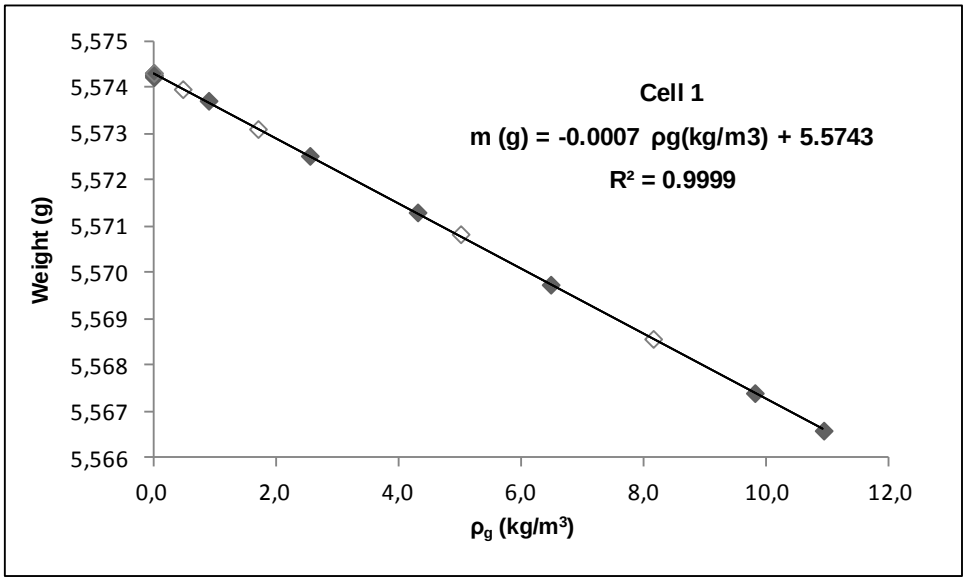

Figure 4.1: Blank calibration of sample holder for Cell 1, used in the adsorption measurements. Filled symbols and open symbols denote adsorption and desorption data, respectively.

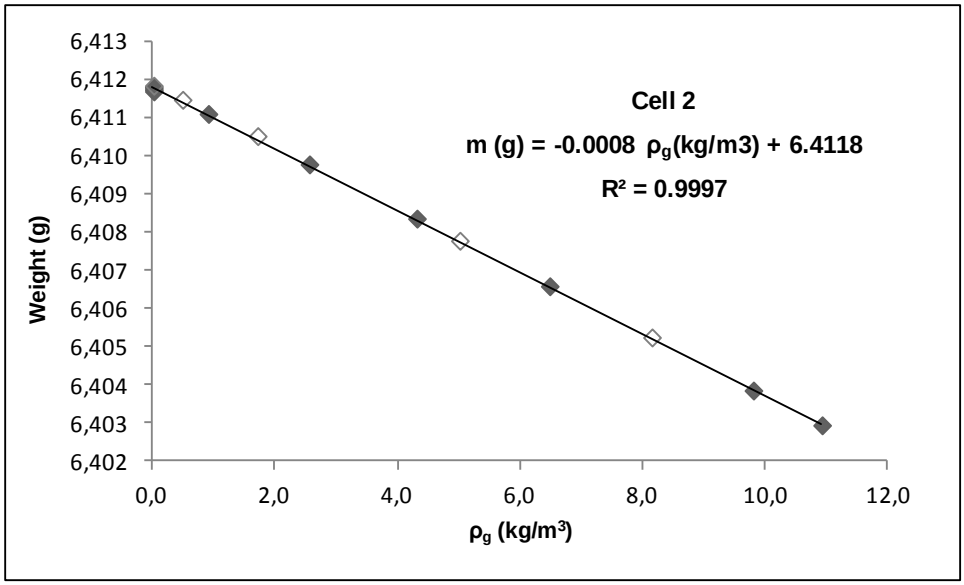

Figure 4.2: Blank calibration of sample holder for Cell 2, used in the adsorption measurements. Filled symbols and open symbols denote adsorption and desorption data, respectively.

Table 4.1: Results of blank calibration of the sample holders used in the adsorption measurements.

Sample holder	Conditions	m_h (g)	V_h (cm^3)	ρ_h (g/cm^3)
Cell 1	293.78K, H_e	5.574	0.703	7.929
Cell 2	293.78K, H_e	6.412	0.808	7.936

On the other hand, adsorption experiments using a non-adsorbing gas, such as helium at high temperature, provide the mass (m_s) and density (ρ_s) of the adsorbent in study, by the equation:

$$m - m_h\left(1 - \frac{\rho_g}{\rho_h}\right) = m_s - \frac{m_s}{\rho_s}\rho_g \qquad \textit{Equation (4.4)}$$

In the present study, it is assumed that helium (H_e) acts as an inert probe that penetrates the entire volume of pores accessible to adsorbents zeolite 5A and MIL-53(Al), without being adsorbed [62]. The experiment was then performed with helium (H_e) for the adsorbents under study, at a temperature of 353.29K and a pressure range from 0 to 35 bar. In Appendix (C.1), Table (C.2) present the experimental findings for the measurements. Figure (4.3) and (4.4), Table (4.2) present the results for the determination of the mass (m_s) and density (ρ_s) for each adsorbent.

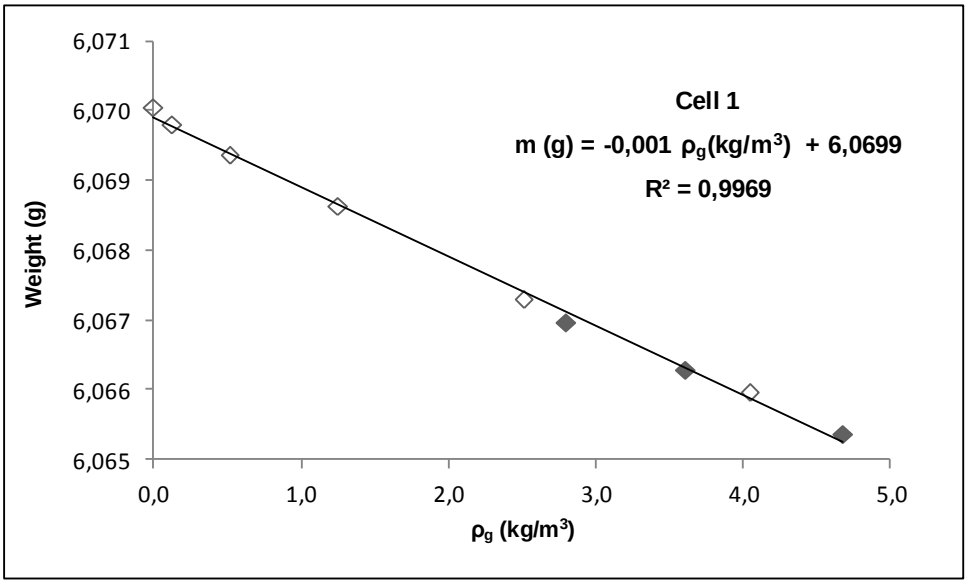

Figure 4.3: Analysis of adsorption equilibrium measurements of the H_e using sample holder no.1. The experiments using a non-adsorbing gas at high temperature provides the mass and density of the zeolite 5A sample. Filled symbols and open symbols denote adsorption and desorption data, respectively.

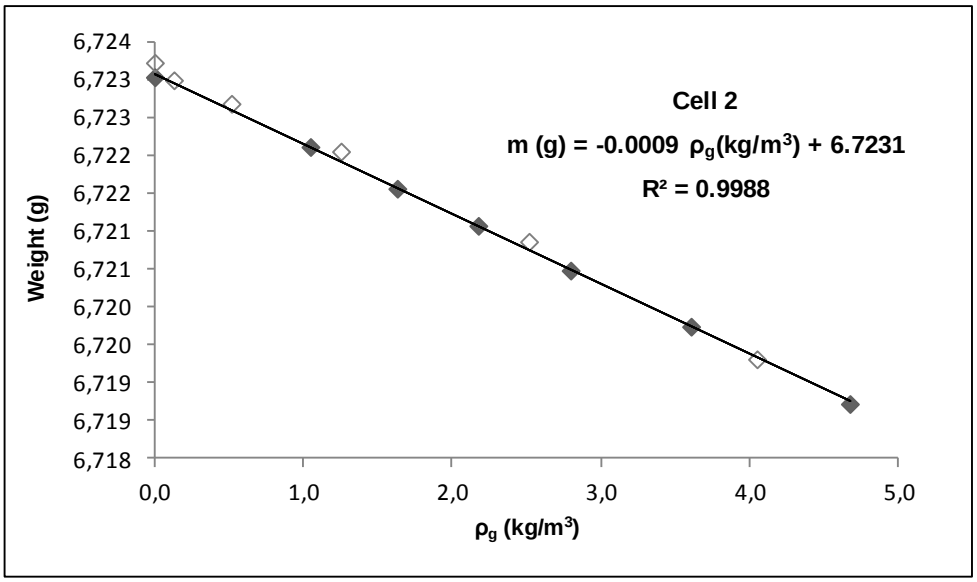

Figure 4.4: Analysis of adsorption equilibrium measurements of the H_e using sample holder no.2. The experiments using a non-adsorbing gas at high temperature provides the mass and density of the MIL-53(Al) sample. Filled symbols and open symbols denote adsorption and desorption data, respectively.

Table 4.2: Results of adsorption equilibrium measurements of the H_e. Cell 1, contains the sample of zeolite 5A, and Cell 2 the sample of MIL-53 (Al).

Sample Cell	Conditions	m_s (g)	V_s (cm^3)	ρ_s (g/cm^3)
Cell 1	353.29K, H_e	0.496	0.290	1.707
Cell 2	353.29K, H_e	0.311	0.142	2.198

Finally, once known the mass values (m_h) and density (ρ_h) of the sample holder, the mass (m_s) and density (ρ_s) of the sample of adsorbent, and (ρ_g) being the density of the bulk gas at each equilibrium point of the isotherm, it is possible to determine the adsorption isotherms of excess, for each of the adsorbents studied, by the equation:

$$m_s q_{ex} = m - m_h\left(1 - \frac{\rho_g}{\rho_h}\right) - m_s\left(1 - \frac{\rho_g}{\rho_s}\right) \qquad \textit{Equation (4.5)}$$

$$\Leftrightarrow\ q_{ex} = \frac{m - m_h}{m_s} - 1 + \left(\frac{1}{\rho_s} + \frac{V_h}{m_s}\right)\rho_g$$

where, (V_h) corresponds to the volume of all moving parts present in the measuring cell (such as the holding basket) that are subject to the buoyancy force exerted by the gas.

Knowing q_{ex} is then possible to determine the absolute amount of adsorption (q_t) from the Eq. (4.6) [6]. Finally, the total amount of is given by:

$$q_t = q_{ex}\left(\frac{\rho_a}{\rho_a - \rho_g}\right) \qquad \textit{Equation (4.6)}$$

In gravimetric adsorption equilibrium measurements for microporous solids, the thermodynamic property most readily determinable is that which Gumma and Talu denote as *net* adsorption [63]. This is an alternative concept where q_{net} is then defined as the total amount of gas present in the measuring cell (with the adsorbent), minus the amount that would be present in the empty cell (without the adsorbent), at the same pressure and temperature conditions [63].

In the case of a gravimetric experiment, parameter q_{net} can be calculated directly from the experimental data since it is independent of the characteristics of adsorbents, such as pore volume, density of the solid matrix and the volume of impervious solid.

Note that *net* values are always lower than the excess and the absolute adsorption, and negative q_{net} value, indicates that the overall density of the cell with the solid is lower than in the empty container. Therefore, by adopting the approach of net adsorption, the only buoyancy forces taken into account, in order to correct the influence of the gas density in relation to the measured apparent weight of the sample, are the displacements of gas by the sample holder, which are obtained with simple blank experiments, performed at different pressures with the empty cell. Therefore, q_{net} is given by the equation:

$$q_{net} = \frac{m - m_s - m_h + V_h\,\rho_g}{m_s} \qquad \textit{Equation (4.7)}$$

where q_{net} is the expression per unit mass of adsorbent, m is the apparent weight of the sample measured by the balance, m_s is the mass of the sample of adsorbent (measured after vacuum degassing and thermal pretreatment), m_h is the mass of the sample holder, V_h is the volume of all moving parts present in the measuring cell (such as the holding basket) that are subject to the buoyancy force exerted by the gas, and ρ_g is the gas density at the pressure and temperature conditions of the experiment.

However, adsorption measurements, are commonly presented in terms of excess adsorption, q_{ex} , which can be positive or negative, and which corresponds to the total amount of gas introduced into the measuring cell minus the amount that remains in the gas phase upon equilibration of the system, in other words, q_{ex} is the amount of gas in excess of the amount that would be present in the same system, at the same pressure and temperature, if the gas did not adsorbed in the solid [57]. The excess amount, q_{ex}, is related to q_{net} trough the equation:

$$q_{net} = q_{ex} - \frac{\rho_g}{\rho_s} \qquad \textit{Equation (4.8)}$$

$$\Leftrightarrow q_{ex} = q_{net} + V_S \rho_S$$

where $V_S = \frac{1}{\rho_S}$ is the specific volume impenetrable to the adsorbate.

The relations between the absolute adsorption (q_t) and the other two adsorption quantities (q_{net} and q_{ex}), are given by:

$$q = q_{ex} + V_p \rho_g = q_{net} + (V_p + V_s) \rho_g \qquad \textit{Equation (4.9)}$$

where, V_p is the accessible pore volume of the adsorbent.

4.1.1. Adsorption Isotherms

After defining the amount adsorbed as *net*, excess and absolute adsorptions, through equations (4.7), (4.8) and (4.9), the experimental adsorption/desorption equilibria data can be represented in Figures (C.1) to (C.39), Appendix (C.2), where are include the Tables (C.3) to (C.12) with the experimental data.

As an example, Figure (4.5) illustrates the net (q_{net}), excess (q_{ex}) and total (q_t) amounts adsorbed for nitrogen at 303.22K for MIL-53(Al). It is possible to see that, approximately, at pressures below 1 bar the differences between net (q_{net}), excess (q_{ex}), and total adsorption (q_t) are negligible. At higher pressures, the three measurements of adsorption start to deviate from each other. For the high pressure region, the net adsorption is the lowest of the three quantities, followed by excess and finally by total adsorption, that is the

highest of the three. These relationships correspond to the whole investigated temperature range, for all the gases in study both in the case of zeolite 5A as MIL-53(Al).

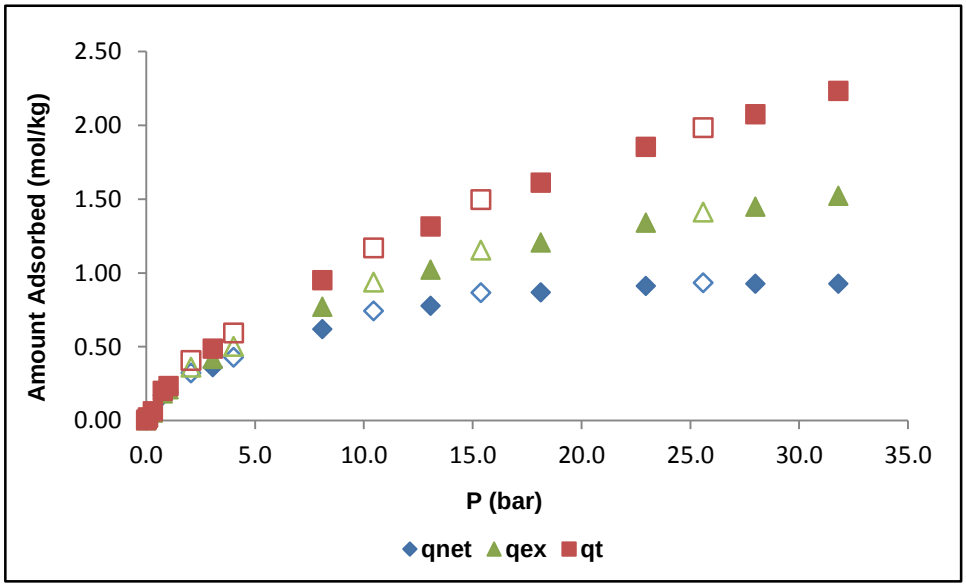

Figure 4.5: Experimental single-component adsorption for N_2 at 303.22K for MIL-53(Al). Filled symbols and open symbols denote adsorptionb and desorption data, respectively.

In order to better understand the results of the adsorption process, it is possible to see Figure (4.6) that shows the adsorption isotherm of carbon dioxide (CO_2) obtained experimentally for the MIL-53(Al). Figure (4.6) shows the total adsorbed amount (mol/kg) in function of pressure (bar), for the temperatures that were measured, 303.16K, 323.18K and 353.37K. In the Appendix (C.2) is possible to find the remaining graphics with this same approach for each gas.

It is then possible to verify that for both adsorbers and for all gases studied, the total adsorbed amount (mol/kg) increases with increasing pressure (bar) until reaching an approximately constant level. The exact location of this level depends on the molecular nature of the adsorbate, being achieved, generally, earlier for lighter molecules. We can also conclude that apparently isotherms obtained are of the Langmuir type (Type I). It is also possible to assert that as expected, at low temperatures the amount adsorbed is larger, since the adsorption is an exothermic process.

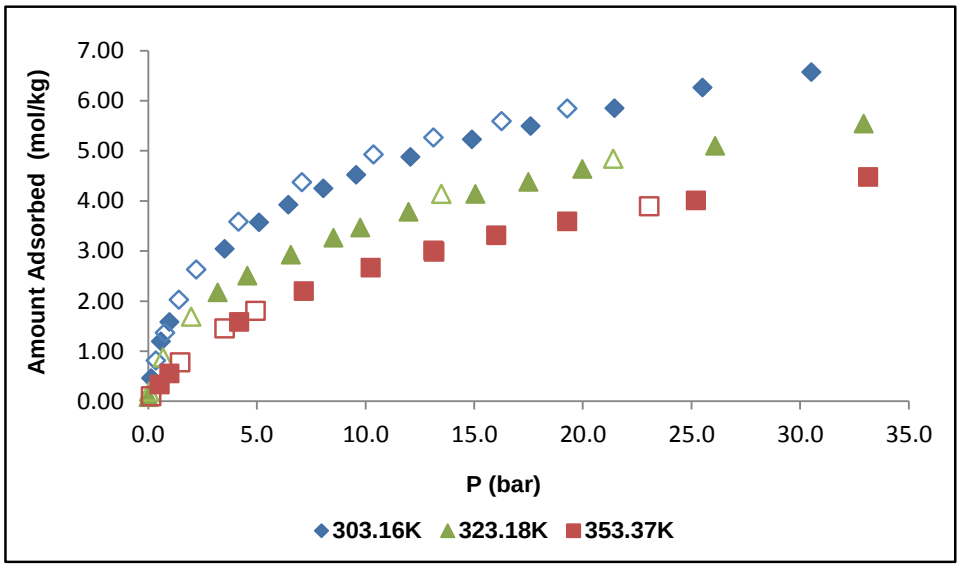

Figure 4.6: Experimental single-component adsorption for CO_2 at 303.16K, 323.18K and 353.37K for MIL-53(Al). Filled symbols and open symbols denote adsorption and desorption data, respectively.

4.2. Theorical Methods

Over the years, there were formulated theoretical models capable to describe the behavior of the isotherms.

Concerning the single-component isotherm models, as the case in study in this work, it is known that the minimum number of parameters required to fit a non-linear isotherm model is three, as in the elementary Langmuir isotherm model [64].

Several are the models of isotherms that have been employed in the literature in the context of the modeling adsorption equilibrium of gases. The Langmuir-Freundlich (LF) (also known as Sips), Toth and Unilan isotherms, among others, are generally popular, because of their ability to model a wide variety of equilibrium data and possess four independent parameters, thereby providing an extra degree of freedom as compared to the simple Langmuir isotherm. The last isotherm model reviewed here is the potential theory either in the form of the Dubinin-Asthakov equation or of the model proposed by S. Ozawa and Ogino [65, 66]. All of these models mentioned here, may be explicitly solved for the solid charge balance.

The results indicate that the Langmuir-Freundlich, Toth and Potential theory isotherm models fit the isotherm data equally well with an average precision error of less than 2%. However, it should be pointed out that there is less certainty as to the correct temperature dependency of the parameters of the Toth isotherm than of the parameters of the other isotherm models. On the other hand, the potential theory has attractive features that make it

especially useful for predicting single-component adsorption equilibrium from a limited set of experimental measurements [26, 65, 67]:

✓ The characteristic curve is temperature independent and therefore, only adsorption equilibrium measurements at one temperature are necessary to obtain the characteristic curve, and this is sufficient to describe the adsorption at all temperatures for the same gas-solid system.

✓ The theory can be generalized if an affinity coefficient is used as a shifting factor to bring the characteristic curves of all gases on the same adsorbent into a single curve. This formulation is perhaps the best attempt to obtain a universal isotherm which adsorption data of one reference gas are extended to other gases.

As such, for the realization of this thesis the models studied were the Langmuir - Freundlich (Sips), Toth and the Potential Theory.

4.2.1. Sips and Toth Isotherm Models

Knowledge of the adsorption equilibrium and the heat of adsorption are essential for proper design of any gas-phase adsorption process [6]. It was then used, individual adjustment at different temperatures for each component.

An extension of the Freundlich equation (also called Sips equation or Langmuir - Frendlich model) and the Toth model were the empirical isotherm equations applied [68].

These isotherm models were considered, since they have been extensively used to model gas adsorption on microporous adsorbents. In order to obtain a global isotherm equation for each component, at different temperatures, the data was fitted using *TableCurve 3D, v.4.0*.

The Sips isotherm can be written as,

$$q_t = q_{ts} \frac{(bP)^{1/n}}{1+(bP)^{1/n}} \qquad \textit{Equation (4.10)}$$

where the parameters obtained are the maximum adsorbed amount (q_{ts}), b is the affinity constant and measures how strong the adsorbate molecule is attracted on to a surface, n is one parameter. The parameter n that characterizes the system adsorbate/adsorbent heterogeneity, is usually greater than 1, and the larger it is, the more heterogeneous is, usually, the system. P is the pressure and q_t is the data of the adsorbed amount.

The affinity constant b, and the parameter n can be written as a function of temperature, by:

$$b = b_0 \exp\left[\frac{Q}{R_g T_0}\left(\frac{T_0}{T} - 1\right)\right] \qquad \textit{Equation (4.11)}$$

$$\frac{1}{n} = \frac{1}{n_0} + \alpha\left(1 - \frac{T_0}{T}\right) \qquad \textit{Equation (4.12)}$$

here the b_0 is the affinity constant at a reference temperature, T_0, n_0 is the parameter n at the same reference temperature and α is a constant parameter. R_g is the ideal gas constant and Q is the heat of adsorption.

Another model used was Toth's. The Toth isotherm can be written as

$$q_t = q_{ts} \frac{bP}{[1 + (bP)^t]^{1/t}} \qquad \textit{Equation (4.13)}$$

where the parameters obtained are the maximum adsorbed amount (q_{ts}), b is the affinity constant defined the same way as for the model of Sips, Eq. (4.11). t is a parameter, P is the pressure and q_t is the data of the amount adsorbed.

The parameter t can be written as a function of temperature, by:

$$t = t_0 + \alpha\left(1 - \frac{T_0}{T}\right) \qquad \textit{Equation (4.14)}$$

here t_0 is the parameter at a reference temperature, T_0, and α is a constant parameter.

4.2.1.1. Isosteric heat of Adsorption

One of the decisive quantities to study in adsorption is heat of adsorption, since the knowledge of this value is very important for the characterization and optimization of an adsorption process [69].

The heat of adsorption is usually estimated from the temperature dependence of the adsorption isotherm. The most relevant thermodynamic variable to describe the heat effects during the adsorption process is the differential isosteric heat of adsorption Q_{st} (kJ/mol), that represents the energy difference between the state of the system before and after the adsorption of a differential amount of adsorbate on the adsorbent surface [6, 57].

For any given isotherm model, the isosteric heat of adsorption, Q_{st}, is typically estimated using the Clausius–Clapeyron equation as

$$Q_{st} = R_g T^2 \left(\frac{\partial \ln P}{\partial T}\right)_q \qquad \textit{Equation (4.15)}$$

It is worth mentioning that there are some simplifying assumptions implicit in this equation (e.g. the adsorbed molar volume is neglected and ideal behavior for the bulk gas phase is assumed), which in most cases, however, have negligible impact on the estimated value of Q_{st}.

Applying Eq. (4.15) to the Sips isotherm model, defined by Eq. (4.10) gives [70]:

$$Q_{st} = Q - \alpha n R_g T_0 \ln(bP) = Q - \alpha n^2 R_g T_0 \ln\left(\frac{\theta}{1-\theta}\right) \qquad \textit{Equation (4.16)}$$

where $\theta = \frac{q_t}{q_{ts}}$ is the fractional loading. The heat of adsorption, Q, equals Q_{st} when $\frac{q_t}{q_{ts}}$ is 0.5.

The isosteric heat of adsorption for the temperature-dependent form of the Toth isotherm model, given by Eq. (4.13), is:

$$Q_{st} = Q - \frac{\alpha R_g T_0}{t}\left[ln\frac{\theta}{(1-\theta^t)^{1/t}} - \frac{ln\theta}{(1-\theta)^t}\right] \qquad \textit{Equation (4.17)}$$

In which the parameter Q equals the isosteric heat of adsorption, Q_{st} when the fractional loading (θ) is zero.

However, since the isosteric heat of adsorption is defined by the amount of heat released when an infinitesimal number of molecules of the fluid is transferred to the adsorbed phase.

It can be considered that $Q_{st} = Q_{sp}(P,T)$ or $Q_{st} = Q_{sp}(T,q)$, but in practice Q_{st} depends very little on temperature, unless it is considering a range of very extensive temperature. In the case of this study, the temperature range 303.15 - 373.15K is sufficiently small, thereby justifying the assumption that Q_{st} is independent of temperature. Let's consider then that $Q_{st} \approx Q_{st}(q)$, in this case it is possible to calculate Q_{st} from the adsorption isotherms obtained experimentally at the three temperatures using the integrated form of the Clausius–Clapeyron, Eq. (4.15) [47, 57]:

$$\ln(P)_{qT} = constant - \frac{Q_{st}}{R_g T} \qquad \textit{Equation (4.18)}$$

Eq. (4.18) shows that $ln(P)$ should vary linearly with $\frac{1}{T}$ for a certain fixed amount of adsorbed amount q_t and that the slope of the straight line gives us the value of $-\frac{Q_{st}}{R_g}$. Is then possible to determine the value of the isosteric heat of adsorption, Q_{st}.

4.2.1.2. Adsorption Results using Sips and Toth approaches

A detailed study of adsorption isotherms, with the aim of obtaining global Adjustments for adsorbate was then performed. Sips and the Toth model were the empirical isotherm equations applied. In order to obtain a global isotherm equation for each component, at different temperatures, the data was fitted using *TableCurve 3D, v.4.0*. This software combines a powerful surface fitter, that has the ability to describe three dimensional empirical data, in this case, the amount adsorbed (mol/kg) and the pressure (bar) are plotted in order to the working temperatures (K). Through the parameters calculated by *TableCurve 3D, v.4.0.* it was possible to determine the best fit for the experimental data.

The average relative error (ARE%) in the estimated amount adsorbed is defined as:

$$ARE\% = \frac{100}{N_{exp}} \sum \frac{|q_{mod} - q_{exp}|}{q_{exp}} \qquad \textit{Equation (4.19)}$$

The average relative error (ARE%) in the estimated amount adsorbed is defined as where the subscripts 'mod' and 'exp' denote estimated values predicted by the model and experimental values, respectively, and N_{exp} is the number of data points. Except for the very low pressure range, where the experimental errors are more pronounced, the low values for the individual and overall ARE's, as well as for the correlation coefficient (R^2), indicate the good quality of the fitting. Therefore, it is fair to state that the adjustments made by Sips and Toth are reasonably accurate over a broad range of experimental conditions for the adsorption of the various adsorbates on the adsorbents considered in this study.

The dependencies b, n and t in temperature were considered in the models. The Table (4.3) and (4.4) show the best results obtained with the two equations of isothermal type, in the fit of the data, performed to the MOF MIL-53(Al) and the 5A zeolite, respectively, for the gases presented.

Figures (4.7) – (4.18) show the fitting degree between these equations and the experimental data obtained. The fit is in excellent agreement with the experimental points, describing the data of the components on the MIL-53(Al), as in zeolite 5A the samples, with good success. The coefficient R^2 is higher than 0.99 in all cases.

Table 4.3 : Parameters obtained from the data fitting with the Sips and Toth models for the MIL-53(Al).

Parameter	Metal-Organic Framework: MIL-53(Al)							
	N_2		CO_2		C_2H_6		C_2H_4	
	Sips	Toth	Sips	Toth	Sips	Toth	Sips	Toth
q_{ts} (mol/kg)	5.931	6.173	9.039	9.285	9.358	8.989	6.159	6.566
b_0 (bar^{-1})	0.017	0.043	0.113	0.294	0.102	3.249	0.268	1.116
α	0.199	0.100	0.142	0.010	0.299	0.0500	0.094	0.085
n_0 or t_0	1.207	0.567	1.437	0.617	2.259	0.370	1.603	0.497
Q (kJ/mol)	12.04	14.19	24.99	24.94	31.15	32.17	27.55	25.00
T_0 (K)	303.22	303.22	303.16	303.16	303.16	303.16	303.18	303.18
Are (%)	5.511	9.705	5.675	8.676	6.034	9.846	8.469	10.516

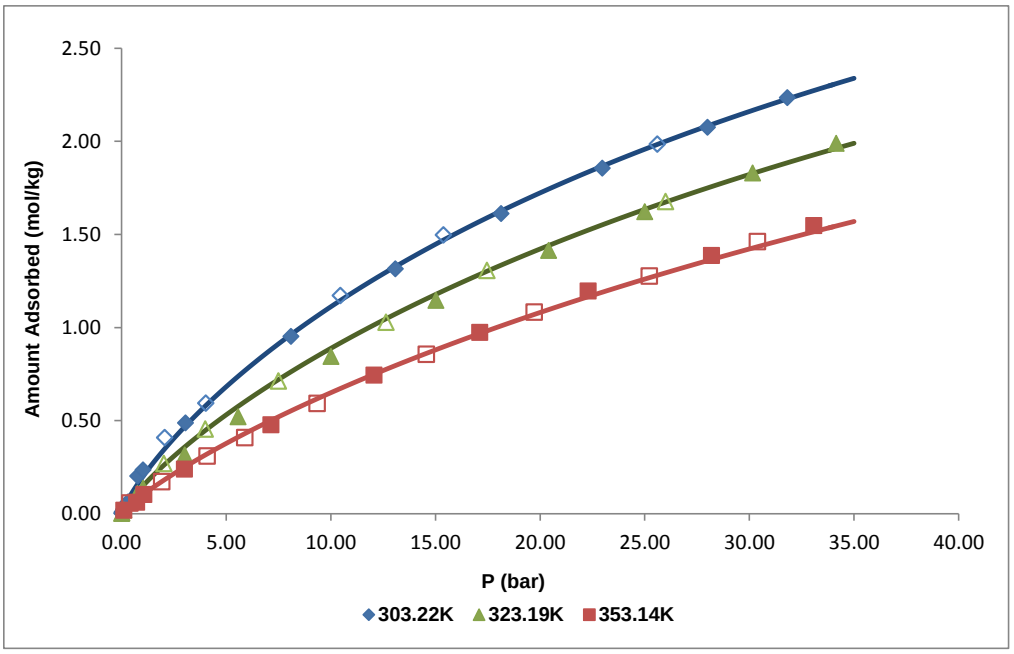

Figure 4.7: Global fitting of the experimental N_2 adsorption data in MIL-53(Al) by the Sips isotherm. Filled symbols and open symbols denote adsorption and desorption data, respectively.

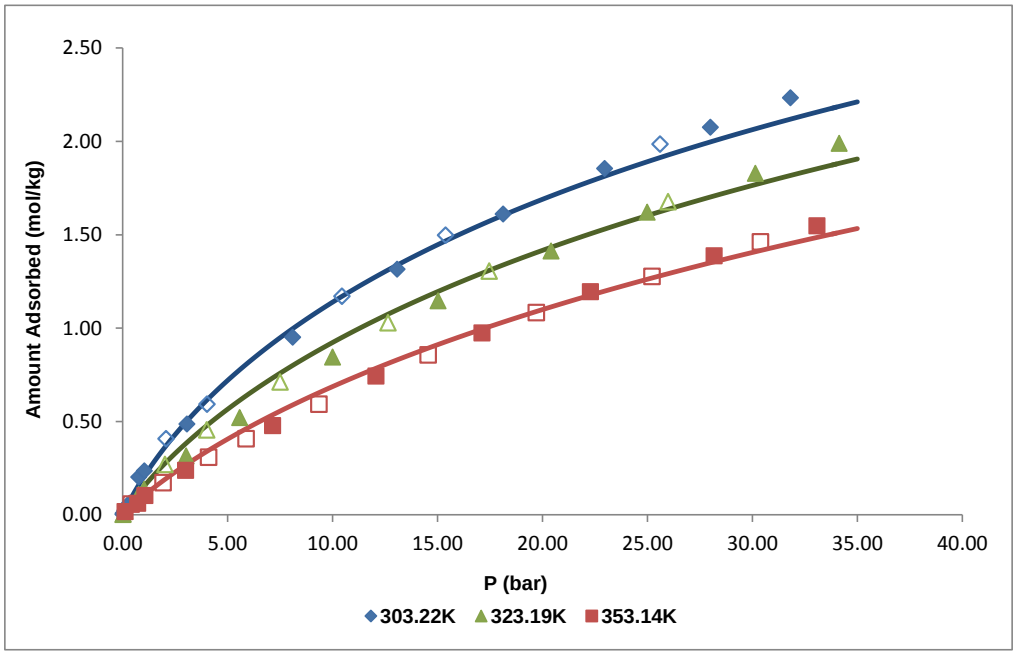

Figure 4.8: Global fitting of the experimental N_2 adsorption data in MIL-53(Al) by the Toth isotherm. Filled symbols and open symbols denote adsorption and desorption data, respectively.

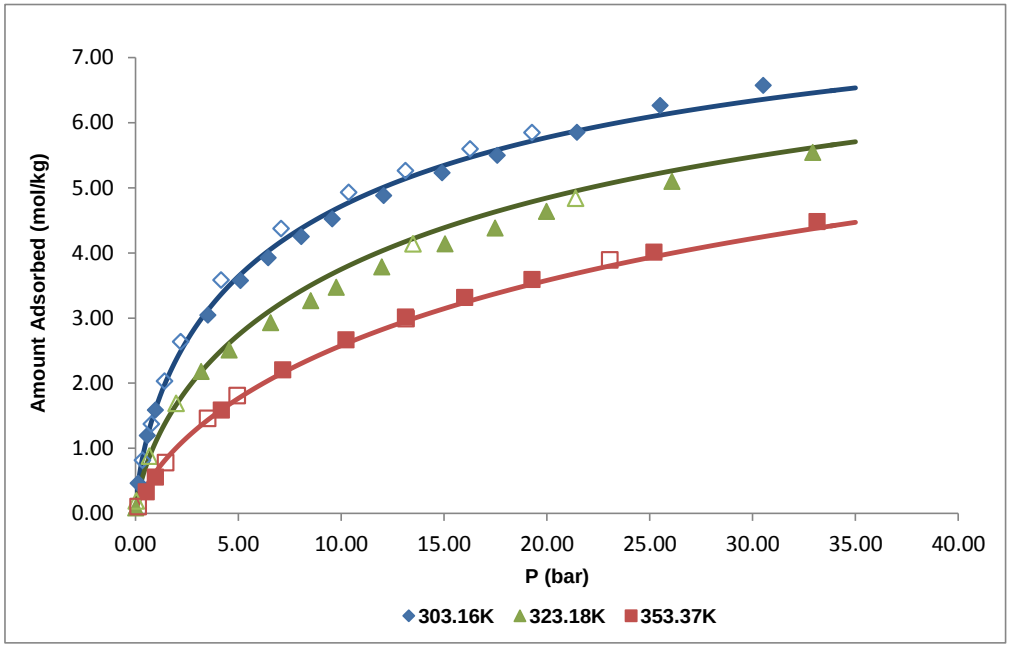

Figure 4.9: Global fitting of the experimental CO_2 adsorption data in MIL-53(Al) by the Sips isotherm. Filled symbols and open symbols denote adsorption and desorption data, respectively.

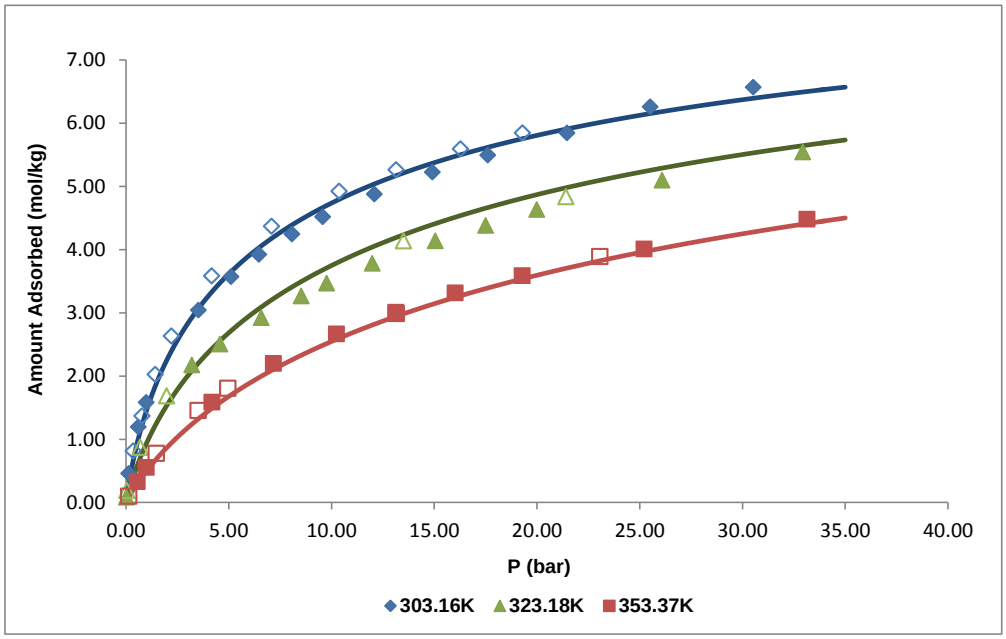

Figure 4.10 : Global fitting of the experimental CO_2 adsorption data in MIL-53(Al) by the Toth isotherm. Filled symbols and open symbols denote adsorption and desorption data, respectively.

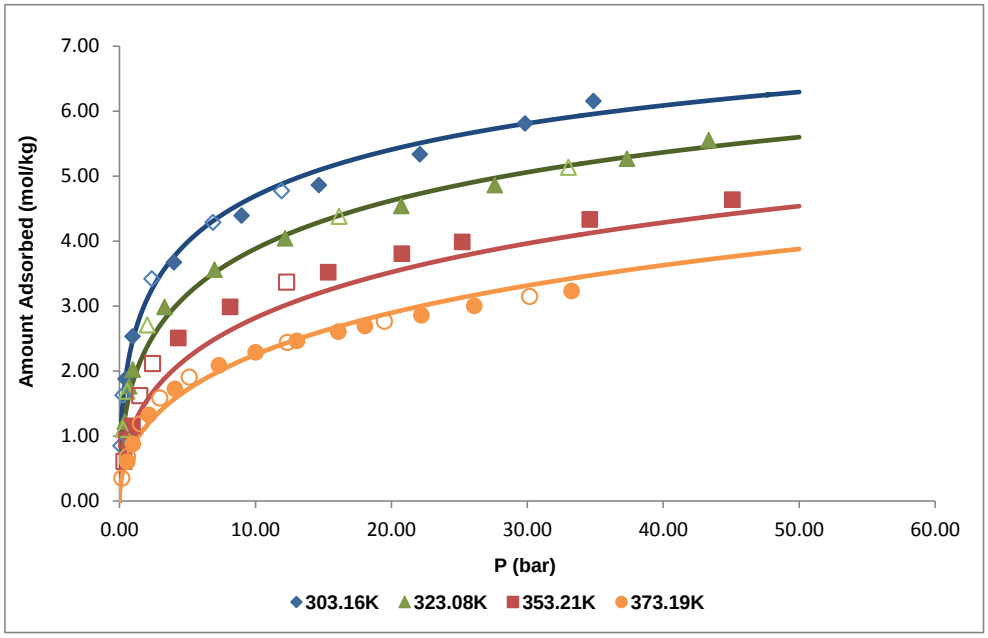

Figure 4.11: Global fitting of the experimental C_2H_6 adsorption data in MIL-53(Al) by the Sips isotherm. Filled symbols and open symbols denote adsorption and desorption data, respectively.

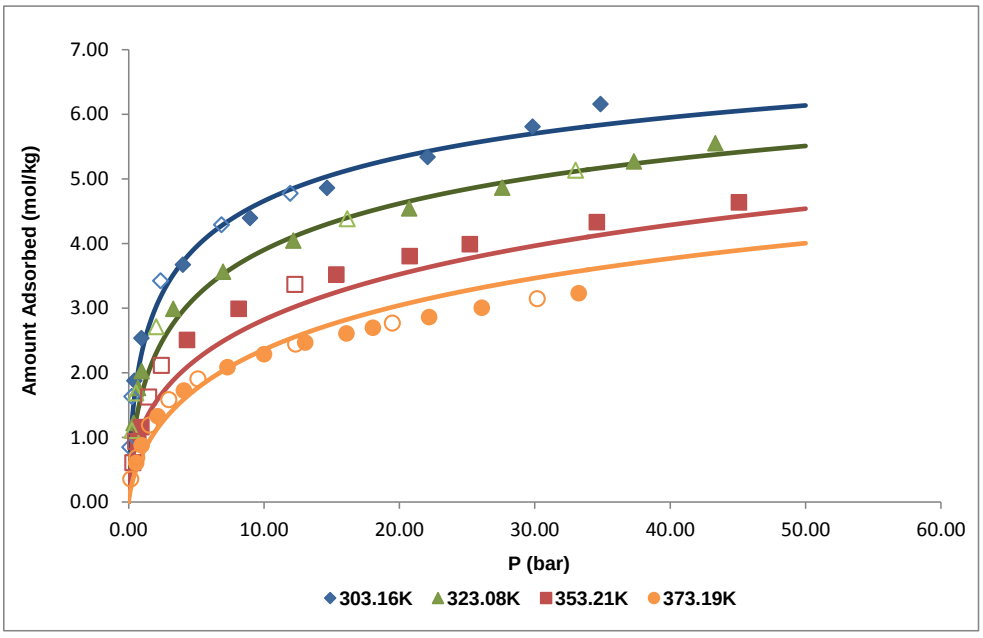

Figure 4.12 : Global fitting of the experimental C_2H_6 adsorption data in MIL-53(Al) by the Toth isotherm. Filled symbols and open symbols denote adsorption and desorption data, respectively.

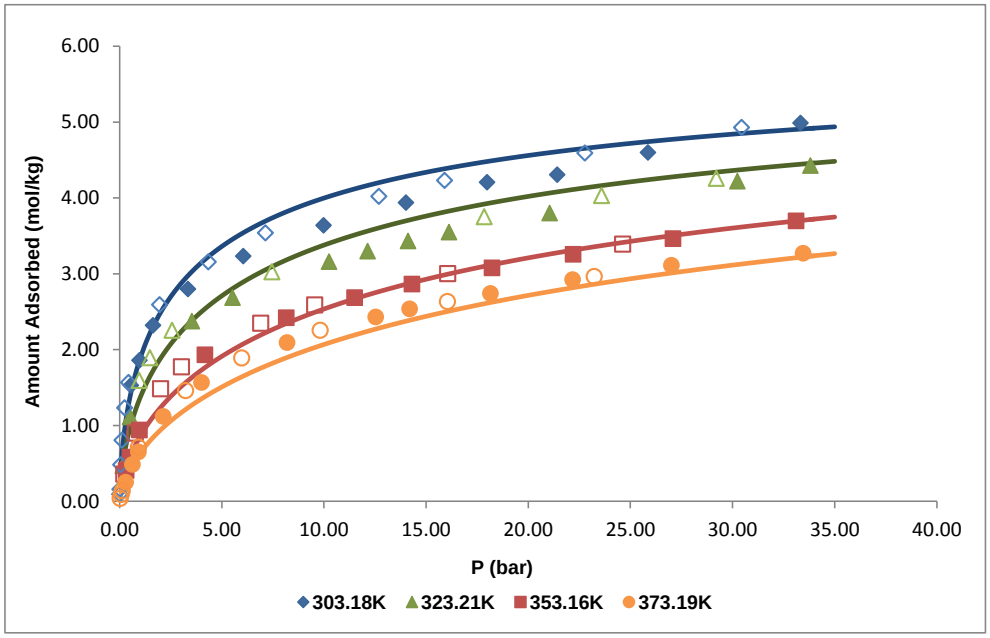

Figure 4.13: Global fitting of the experimental C_2H_4 adsorption data in MIL-53(Al) by the Sips isotherm. Filled symbols and open symbols denote adsorption and desorption data, respectively.

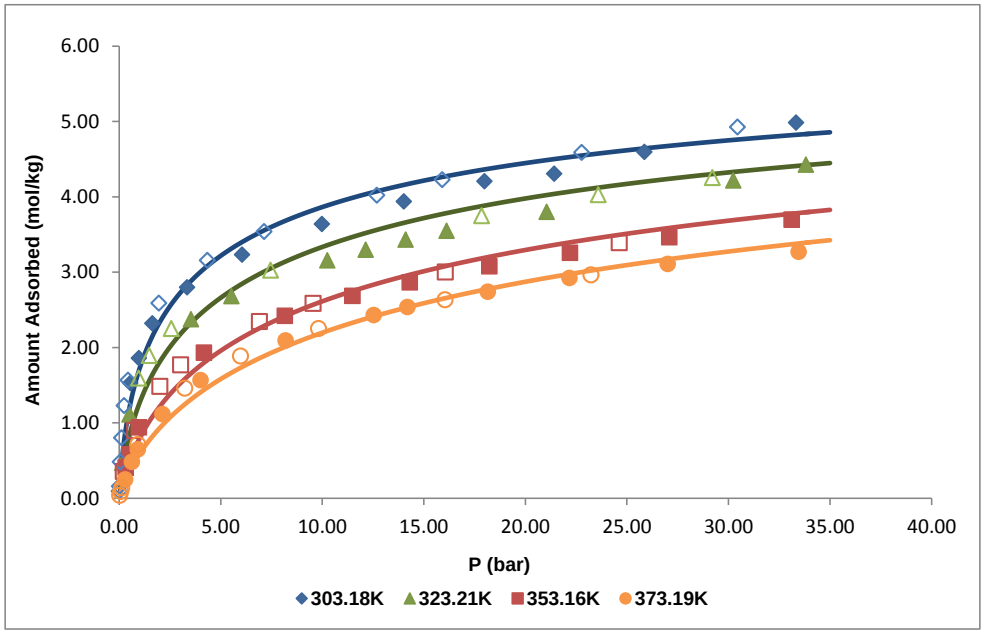

Figure 4.14: Global fitting of the experimental C_2H_4 adsorption data in MIL-53(Al) by the Toth isotherm. Filled symbols and open symbols denote adsorption and desorption data, respectively.

Table 4.4 : Parameters obtained from the data fitting with the Sips and Toth models for the zeolite 5A.

Parameter	Zeolite 5A			
	CO_2		C_2H_4	
	Sips	Toth	Sips	Toth
q_{ts} (mol/kg)	5.861	5.490	4.369	4.160
b_0 (bar^{-1})	2.321	9.998	0.742	5.559
α	0.085	0.095	0.099	0.019
n_0 or t_0	2.533	0.493	2.378	0.462
Q (kJ/mol)	38.99	33.92	29.52	26.00
T_0 (K)	303.16	303.16	323.21	323.21
Are (%)	5.993	8.969	4.075	10.799

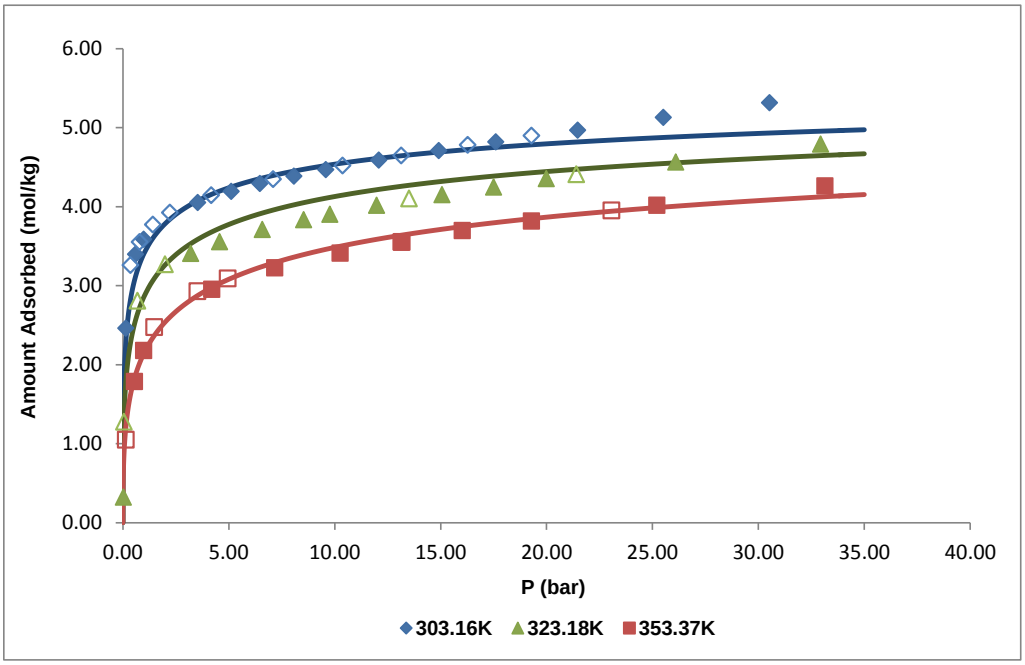

Figure 4.15: Global fitting of the experimental CO_2 adsorption data in zeolite 5A by the Sips isotherm. Filled symbols and open symbols denote adsorption and desorption data, respectively.

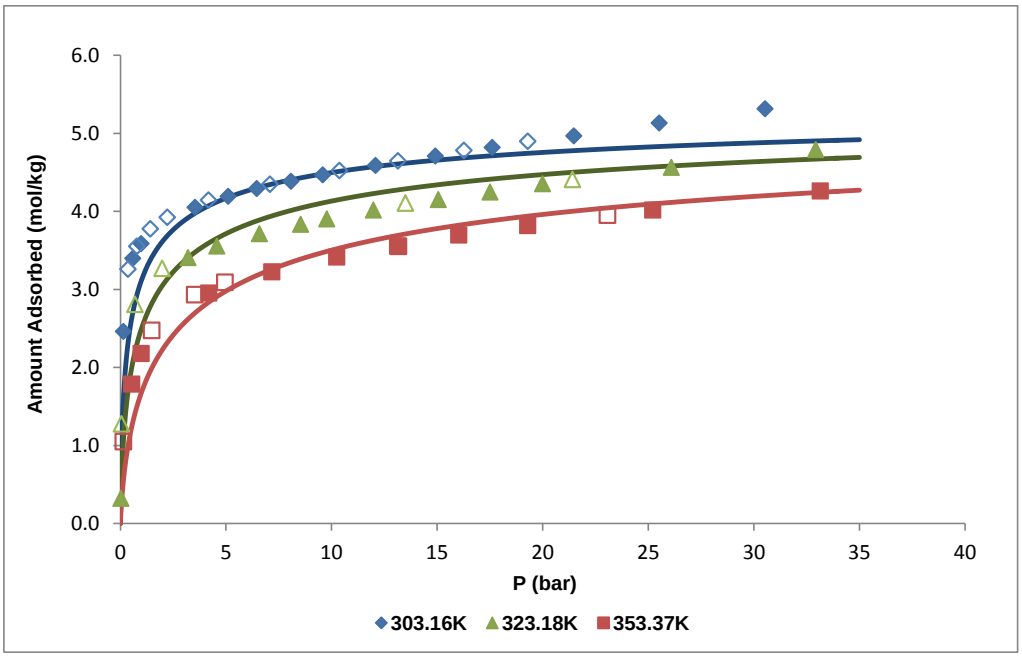

Figure 4.16: Global fitting of the experimental CO_2 adsorption data in zeolite 5A by the Toth isotherm. Filled symbols and open symbols denote adsorption and desorption data, respectively.

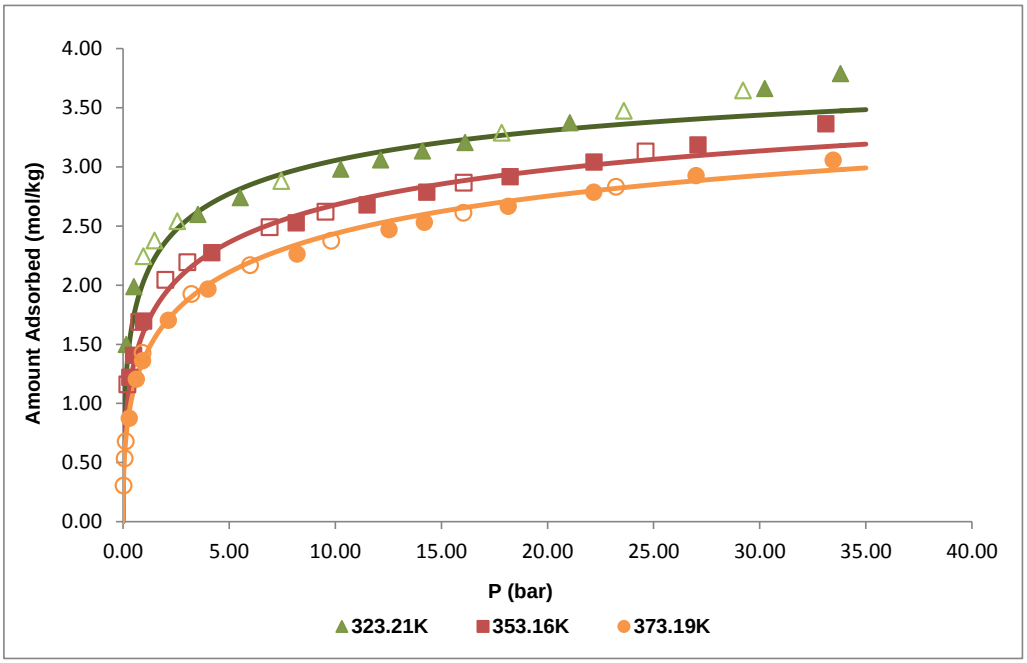

Figure 4.17: Global fitting of the experimental C_2H_4 adsorption data in zeolite 5A by the Sips isotherm. Filled symbols and open symbols denote adsorption and desorption data, respectively.

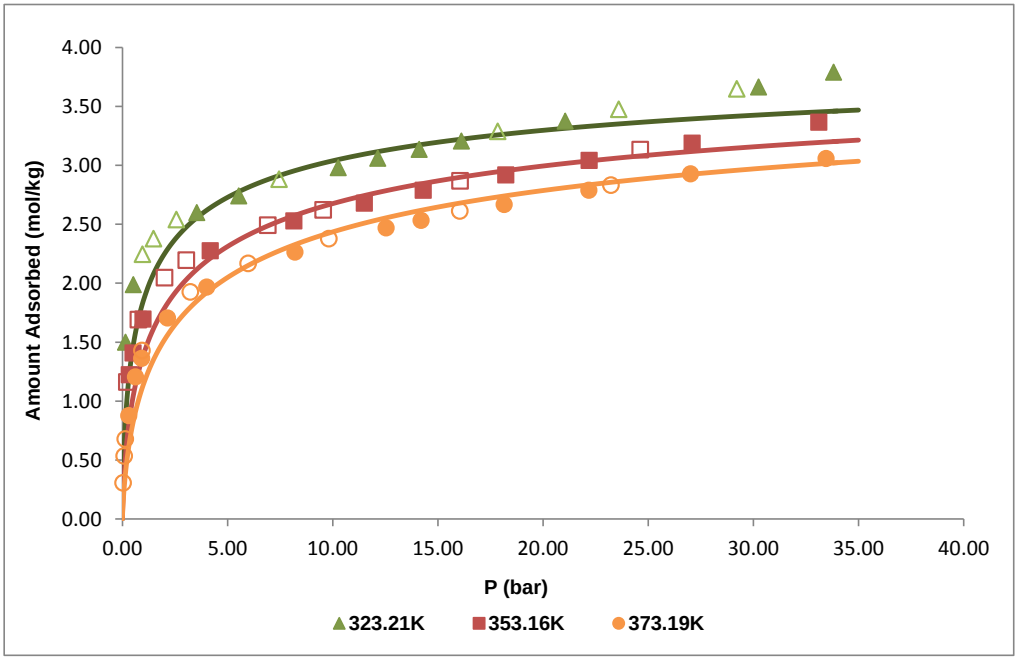

Figure 4.18: Global fitting of the experimental C_2H_4 adsorption data in zeolite 5A by the Toth isotherm. Filled symbols and open symbols denote adsorption and desorption data, respectively.

In the case of MIL-53(Al), the results obtained by global adjustments made to the nitrogen (N_2), carbon dioxide (CO_2) [71, 72, 51, 53] are consistent with the literature, since for ethane (C_2H_6) and ethylene (C_2H_4), although data are scarce in the literature, we can say that the results obtained are consistent [73, 74, 75]. For the MIL-53(Al), the global settings, indicate that the one that best fits the experimental measurements, is the Sips model, because the value of mean relative error is considerably lower compared with the adjustment made by Toth model.

Regarding 5A zeolite, to the global adjustments performed to carbon dioxide (CO_2) and ethylene (C_2H_4), the results obtained are in accordance with the literature [76, 41]. We can still say that in both gases, the adjustment by the Sips model proved best, with a mean value of lower relative error compared with the adjustment made by the Toth model.

Comparing the adsorption capacity of MIL-53(Al) and 5A zeolite is clearly visible that the MIL-53(Al) presents a higher adsorption capacity. However in both adsorbents is verifiable the preferential adsorption capacity for carbon dioxide, which is a good indication that these materials have a strong potential in the capture and storage of carbon dioxide, in the purification of biogas or purification of methane from natural gas.

The excellent agreement between the fittings of both models and the experimental data demonstrates that these isotherm models can be confidently employed to accurately correlate the adsorption equilibria of the all adsorbates.

In Appendix (D.1), Figures (D.1) to (D.12), are found the 3D images, taken directly from the *software* used to perform the global settings, *TableCurve, v.4.0*.

Figures (4.19) - (4.24), compare the single-component adsorption isotherms at 303.15K for CO_2/N_2, CO_2/CH_4, and C_2H_6/C_2H_4, respectively. The results are represented both in an absolute scale and also in log-log scale to show the adsorption behavior in the low pressure range. The symbols represent the experimental points (the filled symbols represent adsorption and the empty symbols desorption) and the lines represent the Sips model fitting.

Figures (4.19) and (4.20) compare the adsorption isotherms of pure CO_2 and N_2 at 303.15K on MIL-53(Al). It can be seen that CO_2 is much more adsorbed than nitrogen (N_2) for all the pressure range studied.

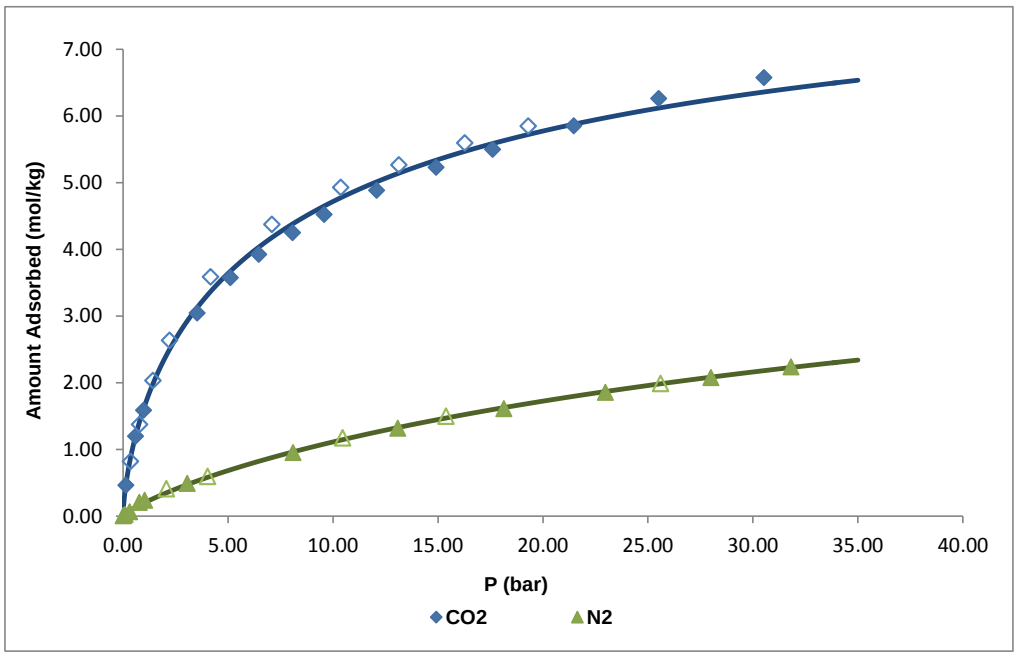

Figure 4.19: Single-component adsorption isotherms for CO_2 and N_2 at 303.15K. Symbols denote experimental data (filled symbols and open symbols denote adsorption and desorption data, respectively) and lines are the predictions from the Sips isotherm model.

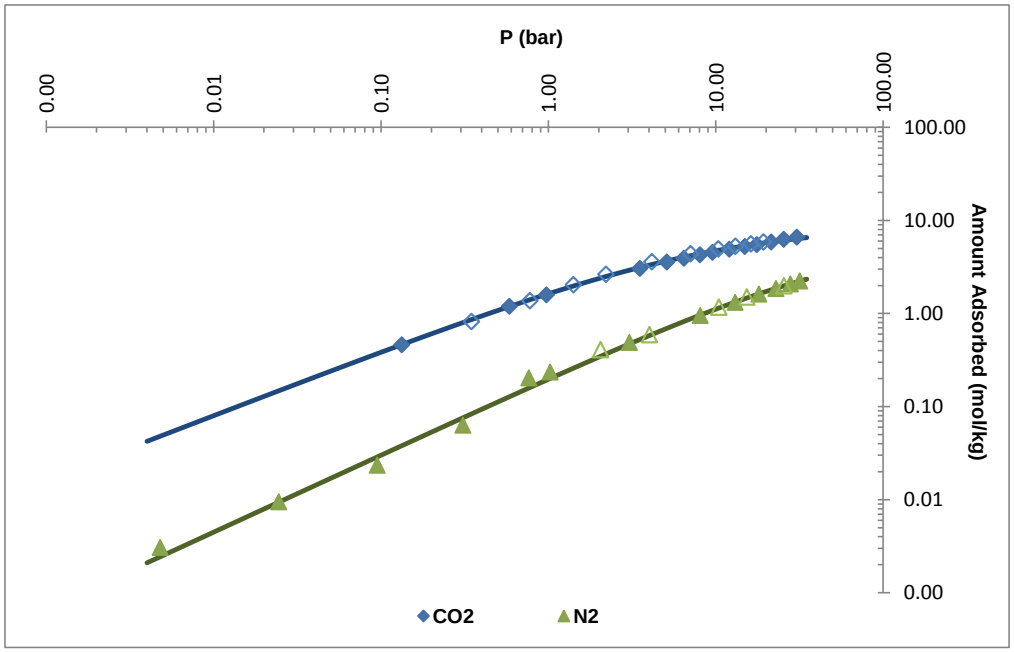

Figure 4.20: Graph in log scale of the single-component adsorption isotherms for CO_2 and N_2 at 303.15K. Symbols denote experimental data (filled symbols and open symbols denote adsorption and desorption data, respectively) and lines are the predictions from the Sips isotherm model.

In Figures (4.21) and (4.22) it can be seen the comparison between the pure isotherms of CO_2 and CH_4 at 303.15K on MIL-53(Al). It should be noted that the CH_4 data was measured previously by Lyubchyk *et al* [47]. The represented results show that CO_2 is, once more, the more adsorbed species although the difference between the adsorption capacity of the adsorbent towards CO_2 and CH_4 is smaller than between CO_2 and N_2. This means that the adsorbent is more selective for the CO_2/N_2 separation than for CO_2/CH_4.It was concluded that carbon dioxide is the most adsorbed component.

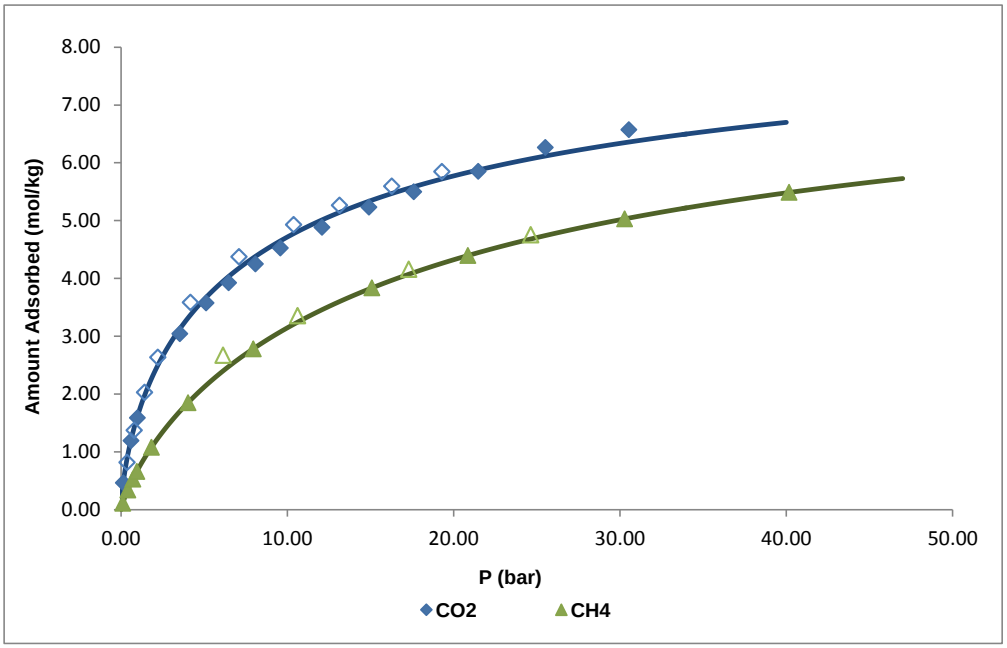

Figure 4.21: Single-component adsorption isotherms for CO_2 and CH_4 at 303.15K. Symbols denote experimental data (filled symbols and open symbols denote adsorption and desorption data, respectively) and lines are the predictions from the Sips isotherm model.

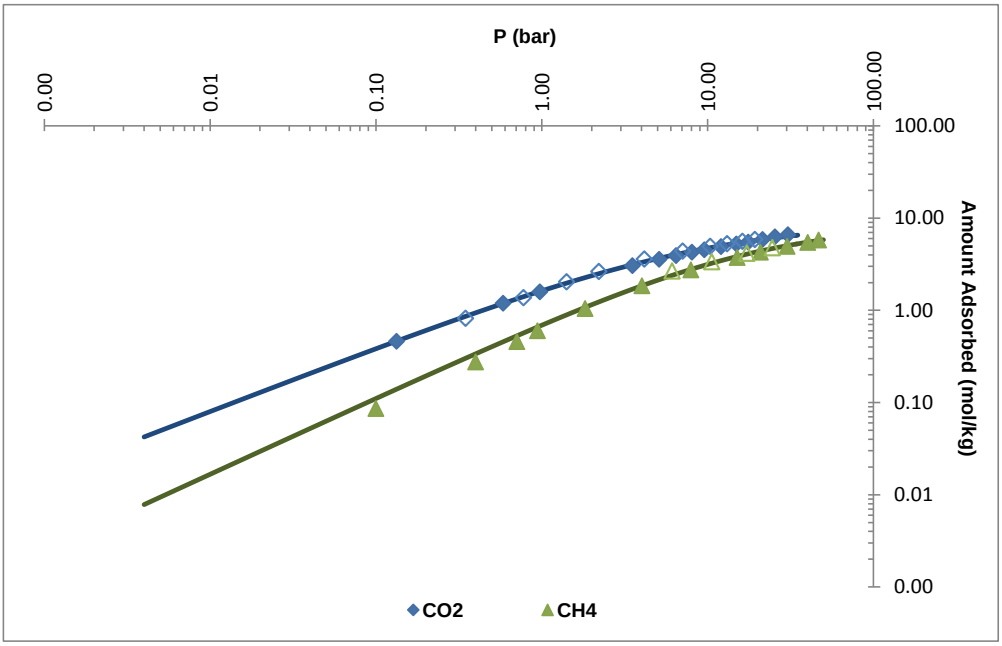

Figure 4.22: Graph in log scale of the single-component adsorption isotherms for CO_2 and CH_4 at 303.15K. Symbols denote experimental data (filled symbols and open symbols denote adsorption and desorption data, respectively) and lines are the predictions from the Sips isotherm model.

The adsorption isotherms of C_2H_6 and C_2H_4, at 303.15K over MIL-53(Al) are represented in Figures (4.23) and (4.24). The results indicate that ethane (C_2H_6) is the most adsorbed component, although at low pressures (below 1 bar) the adsorbed amounts were found to be very similar for the two gases.

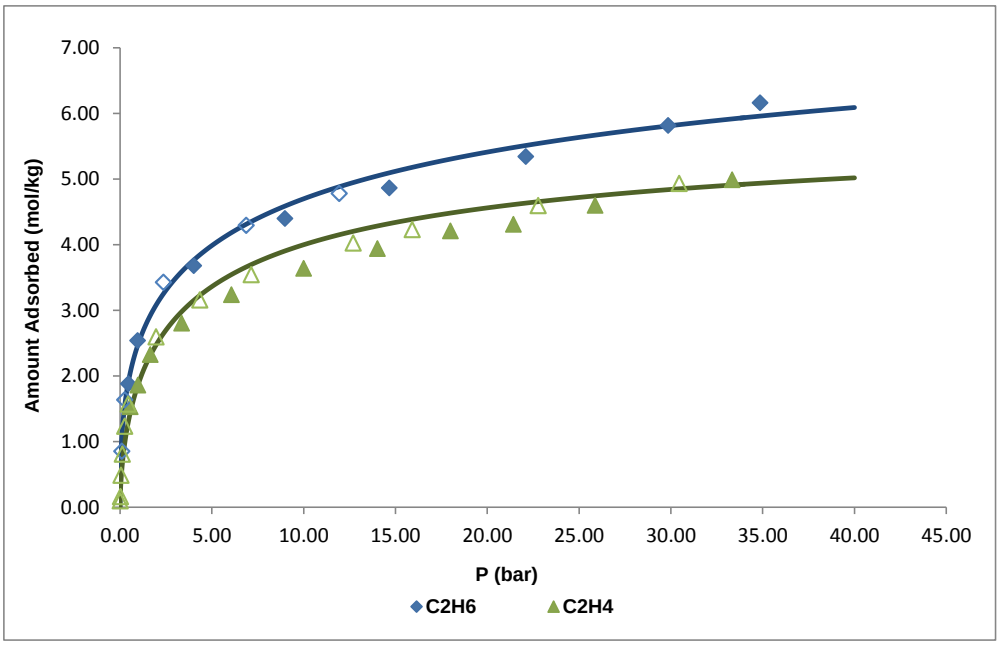

Figure 4.23 : Single-component adsorption isotherms for C_2H_6 and C_2H_4 at 303.15K. Symbols denote experimental data (filled symbols and open symbols denote adsorption and desorption data, respectively) and lines are the predictions from the Sips isotherm model.

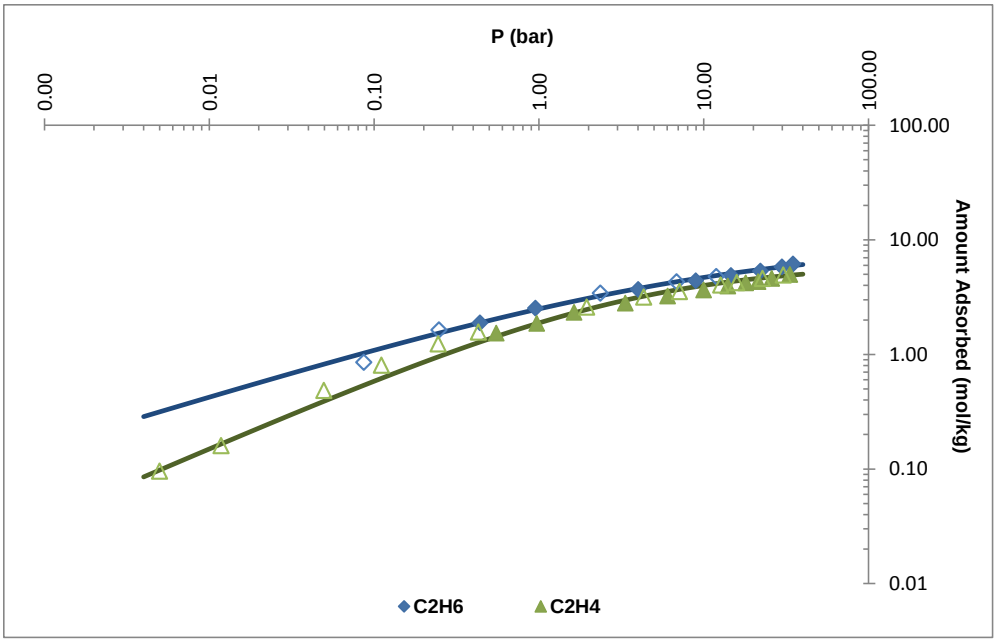

Figure 4.24: Graph in log scale of the single-component adsorption isotherms for C_2H_6 and C_2H_4 at 303.15K. Symbols denote experimental data (filled symbols and open symbols denote adsorption and desorption data, respectively) and lines are the predictions from the Sips isotherm model.

The equilibrium selectivity factor, $\alpha_{i/j}$, was also determined by:

$$\alpha_{i/j} = \frac{q_i}{q_j} \qquad \textit{Equation (4.19)}$$

Figure (4.25) presents the selectivity of CO_2/N_2 (blue line) and CO_2/CH_4 (green line), at 303.15 K, as a function of pressure. It is verified that both selectivities decreases with the increase of pressure. Also, it can be observed that the CO_2/N_2 selectivity is higher than the CO_2/CH_4 selectivity for all the pressure range studied.

Figure (4.26) shows the selectivity of C_2H_6/C_2H_4 at 303.15, as a function of pressure. The results show that the selectivity decreases with pressure, and the selectivity values are lower than for the CO_2/N_2 and CO_2/CH_4 pairs.

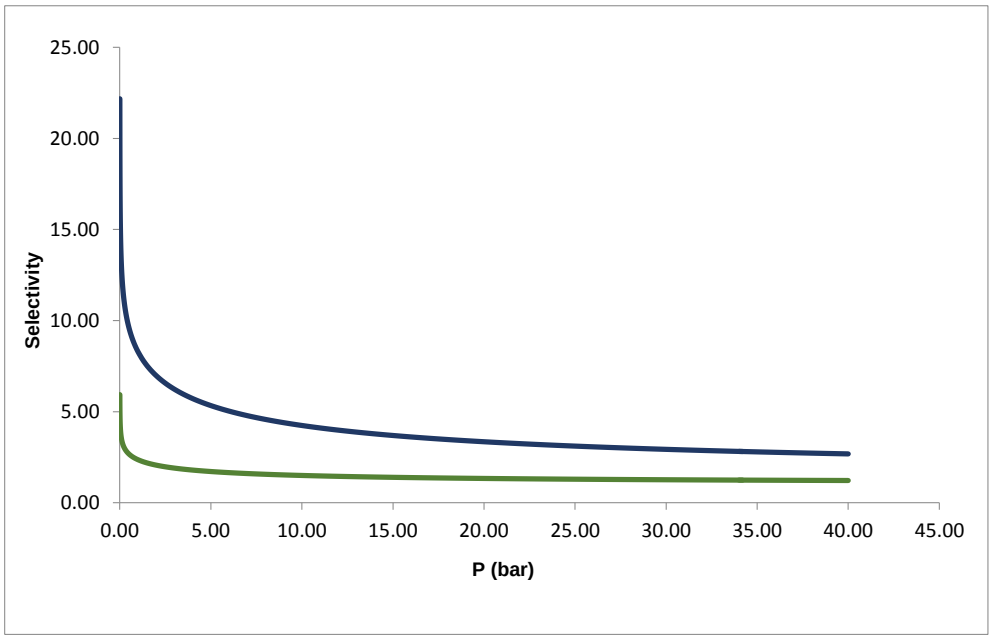

Figure 4.25: Selectivity of CO_2/N_2 (blue line) and CO_2/CH_4 (green line) as a function of pressure at 303.15K.

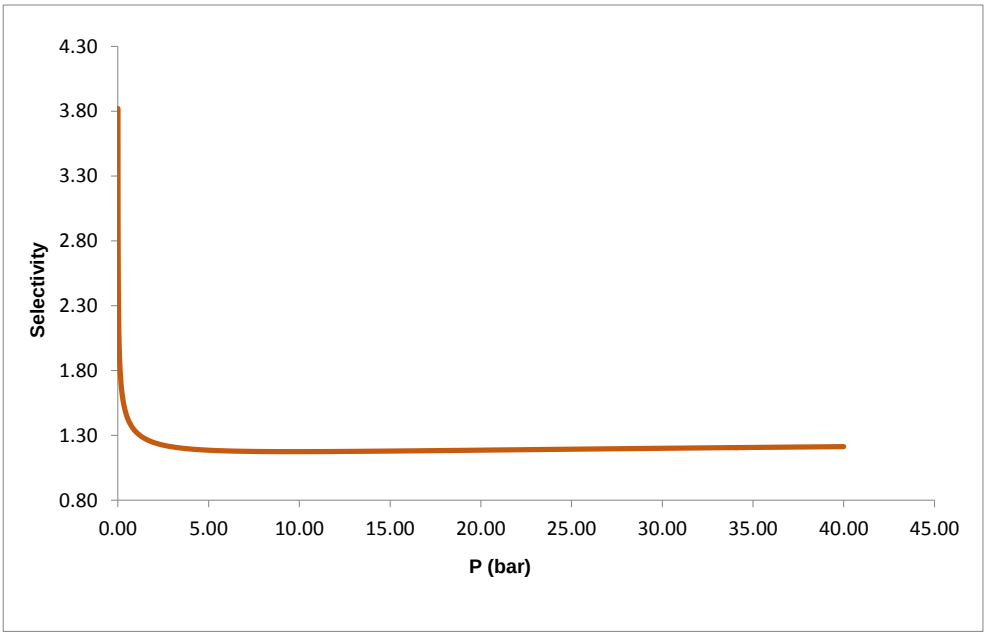

Figure 4.26: Selectivity of C_2H_6/C_2H_4 as a function of pressure at 303.15K.

As already mentioned, the isosteric, Q_{st} heat is a quantity of great importance for the characterization and optimization of adsorption processes.

The isosteric heats were then determined using the two models studied here, Sips and Toth, taking into account the temperature dependence. However, it was also taken into account the assumption that the range of working temperatures was small enough to consider the Q_{st} independent of temperature. Therefore, Figures (4.27) - (4.32) have a isosteric heat as a function of the fractional loading (θ) for both MIL-53(Al) and for zeolite 5A and for each of the adsorbates. The Q_{st} calculated by Sips model is represented for each of the temperature at which the adsorption equilibrium were determined (303.15 - 373.15K). The most salient, black, circular shaped symbols, represent the calculated Q_{st} ,considering that the range of temperatures (303.15 - 373.15K) is small enough to assume that Q_{st} is independent of temperature [47, 57].

Appendix (D.2) in Figures (D.13) - (D.18) are shown the variation of the isosteric heats as a function of the fractional loading (θ), considering the model Toth and Q_{st} temperature dependent, for each gas, at temperatures at which adsorption equilibria were measured. Each symbol corresponds to the value of Q_{st} calculated for the pressure and temperature of a point on the experimental adsorption isotherms.

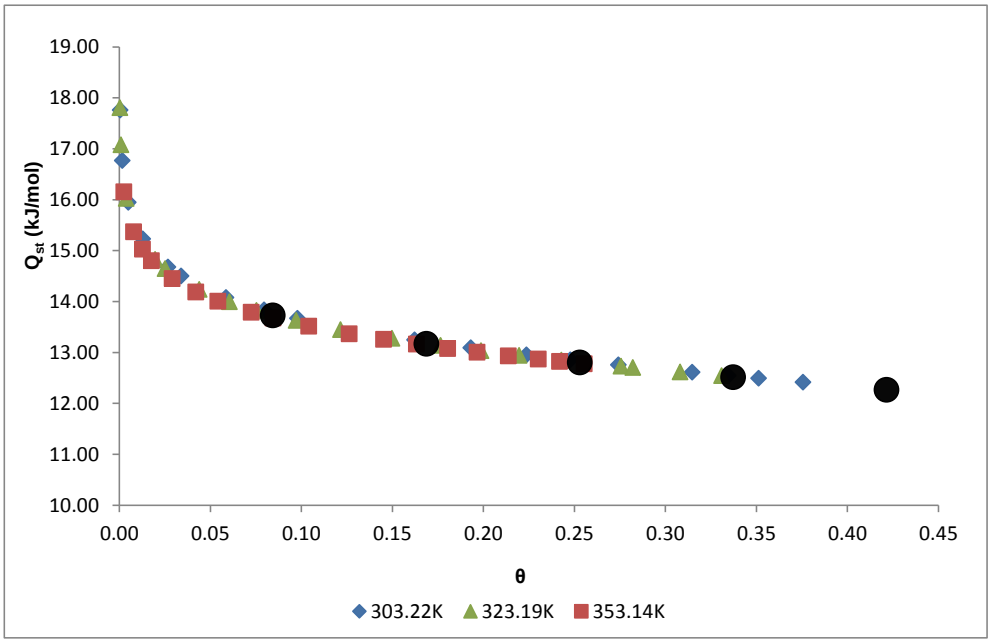

Figure 4.27: Isosteric heats of adsorption for N_2 in MIL-53(Al), as a function of loading, determined from the temperature dependence of the Sips isotherm model. The symbols in black represent the Q_{st} independent of temperature.

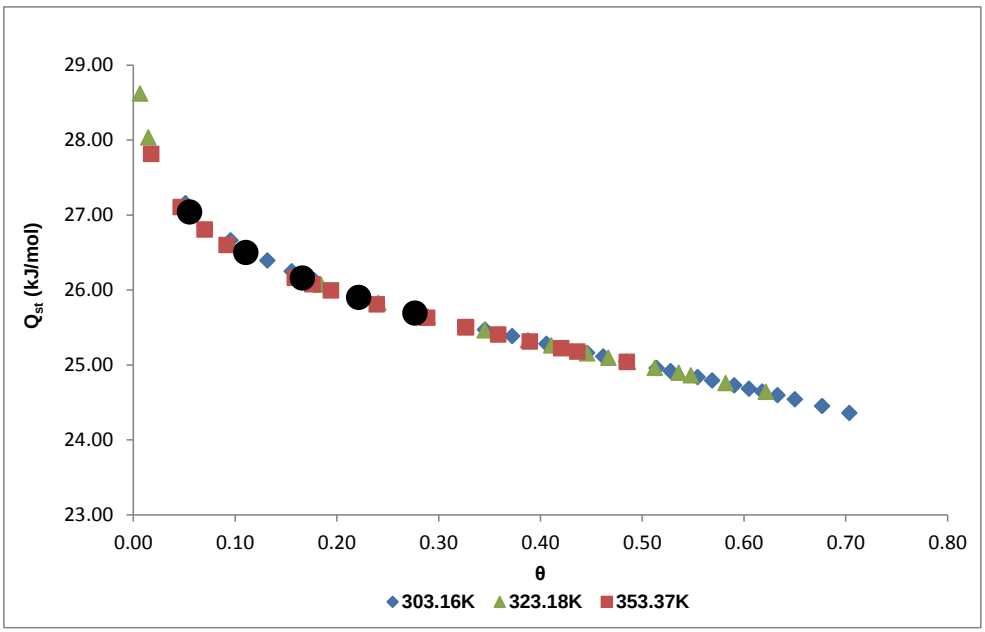

Figure 4.28: Isosteric heats of adsorption for CO_2 in MIL-53(Al), as a function of loading, determined from the temperature dependence of the Sips isotherm model. The symbols in black represent the Q_{st} independent of temperature.

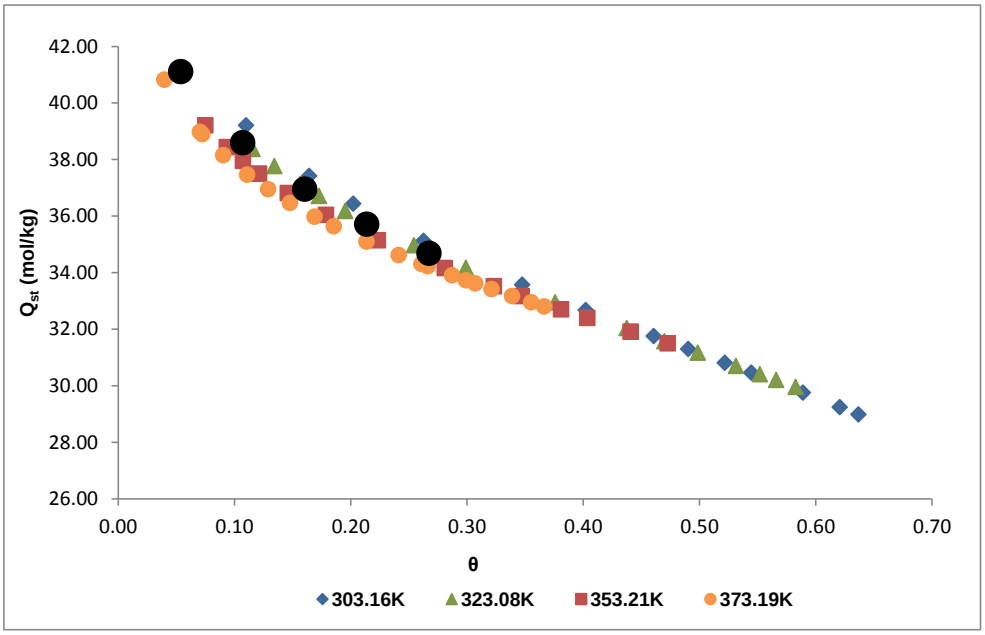

Figure 4.29: Isosteric heats of adsorption for C_2H_6 in MIL-53(Al), as a function of loading, determined from the temperature dependence of the Sips isotherm model. The symbols in black represent the Q_{st} independent of temperature.

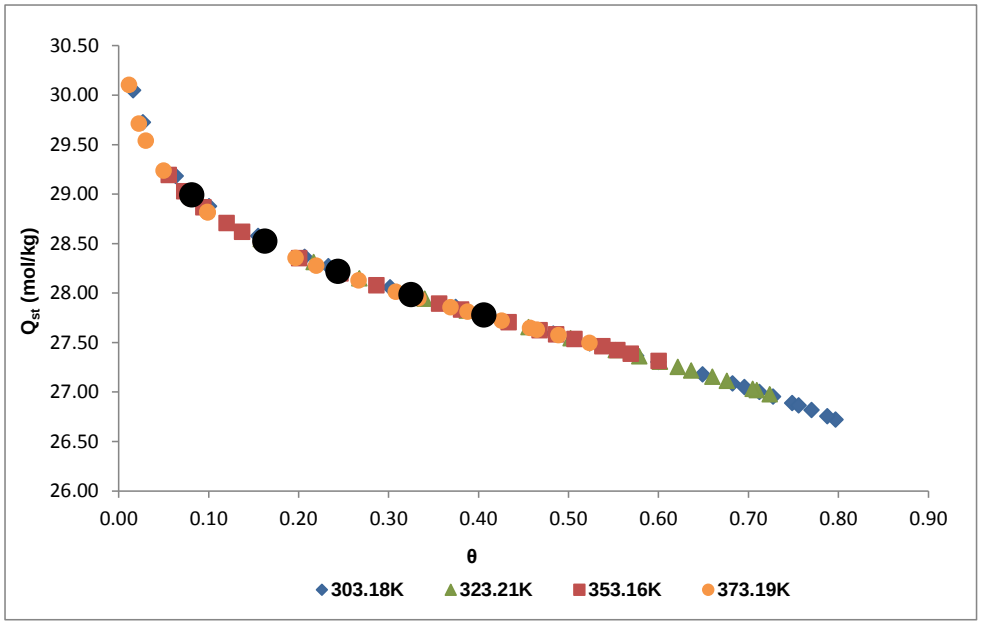

Figure 4.30: Isosteric heats of adsorption for C_2H_4 in MIL-53(Al), as a function of loading, determined from the temperature dependence of the Sips isotherm model. The symbols in black represent the Q_{st} independent of temperature.

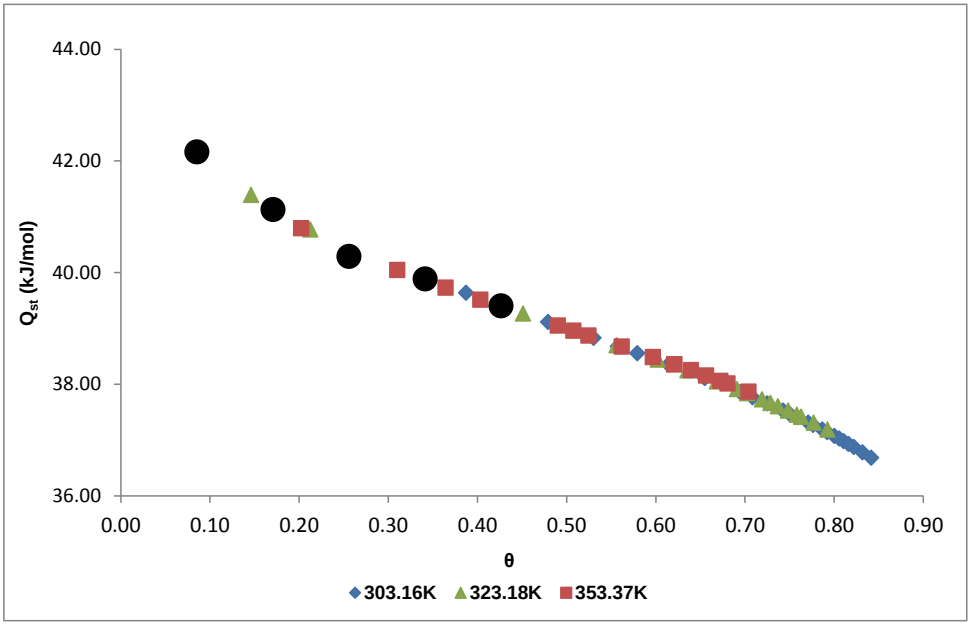

Figure 4.31: Isosteric heats of adsorption for CO_2 in zeolite 5A, as a function of loading, determined from the temperature dependence of the Sips isotherm model. The symbols in black represent the Q_{st} independent of temperature.

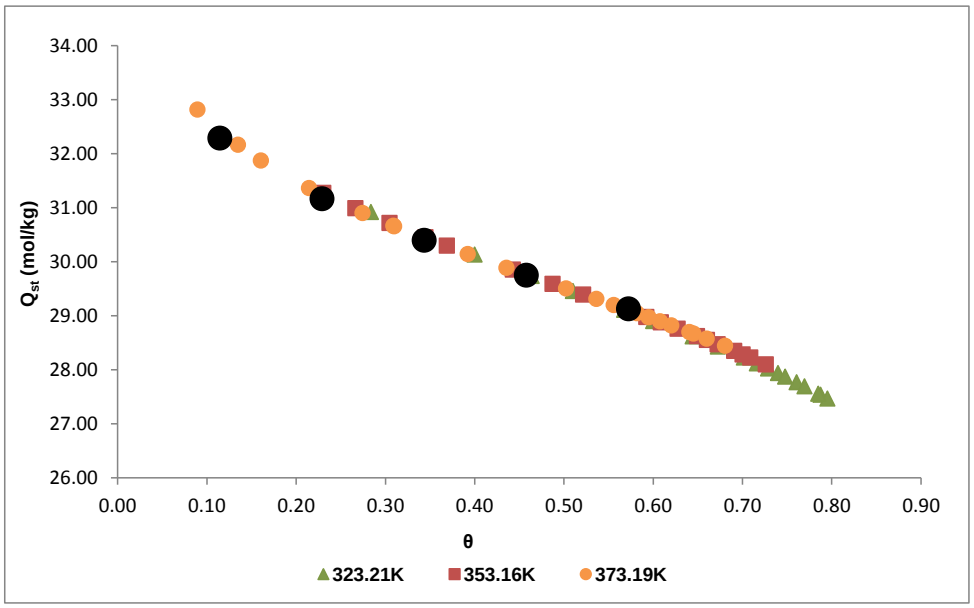

Figure 4.32: Isosteric heats of adsorption for C_2H_4 in zeolite 5A, as a function of loading, determined from the temperature dependence of the Sips isotherm model. The symbols in black represent the Q_{st} independent of temperature.

We conclude that for the MIL-53(Al), in the case of nitrogen (N_2) Q_{st} decreases with the increase of fractional loading (θ) until it reaches a plateau. However, MIL-53(Al) to carbon dioxide (CO_2), ethane (C_2H_6) and ethylene (C_2H_4), is more similar to the zeolite 5A in carbon dioxide (CO_2) and ethylene (C_2H_4) that is, the behavior of Q_{st} as a function of the the fractional loading (θ) is not that linear. The isosteric heat of adsorption begins to decrease in a gradual manner, and then in a more dramatic fashion. In this case, it cannot be neglected, then the isosteric heat of adsorption varies with the surface coverage.

4.2.2. Adsorption Potential Theory

Adsoption equilibrium on microporous adsorbents can be correlated using the Adsorption Potential Theory (APT). APT was developed by Dubinin and co-workers [65, 67] from the original work of Polanyi [77]. This theory has been widely used for the correlation of adsorption on different materials [26, 78, 79, 80].

APT assumes liquid-like behavior of the species adsorbed within the micropores although its properties may differ from the properties of liquid bulk at the same temperature due to the influence of the adsorbent force field. The difference in free energy between the adsorbed phase and the saturated liquid adsorbate at the same temperature can be obtained from the ratio between the equilibrium pressure and the saturation vapor pressure [19]. This is referred as the adsorption potential (ϕ) which is defined by:

$$\phi = R_g T ln\left(\frac{P_S}{P}\right) \qquad \textit{Equation (4.20)}$$

where R_g is the ideal gas constant, T is the temperature, P_S is the saturation vapor pressure of the adsorbated and P is the equilibrium pressure at temperature T. It should be noticed that due to the non-ideal gas behavior for high pressures P and P_S, should be replaced by the corresponding fugacity, f and f_S. The APT relates ϕ with the volume of the adsorbed phase (W) for a given gas-solid system in a relation that is generally referred as the characteristic curve.

$$W = q_t V_m = W(\phi) \qquad \textit{Equation (4.21)}$$

The APT is extremely when we desire to predict single-component adsorption equilibria and only a limited set of experimental measurements are available. The main advantage of this approach is that with a limited set of experimental data, the adsorption can be described for different temperatures [26, 19, 78].

Generalization of the APT theory was also proposed [81]. For this purpose, an affinity coefficient (β) can be used with the objective of collapsing the characteristic curves of various gases on an adsorbent into a unique characteristic curve. Applying this assumption Eq. 21 must be replaced by:

$$W \equiv q_t V_m = W\left(\tilde{\phi}\right) \qquad \textit{Equation (4.22)}$$

with,

$$\tilde{\phi} \equiv \frac{\phi}{\beta}$$ *Equation (4.23)*

The affinity coefficient, β, can be estimated obtained from correlation with the molecular parachor, as demonstrated by Wood and co-workers [82, 83].

$$\beta = 8.27 \times 10^{-3}(parachor)^{0.90}$$ *Equation (4.24)*

Below the adsorbate critical temperature (T_c), V_m is estimated from the modified Rackett equation [84], assuming to be equal to the molar volume of the saturated liquid at the temperature condition.

$$V_m = \frac{R_g T_c}{P_c} Z_{Ra} \left[1 + \left(1 - \frac{T}{T_c}\right)\right]^{2/7}$$ *Equation (4.25)*

where, P_c is the critical pressure of the adsorbate and Z_{Ra} is the Rackett compressibility factor. The Wagner equation was used to estimate the saturated vapor pressure [85].

$$ln\left(\frac{P_S}{P_c}\right) = \frac{Ax + Bx^{1.5} + Cx^3 + Dx^6}{1 - x}$$ *Equation (4.26)*

where,

$$x = 1 - \frac{T}{T_c}$$ *Equation (4.27)*

and A, B, C, and D are adsorbate-specific constants [85].

Above the adsorbate critical temperature definition of the adsorbed phase is not straightforward and in this work the work of Agarwal and Schwarz was followed [86]. The saturated vapor pressure was estimated by:

$$P_S = \left(\frac{T}{T_c}\right)^2 P_c$$ *Equation (4.28)*

and V_m was obtained by

$$V_m = V_b \exp[\Omega(T - T_b)] \qquad \textit{Equation (4.29)}$$

where T_b and V_b are, respectively, the temperature and molar volume of the liquid adsorbate at normal boiling point, and Ω is the adsorbate estimated thermal expansion coefficient in a superheated liquid state [66] and is obtained by,

$$\Omega = ln \frac{{}^{V_c}/_{V_b}}{T_c - T_b} \qquad \textit{Equation (4.30)}$$

In order to determine a isotherm relation for future application in process modelling, the characteristic curve was fitted to the Dubinin-Astakhov (D-A) equation, expressed by:

$$W = W_s \, exp\left(-\gamma \tilde{\phi}^{n'}\right) \qquad \textit{Equation (4.31)}$$

where ${}^{W}/_{W_s}$ is the fractional filling of the specific micropore volume (W_s) accessible to the adsorbate and γ and n' are parameters related to the characteristic energy for the system and the pore size distribution, respectively. These parameters were obtained from the linear fitting of

$$ln\left[ln\left({}^{W_s}/_{W}\right)\right] \quad versus \quad ln(\phi)$$

$$ln\left[ln\left({}^{W_s}/_{W}\right)\right] = \ln\gamma + n' \ln\phi \qquad \textit{Equation (4.32)}$$

Also, if $ln\left({}^{W_s}/_{W}\right)$ is expressed as a function of ϕ, the experimental data can be fitted with a polynomial expansion (in this case a third order polynomial was employed):

$$ln\left({}^{W_s}/_{W}\right) = c_1\phi + c_2\phi^2 + c_3\phi^3 \qquad \textit{Equation (4.33)}$$

This methodology was previously employed in several works with success [79, 6, 70].

4.2.2.1. Results and Discussion

In this work, the APT was applied to the analysis of the adsorption equilibrium experimental data of CO_2, N_2 and also the CH_4 data previously measured in the work of Lyubchyk *et al* [47]. To employ the APT the absolute amount adsorbed (q_t) is needed although from the gravimetric data only *net* or excess adsorbed quantities can be directly obtained. Therefore, (q_t) was determined employing the pore volume reported in previous molecular simulation studies performed by the group. This value provided a starting point for iteration and, finally, the determination of W_s, γ and n.

Table 4.5: Affinity coefficients, β, for CH_4, CO_2 and N_2 on MIL-53(Al) employed in this study.

	CH_4	CO_2	N_2
β (calculated from Eq.24)	0.394	0.480	0.280
β (employed)	0.440	0.370	0.280

The affinity coefficient, β, employed for first calculations were obtained from the Wood correlation (Eq. 23) and such values were tuned in order to obtain a better characteristic curve for the different adsorbates studied. The β values calculated and employed are showed in the Table (4.5).

As an example, we can see that in Figure (4.33), the D–A isotherm model is compared directly to the experimental adsorption/desorption data in, at three temperatures and for the methane (CH_4) in MIL-53(Al). It is observed that there is good agreement between model predictions and the experimental adsorption data for all three adsorbates.

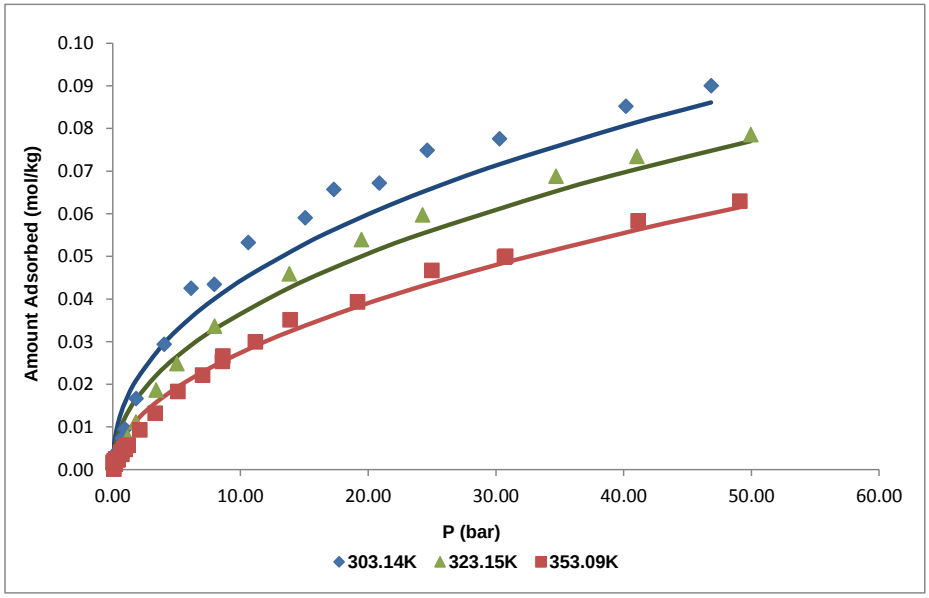

Figure 4.33: Single-component adsorption isotherms for the CH_4, at 303.14K, 323.15K and 353.09K. Symbols denote experimental data and lines are the predictions from the D-A isotherm model.

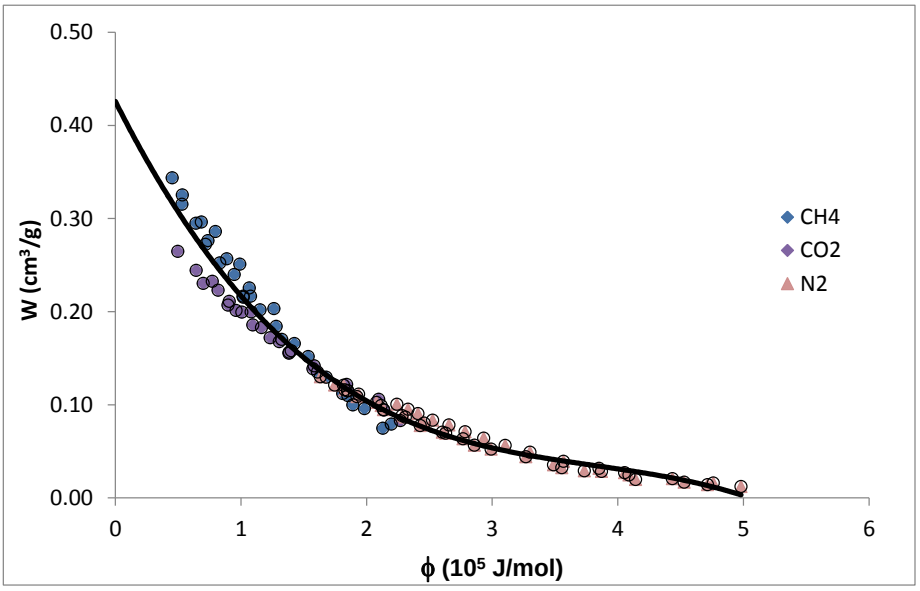

Figure 4.34: Characteristic curve obtained from collapsing the experimental data of CH_4, CO_2 and N_2 in to a single curve. The solid line represents the fitting with the D-A isotherm model.

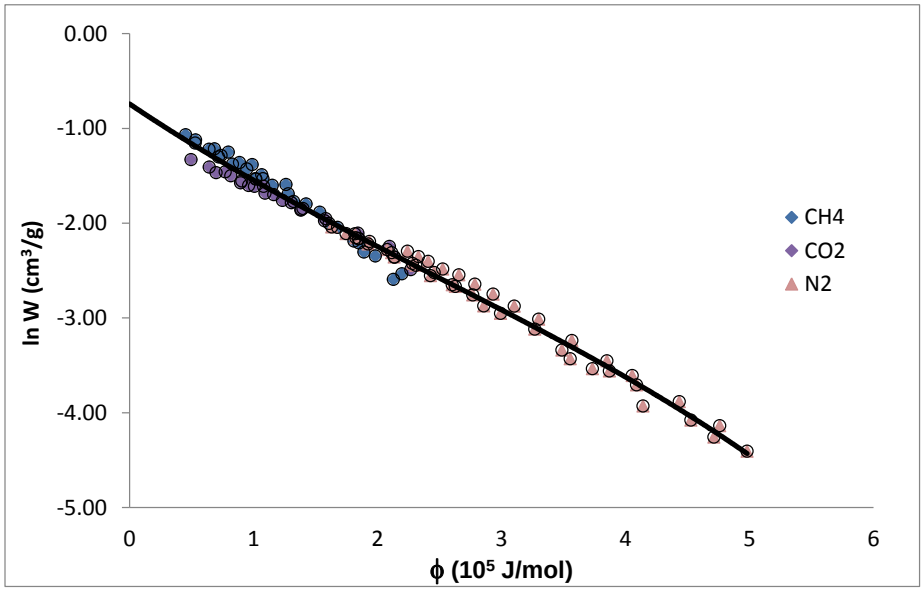

Figure 4.35: Logarithmic representation of the characteristic curve obtained from collapsing the experimental data of CH_4, CO_2 and N_2 in to a single curve. The solid line represents the fitting with the D-A isotherm model.

The characteristic curve obtained with the APT is showed in Figures (4.34) and (4.35), showing that a single curve could be successfully obtained for the three adsorbates considered. The solid lines represented in Figures (4.34) and (4.35) represent the D-A model and it can be seen that the experimental data could be successfully fitted. The fitting allowed the determination of the parameters W_s, γ and n showed in Table (4.6).

Table 4.6: Parameters obtained in the fitting of the experimental data.

W_s (cm³/g)	0.477
γ (J/mol)^n	1.036e-5
n	0.978

The W_s value obtained from the experimental data fitting (0.477cm³/g) in this preliminary study is approximated to the value obtained from molecular simulation (0.562cm³/g). Further refinements in the fitting may enhance the agreement between the specific micropore volume determined both by APT and by molecular simulation.

Chapter V

5. Conclusions and Future Work

In this work, equilibrium adsorption of n-alkanes (C_2 – C_4), ethylene, carbon dioxide and nitrogen were measured and analyzed on two adsorbent materials: metal-organic framework, MIL-53(Al) and zeolite 5A. The data gathered and analyzed is of great importance since it will add an important amount of information to the available literature on the subject. The obtained results are vital for the development of adsorption-based sustainable strategies for gas separation, recovery, capture and storage, employing the studied materials.

Measurements of equilibrium adsorption of pure components (ethane, propane, butane, ethylene, carbon dioxide and nitrogen) were conducted using the gravimetric method. The data obtained covers a wide range of thermodynamic conditions, including temperatures between 303.15K and 373.15K and pressure values between 0 - 50bar.

The adsorption equilibrium data were analyzed through the global fitting employing two isotherm models: the Sips and Toth models. The isosteric heat of adsorption and its dependence with adsorbent loading and was studied.

Results obtained showed that, in general, the adsorption capacity is higher in MIL-53(Al) than 5A zeolite. However, in the two adsorbents, the preferred adsorption capacity for CO_2 is a good indicator that these materials have a strong potential for application in the capture and storage of CO_2 and also in biogas and natural gas purification. The selectivity of MIL-53(Al) towards CO_2/N_2 and CO_2/CH_4 decreases with increasing pressure. Results also showed that this adsorbent is more selective for the CO_2/N_2 separation.

The separation of olefins/paraffins was also taken into account within this work. Therefore species as ethane (C_2H_6) and ethylene (C_2H_4) were also target of study on MIL-53(Al). In this case, C_2H_6 was preferentially adsorbed by the MIL-53(Al) adsorbent although the obtained selectivity decreased with pressure, once more.

Isosteric heat was determined employing both Sips and Toth models, taking into account the temperature dependence. However, the range of working temperatures was small enough to consider the Q_{st} independent of temperature. It was observed that the Q_{st} obtained for the different temperatures are in agreement which confirms that within this temperature range the isosteric heat can be considered temperature independent.

A different analysis of the experimental data of methane, carbon dioxide and nitrogen was performed. This consisted in the application of the Polaniy-Dubinin potential theory of adsorption (APT). The APT allowed collapsing the experimentally obtained data on a single characteristic curve, which is temperature independent. This analysis is useful for extrapolation of the adsorption behavior of gases and vapors for which no experimental data is available. Also, the APT allowed to obtain an adsorbent pore volume (0.477cm^3/g) which was approximate to the value obtained by the group from molecular simulation (0.562 cm^3/g).

The work undertaken within this thesis, allowed obtaining advanced knowledge in the field of adsorption. However, there are several aspects that deserve continued attention beyond this thesis. The following recommendations are proposed:

- ✓ In order to complement the experimental data obtained, it would be interesting to perform molecular simulation and other more fundamental studies, to better understand the adsorption mechanisms on MIL-53(Al). This information would be extremely important to better explain what happens to the flexible structure of MIL-53(Al) during adsorption processes.

- ✓ Since the MIL-53(Al) is presented as a powder, its pelletization would be interesting, since shaped materials are essential to carry out research studies on the adsorption processes such as Pressure Swing Adsorption (PSA).

Appendices

Appendix A: Characterization of Adsorbents

An effective adsorption process, is based on selection of a suitable adsorbent, since the success or failure of the process is directly related to the performance of the adsorbent. As such, the characterization of the adsorbents is a fundamental aspect since it provides qualitative and quantitative information, which serves as a basis for comparison and selection of the best adsorbent for specific applications.

In the present study, the two adsorbents in question, are the 5A zeolite and MOF, MIL-53(Al). In the case of zeolite 5A, this is found in the form of spheres with a mesh between 60 and 80, synthesized by Supelco - Analytical (Bellefonte, USA) (lot.12193 - 50g). For the metal organic framework (MOF) MIL-53(Al), it is presented in the form of crystals synthesized by BASF (Somerset, NJ) under the trademark Basolite A100 and were purchased through Sigma-Aldrich (product no.688738 - 10g). According to the manufacturer, this material has an average pore diameter $\overline{D_p} = 32\ \mu m$.

Although they are several of the characteristics of the adsorbent, which can be determined, and by different methods, we consider only the most relevants will be discussed here. Therefore, the characterization both the zeolite 5A, as the MOF MIL-53(Al) was performed, using techniques such as Mercury Porosimetry, Thermogravimetric Analysis and Nitrogen (N_2) Adsorption at 77K. It is necessary to take into account that relatively to the MOF, which has been the target of the study by the group, the characterization data had already been published in the work of Lyubchyk *et al* [47, 57]. Therefore, these are the results presented here.

Note that before any of these characterization analysis, the two samples were subjected to a pretreatment. In the case of 5A zeolite, the sample was degassed and activated at 623.15K in a muffle (Nabertherm GmbH B170) in the case of the MIL-53(Al) the procedure was the same, but its activation temperature was of 473.15K.

A.1: Mercury Porosimetry

The mercury porosimetry is a technique that, for applying various levels of pressure to a sample immersed in mercury, characterizes the porosity of the material [56].

The samples of zeolite 5A and MIL-53(Al) were then subjected, separately, to an experimental cycle of intrusion-extrusion of mercury, using a porosimeter, Autopore IV 9500 (Micromeritics Instrument Corporation, Norcross, Georgia). It is possible to visualize the intrusion-extrusion curves of the zeolite 5A and the MIL-53(Al) in Figures (A.1) and (A.2), respectively.

Through which it is possible to determine, that in the case of zeolite 5A, this shows an average value of pore diameter of $\overline{D_p} = 5E^{-05}\ \mu m$ and a porosity of 56%. In the case of the MIL-53(Al), it announces an average pore diameter of $\overline{D_p} = 30\ \mu m$ and a porosity of 68%. We can then conclude that in this case the MOF represents a more porous material than the zeolite, as would be already foreseen.

Comparing with the literature data we can state that the values are within the expected values. In the case of zeolite 5A, is predicted to $\overline{D_p} = 4.3E^{-05}\ \mu m$ [26]. For the MIL-53(Al) the average pore diameter is also in accordance with the value reported by the manufacturer of $\overline{D_p} = 32\ \mu m$.

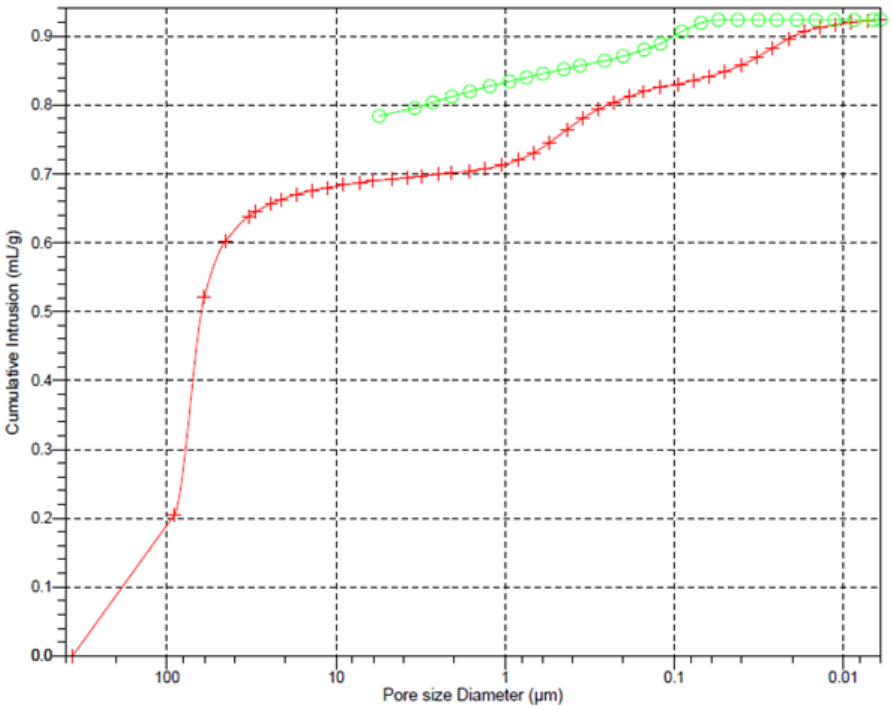

Figure A.1: Experimental Mercury intrusion-extrusion cycle for zeolite 5A. The curves give the volume of mercury (mL Hg/g of sample) penetrated at a given external pressure *P* into the measuring cell. The red curve (–+–+–) depicts the intrusion curve obtained; the green curve (–⊖–⊖–) shows the extrusion curve, obtained by reverting the process.

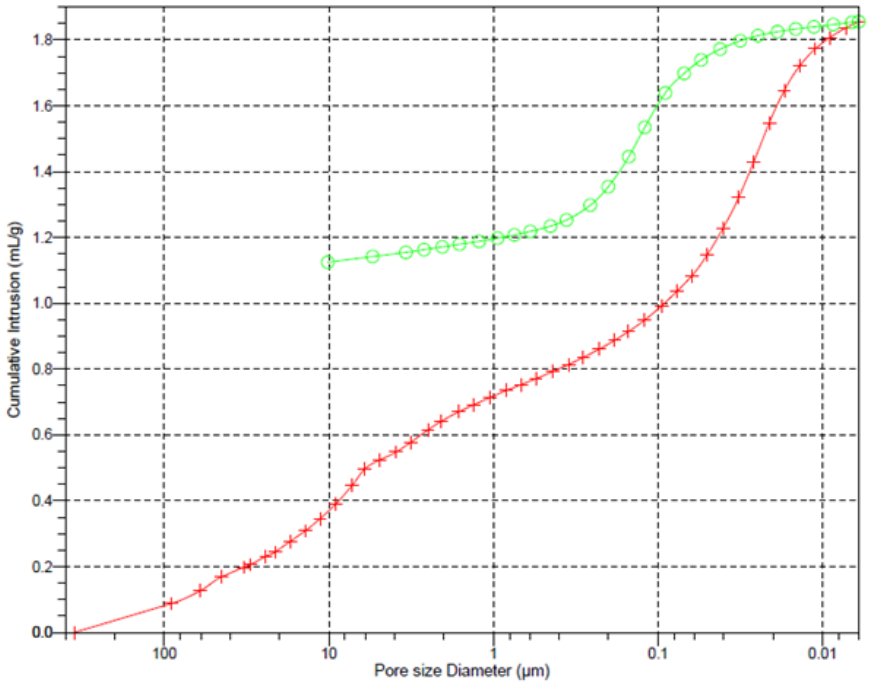

Figure A.2: Experimental Mercury intrusion-extrusion cycle for MIL-53(Al). The curves give the volume of mercury (mL Hg/g of sample) penetrated at a given external pressure *P* into the measuring cell. The red curve (−+−+−) depicts the intrusion curve obtained; the green curve (−⊖−⊖−) shows the extrusion curve, obtained by reverting the process [47].

A.2: Thermogravimetric Analysis (TGA)

Thermogravimetric analysis (TGA) allows us to evaluate the temperature range over which the sample decomposes. This procedure is performed by recording the weight loss as a function of the increasing temperature.

The samples were analyzed by TGA (model Q50 V6.7 Build 203, Universal V4.4, TA Instruments) under a nitrogen (N_2) atmosphere at a heating rate of 5 deg/min.

Typically, the results are presented graphically in a curve of weight percent as function of temperature as it is possible to see in Figure (A.3) and (A.4).

Easily is possible to conclude, by the analysis of Figure (A.3), that in the case of zeolite 5A, the structure can reach up to 823.15K without any decomposition of it. On the other hand, Figure (A.4) proves that MIL-53(Al) shows no deformation in its structure until a temperature of 773.15K [47, 57].

Both the profiles are in complete agreement with similar results, obtained in the literature for TGA made to these materials [87].

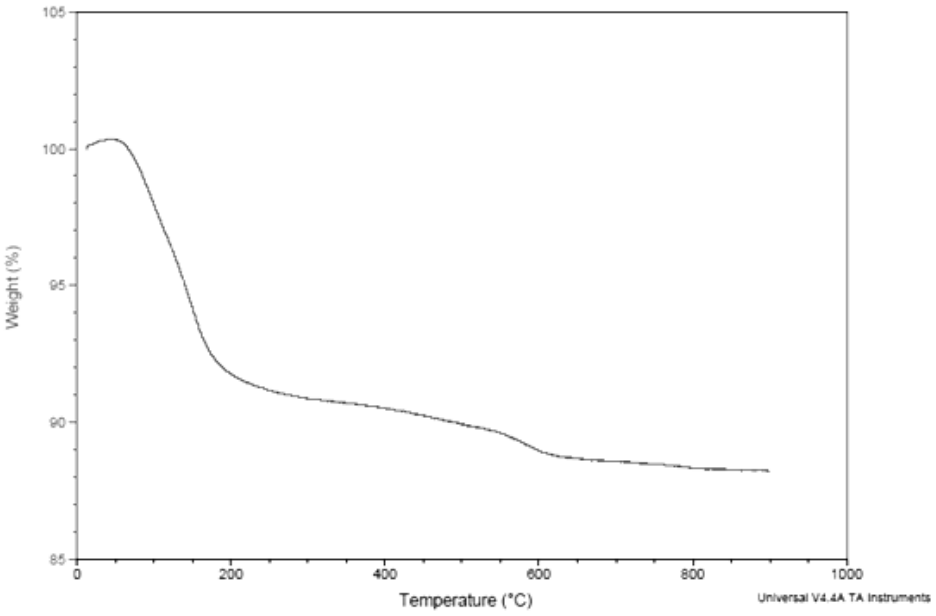

Figure A.3: Representative TGA analysis of zeolite 5A.

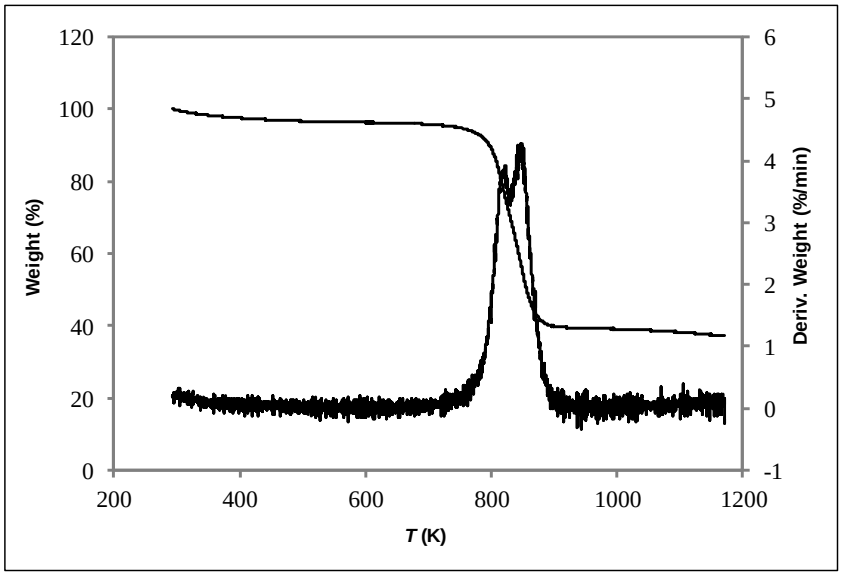

Figure A.4: Representative TGA analysis of MIL-53(Al) powder [47].

A.3: Nitrogen Adsorption at 77K

The nitrogen adsorption at 77K has become a widely used procedure for the determination of surface area and pore size distribution of various porous materials.

The measurement of the isotherm of nitrogen (N_2) for the adsorbents in question was carried out at 77K, using a static volumetric apparatus (Micromeritics Adsorption Analyzer, Model ASAP 2010). Figures (A.5) and (A.6) show the isotherms of nitrogen obtained at 77K, both for zeolite 5A and for MIL-53(Al), respectively.

It is then possible to conclude that for zeolite 5A, the total surface area of the sample, determined by BET surface area method, is 502 m^2/g, of which 448 m^2/g corresponds to the microporous area and the total pore volume is 0.394 cm^3/g, of which 0.233 cm^3/g is the volume of a microporous pores. In the case of the MIL-53(Al) the total surface area of the sample, determined by BET surface area method, is 831 m^2/g, of which 608 m^2/g represent the microporous area, and relatively to the total pore volume, this is of 0.597 cm^3/g, of which 0.332 cm^3/g corresponds to the volume of microporous pores [47, 57].

We can also report that in the case of zeolite 5A, the surface area of 502 m^2/g is found in accordance with the literature values of 571 m^2/g [41, 88]. In the case of the MIL-53(Al) the surface area of 1100-1500 m^2/g reported by the manufacturer is in agreement with the range of values from 1140 to 1270 m^2/g determined by other authors [47, 88].

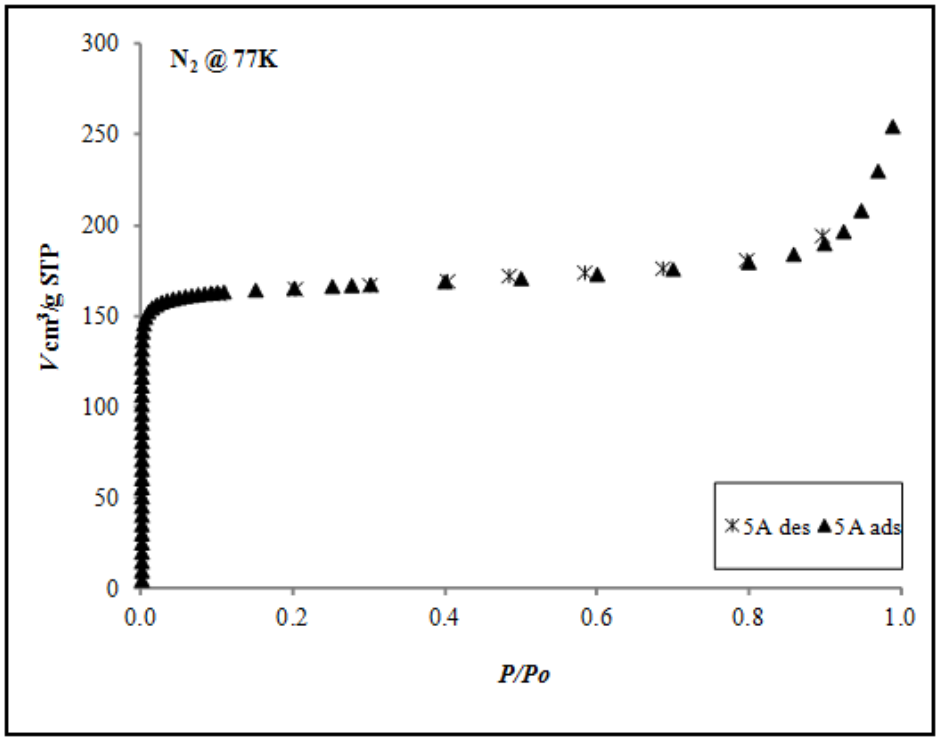

Figure A.5: Adsorption Isotherm of N_2 at 77K for zeolite 5A.

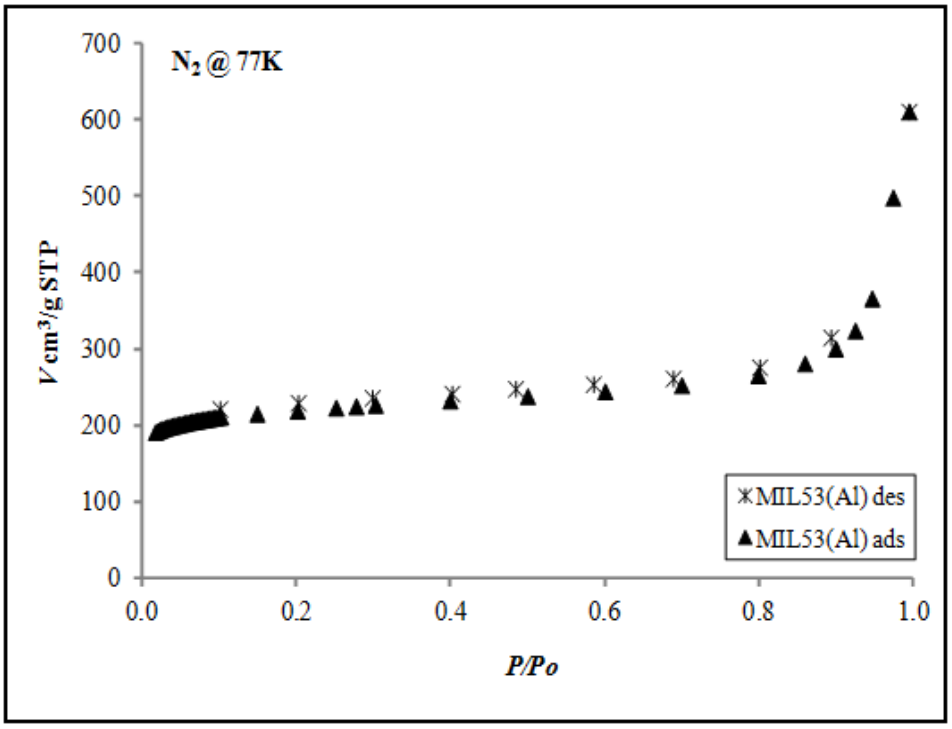

Figure A.6: Adsorption isotherm of N_2 at 77K for MIL-53(Al) [47].

Appendix B: Equipment Description

- **High-pressure Magnetic Suspension Balance (MSB)**

Model: ISOSORP 2000 coupled with a SARTORIUS microbalance Model BP211D.

Supplier: RUBOTHERM GmbH.

Characteristics: for a maximum load of 25g (total measuring volume, i.e. suspension coupling and measuring cell with sample), the balance have a resolution of 0.01mg, an uncertainty than 0.002% of the measured value, a reproducibility than 0.03 mg, for pressures in the range UHV - 150bar and temperatures up to 373.15K.

- **Vaccum Pump (VP)**

Model: EDWARDS 5 C, A65201903I

Supplier: EDWARDS

Pump Serial Number: 139482910

Characteristics: pumping speed 3.0 m^3/h. Motor type: RV3 US/EUR Pump High Volts. Single-phase 50/60Hz , 220 - 240V. Operating temperature of 243K to 343K, maximum total pressure in high flux of 1.2×10^{-1}, maximum total pressure of 2×10^{-3}.

Pump Oil: Edwards Ultragrade 19, hydrocarbon-oil, H11025015, 1Litre.

- **Pressure Generator**

Model: 87-6-5

Supplier: HiP

Characteristics: pressure rating of 5000psi, capacity per stroke 60 ml with teflon packing B-208.

- **Thermostatic Bath – Refrigerator/Heater**

Model: F32-HL

Supplier: JULABO Labortechnik GmbH

Characteristics: working temperature range of 238K to 473K, temperature stability $\pm$ 0,01K, cooling capacity: 293.15, 273.15, 253.15, 243.15K to (Medium: ethanol): 0.45; 0.39; 0.15; 0.06

KW, overall dimensions 31x42x64 cm, bath opening (WxL) 18x12 cm, bath depth 15cm, filling volume 5.5 to 8 liters , weight 38kg.

R**efrigerant:** R134a

- **Pt100 Temperature Probes**

Model: Pt100

Supplier: RS Amidata, Portugal

Characteristics: 4 wires temperature sensors with platinum resistance, that exhibit a typical resistance of 100Ω at 273.15K, typically measure temperatures up 1123.15K, Classe B precision ±0.12Ω at 0.3K. It consists of a thin film of platinum on a plastic film inside a stainless steel involucrum. The relationship between resistance and temperature is relatively linear, but curve fitting is often the most accurate way to make the RTD measurement. The probes were calibrated in the laboratory against a highly accurate Hart Scientific Pt 5613 temperature sensor with an accuracy of ±0.01K.

- **Pressure Transducer (PT): MKS**

Model: MKS Baratron Type 627D

Supplier: MKS Instruments Corporation (USA)

Characteristics: pressure measurements in the range from 1K Torr (1.3157bar) to as low as 0.02 Torr (0.00002bar) Full Scale (FS). The instrument operates with ± 15 VDC (± %5) input at ≤ 250 mA, and provides 0 to 10 VDC output linear with pressure. The 627D transducer is available with optional heater status LEDs, two interface connector lock options, and a variety of fittings. The unit is capable of measuring pressure at ambient temperatures of 288K to 313.15K.

- **Pressure Transducer (PT): OM2**

Model: PX01C1-150A5T

Supplier: OMEGADYNE, Inc. (USA)

Characteristics: pressure range of 0 - 10bar.

- **Pressure Transducer (PT): OM3**

Model: PX01C1-500A5T

Supplier: OMEGADYNE, Inc. (USA)

Characteristics: pressure range of 0 - 35bar.

- **Pressure Transducer (PT): OM4**

Model: PX03C1-3KA5T

Supplier: OMEGADYNE, Inc. (USA)

Characteristics: pressure range for 0 - 69/138/207 bar.

Table B.0.1: Characteristic of the several pressure transducers used in this work.

Name	ACRN.	Supply (VDC)	(Linearity) ACC (%F.S.)	F.S. (bar)	Output (VDC)	Calibration Y=a+bx
Omega 2	OM2	28	0.005	9.124	0 - 5	USB6 xxx Analog Input Multi Sample
Omega 3	OM3	28	0.005	34.830	0 - 5	USB6 xxx Analog Input Multi Sample
Omega 4	OM4	28	0.150	68.931	0 - 5	USB6 xxx Analog Input Multi Sample
Baratron	MKS	$\pm$ 15 VDC $\pm$ 5% $\leq$ 250 mA		1.005	0 - 10	MKS PR 4000B

- **Power Suppliers**

Model: PS 613

Supplier: Velleman

Characteristics: variable voltage of 0 – 30V, 2.5 A DC and two fixed supplies of ±12V and ±5V.

- **Ball Valves**

Model: SS-43S4

Supplier: Swagelok

Characteristics: 1/8”OD fittings, Cv = 2.4, P ≤ 206bar, 283K ≤ T ≤ 338K.

- **Check Valves**

Model: SS-4C-TR-1

Supplier: Swagelok

Characteristics: 1/8”OD fittings, PTFE seals, P_{crack} = 0.06bar, P_{max} = 206 bar.

- **Several Fittings**

Model: Swagelok types (nuts, unions, reducers, elbows, etc.)

Supplier: Swagelok

Characteristics: 1/8” OD fittings.

- **Computer (PC)**

Model: Intel(R) Core(TM) i3-2100 CPU @ 3.10GHz 3.10 GHz

Supplier: Tsunami Computers

Characteristics: Windows 7 Professional, RAM: 8.00 Gb, System type: 64-bit Operating System.

- **Gases**

Supplier: Air Liquide and Praxair (Portugal and Spain).

Characteristics: Compressed Helium (H_e) (99.999%), P = 200 bar from Air Liquide Alphagaz; Compressed Nitrogen (N_2) (99.995%), P = 200 bar from Air Liquide Alphagaz; Carbon dioxide (CO_2) (99.998%), P = 80 bar from Air Liquide Alphagaz; Methane (CH_4) (99.95%), P = 3.5 bar from Praxair Spain Gases; Ethane (C_2H_6) (99.95%), P = 33 bar from Air Liquide Alphagaz; Propane (C_3H_8) (99.95%), P = 6.5 bar from Air Liquide Alphagaz; Butane (C_4H_{10}) (99.95%), P = 0.75 bar from Air Liquide Alphagaz, Ethylene (C_2H_4) (99.5%), P = 80 bar from Air Liquide Alphagaz.

Appendix C: Tables and Figures of Experimental Results

In this appendix, there are all the tables with the experimental results obtained, from the tables with measurements of the blanks made to the two empty cells and the respective adsorbents, to the tables with the experimental measurements of each sorption isotherm.

C.1: Gravimetric Technique for Adsorption Measurements

Two cell samples were used according to the size of the respective adsorbent. As such, there was a referential blank calibration of the cells (without sample). Table (C.1) shows the values of these measurements performed at 293.78K using helium (H_e). Through the analysis of results of this experiment, it is possible to get to know the values of mass (m_h) and density (ρ_h) of the sample holder.

Table C.1: The experimental data obtained from the referential blank calibration of the cell (without sample). Experiment performed at 293.78K using as gas, helium (H_e).

293.78K			
P (bar)	ρ_g (kg/m^3)	Weight (g) Cell 1	Weight (g) Cell 2
0.000	0.000	5.574	6.412
0.313	0.001	5.574	6.412
0.615	0.001	5.574	6.412
0.945	0.002	5.574	6.412
5.460	0.893	5.574	6.411
15.628	2.543	5.573	6.410
26.562	4.298	5.571	6.408
40.231	6.467	5.570	6.407
61.568	9.793	5.567	6.404
68.872	10.915	5.567	6.403
50.888	8.137	5.569	6.405
30.948	4.999	5.571	6.408
10.406	1.698	5.573	6.411
2.881	0.472	5.574	6.411
0.002	0.000	5.574	6.412

In the present study, it is assumed that helium (H_e) acts as an inert probe that penetrates the entire volume of pores accessible to adsorbents (MIL-53(Al) and zeolite 5A), without being adsorbed [62]. Therefore, an experiment was conducted at a high temperature,

using helium (H_e), aimed at determining the mass (m_s) and density (ρ_s) of each of the adsorbents studied. Table (C.2) shows the values of the performed measurements. Note that in cell 1 is present the sample of zeolite 5A, and that in cell 2 is the MOF: MIL-53(Al).

Table C.2: Experimental data obtained from measurements of equilibrium adsorption of helium (H_e) at 353.29K. Cell 1, containing the sample of zeolite 5A and the cell 2, containing the sample of MIL-53(Al).

353.29K					
P (bar)	Cell 1		P (bar)	Cell 2	
	ρ_g (kg/m^3)	Weight (g)		ρ_g (kg/m3)	Weight (g)
0.000	0.000	6.069	0.000	0.000	6.723
20.681	2.797	6.067	7.701	1.047	6.722
26.735	3.608	6.066	12.022	1.631	6.722
34.765	4.676	6.065	16.063	2.176	6.721
30.064	4.051	6.066	20.681	2.797	6.720
18.596	2.517	6.067	26.735	3.608	6.720
9.220	1.252	6.069	34.765	4.676	6.719
3.788	0.516	6.069	30.064	4.051	6.719
0.942	0.128	6.070	18.596	2.517	6.721
0.000	0.000	6.070	9.220	1.252	6.722
			3.788	0.516	6.723
			0.942	0.128	6.723
			0.000	0.000	6.723

C.2: Adsorption Isotherms

The adsorption isotherms of alkanes (ethane (C_2H_6), propane (C_3H_8) and butane (C_4H_{10})), ethylene (C_2H_4), carbon dioxide (CO_2) and nitrogen (N_2) were measured experimentally for a range of temperature of 303.15 - 373.15K and a pressure range of 0 to 50 bar. For the experimental work, the standard static gravimetric method was used.

Each data point is reported as net (q_{net}), excess (q_{ex}), and total adsorption (q_t). For the calculation of q_{ex} and q_t, in the case of zeolite 5A are used values of V_p = 0.394 cm^3/g, from the characterization of the material and ρ_s = 1.707 g/cm^3, determined experimentally, by adsorption isotherm of helium (H_e). In the case of MIL-53(Al) the values used are V_p = 0.562 cm^3/g and ρ_s = 2.129 g/cm^3, determined by molecular simulation and that had already been published by the working group [47].

The experimental adsorption equilibrium data are listed in Tables (C.3) to (C.12). Figures (C.1) to (C.39) show the quantities adsorbed (mol/kg) in relation to the pressure (bar), for the adsorbents and adsorbates in study, at different temperatures.

- **Metal-Organic Framework: MIL-53(Al)**

Table C.3: Isotherm data of nitrogen (N_2) on sample of MIL-53(Al).

303.22K				323.19K				353.14K			
P (bar)	q_{net} (mol/kg)	q_{ex} (mol/kg)	q_t (mol/kg)	P (bar)	q_{net} (mol/kg)	q_{ex} (mol/kg)	q_t (mol/kg)	P (bar)	q_{net} (mol/kg)	q_{ex} (mol/kg)	q_t (mol/kg)
0.005	0.003	0.003	0.003	0.005	0.002	0.002	0.002	0.106	0.014	0.016	0.018
0.025	0.008	0.009	0.009	0.018	0.004	0.004	0.005	0.716	0.037	0.048	0.062
0.095	0.019	0.021	0.023	0.101	0.016	0.018	0.020	1.055	0.066	0.083	0.103
0.309	0.05	0.056	0.063	0.754	0.080	0.094	0.109	2.998	0.134	0.182	0.239
0.764	0.171	0.185	0.202	1.017	0.097	0.115	0.136	7.136	0.227	0.341	0.478
1.028	0.193	0.212	0.235	3.015	0.200	0.252	0.315	12.057	0.321	0.514	0.744
3.054	0.362	0.419	0.487	5.564	0.307	0.405	0.521	17.117	0.374	0.648	0.974
8.096	0.62	0.771	0.952	10.001	0.461	0.636	0.845	22.287	0.415	0.770	1.196
13.075	0.779	1.023	1.315	15.017	0.569	0.832	1.146	28.180	0.402	0.850	1.387
18.129	0.868	1.206	1.611	20.401	0.630	0.987	1.413	33.076	0.392	0.918	1.548
22.961	0.913	1.342	1.855	24.989	0.663	1.100	1.622	30.384	0.400	0.883	1.461
27.997	0.927	1.45	2.075	30.145	0.673	1.200	1.829	25.217	0.394	0.796	1.277
31.807	0.928	1.523	2.234	34.137	0.681	1.277	1.990	19.708	0.393	0.707	1.083
25.598	0.935	1.413	1.985	25.984	0.680	1.134	1.677	14.553	0.346	0.579	0.857
15.377	0.867	1.155	1.498	17.460	0.636	0.941	1.306	9.345	0.265	0.414	0.593
10.448	0.743	0.938	1.171	12.634	0.543	0.764	1.028	5.877	0.202	0.296	0.408
4.017	0.429	0.504	0.593	7.497	0.425	0.556	0.712	4.088	0.166	0.231	0.309
2.058	0.324	0.362	0.408	3.999	0.302	0.371	0.455	1.916	0.105	0.136	0.173
				2.016	0.192	0.228	0.270	0.399	0.043	0.050	0.057

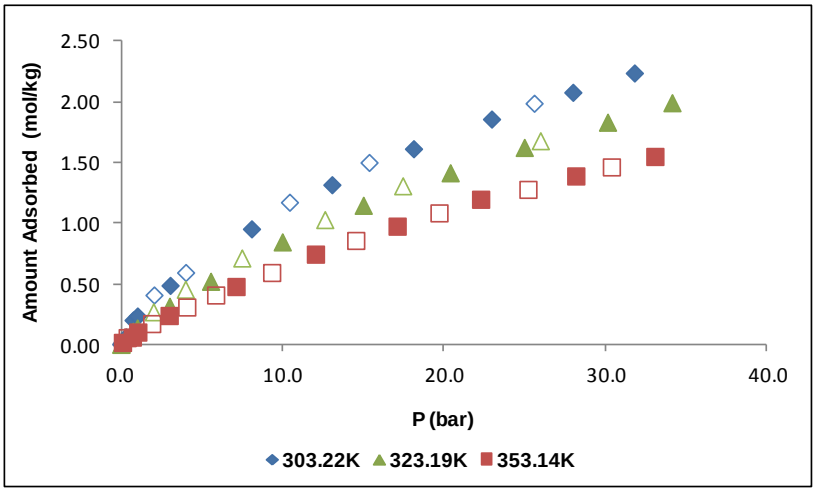

Figure C.1: Experimental single-component adsorption for N_2 at 303.22K, 323.19K and 353.14K for MIL-53(Al). Filled symbols and open symbols denote adsorption and desorption data, respectively.

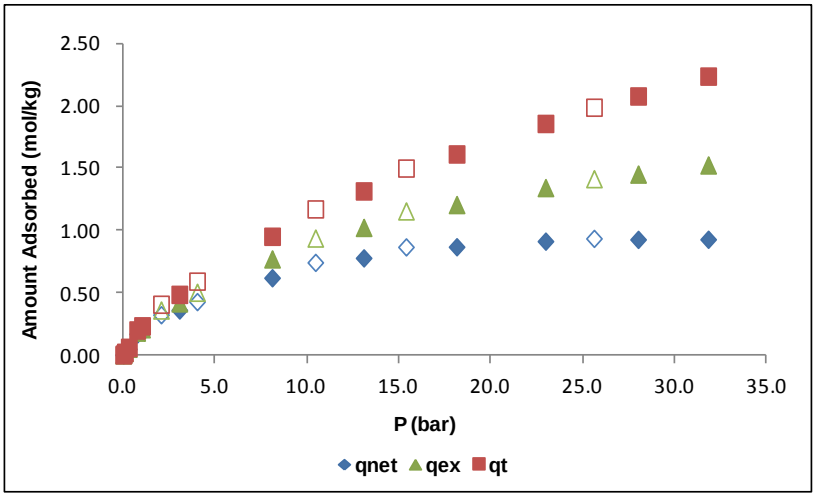

Figure C.2: Experimental single-component adsorption for N_2 at 303.22K for MIL-53(Al). Filled symbols and open symbols denote adsorption and desorption data, respectively.

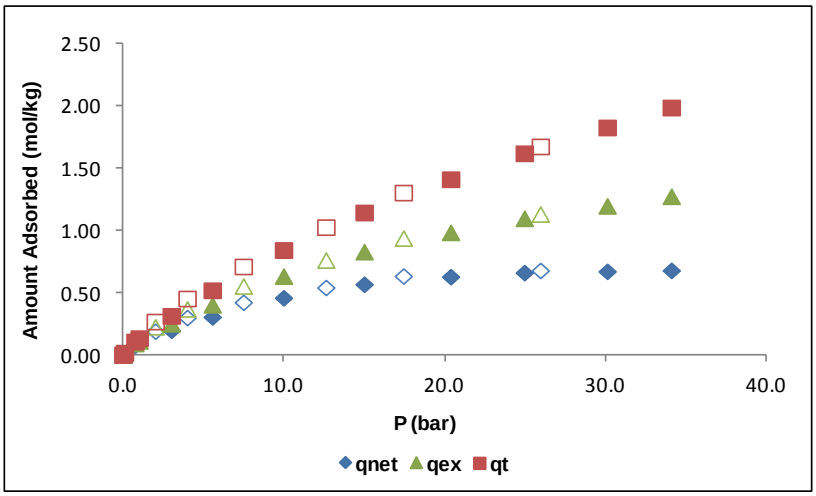

Figure C.3: Experimental single-component adsorption for N_2 at 323.19K for MIL-53(Al). Filled symbols and open symbols denote adsorption and desorption data, respectively.

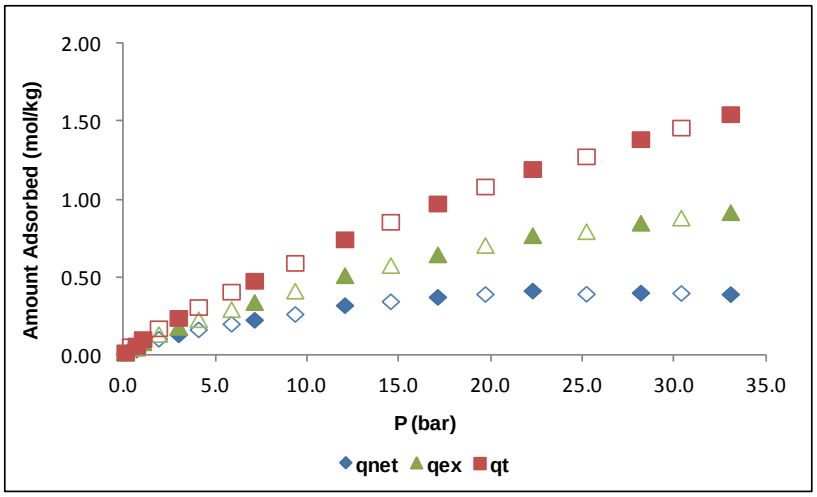

Figure C.4: Experimental single-component adsorption for N_2 at 353.14K for MIL-53(Al). Filled symbols and open symbols denote adsorption and desorption data, respectively.

Table C.4: Isotherm data of carbon dioxide (CO_2) on sample of MIL-53(Al).

303.16K				323.18K				353.37K			
P (bar)	q_{net} (mol/kg)	q_{ex} (mol/kg)	q_t (mol/kg)	P (bar)	q_{net} (mol/kg)	q_{ex} (mol/kg)	q_t (mol/kg)	P (bar)	q_{net} (mol/kg)	q_{ex} (mol/kg)	q_t (mol/kg)
0.133	0.456	0.459	0.462	0.013	0.085	0.085	0.085	0.534	0.313	0.322	0.332
0.586	1.170	1.181	1.194	3.193	2.054	2.111	2.178	0.976	0.522	0.538	0.557
0.974	1.545	1.563	1.585	4.558	2.331	2.412	2.509	4.182	1.439	1.507	1.588
3.523	2.897	2.964	3.043	6.573	2.667	2.785	2.926	7.166	1.946	2.063	2.203
5.101	3.361	3.458	3.575	8.526	2.928	3.082	3.266	10.242	2.296	2.465	2.667
6.454	3.651	3.776	3.924	9.764	3.082	3.259	3.471	13.126	2.534	2.752	3.013
8.066	3.905	4.062	4.249	11.976	3.303	3.522	3.785	16.012	2.727	2.995	3.316
9.572	4.111	4.298	4.522	15.052	3.524	3.804	4.139	19.281	2.872	3.199	3.590
12.074	4.355	4.595	4.881	17.492	3.661	3.990	4.383	25.205	3.055	3.490	4.011
14.903	4.571	4.870	5.229	19.981	3.803	4.183	4.637	33.140	3.192	3.779	4.482
17.596	4.706	5.065	5.495	26.086	3.978	4.488	5.098	23.055	3.025	3.421	3.894
21.459	4.864	5.313	5.850	32.926	4.081	4.747	5.544	13.155	2.510	2.729	2.990
25.505	5.059	5.606	6.261	21.400	3.941	4.350	4.840	4.946	1.631	1.711	1.807
30.518	5.082	5.760	6.571	13.496	3.591	3.840	4.138	3.511	1.332	1.389	1.457
19.286	4.973	5.371	5.848	1.976	1.613	1.648	1.689	1.468	0.728	0.752	0.780
16.266	4.870	5.200	5.595	0.685	0.849	0.861	0.876	0.129	0.098	0.100	0.102
13.133	4.689	4.951	5.264	0.041	0.189	0.190	0.191				
10.365	4.481	4.684	4.927								
7.079	4.071	4.208	4.371								
4.162	3.410	3.490	3.584								
2.209	2.543	2.584	2.634								
1.412	1.971	1.998	2.030								
0.777	1.340	1.355	1.372								
0.348	0.804	0.810	0.818								

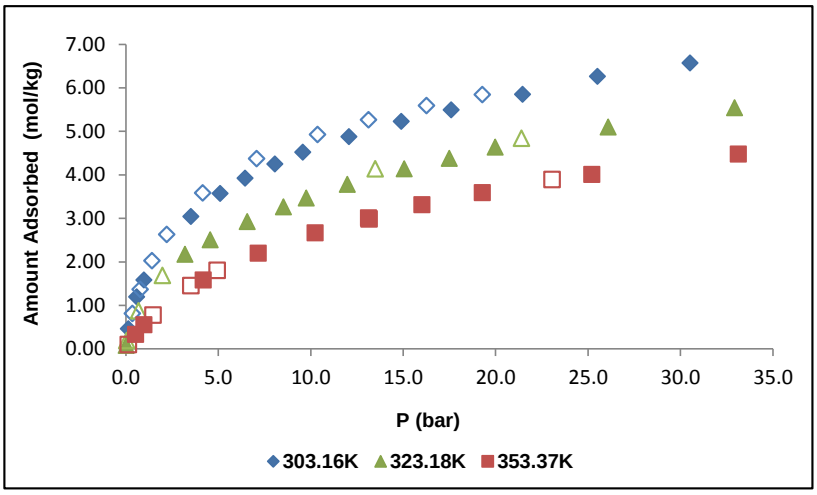

Figure C.5: Experimental single-component adsorption for CO_2 at 303.16K, 323.18K and 353.37K for MIL-53(Al). Filled symbols and open symbols denote adsorption and desorption data, respectively.

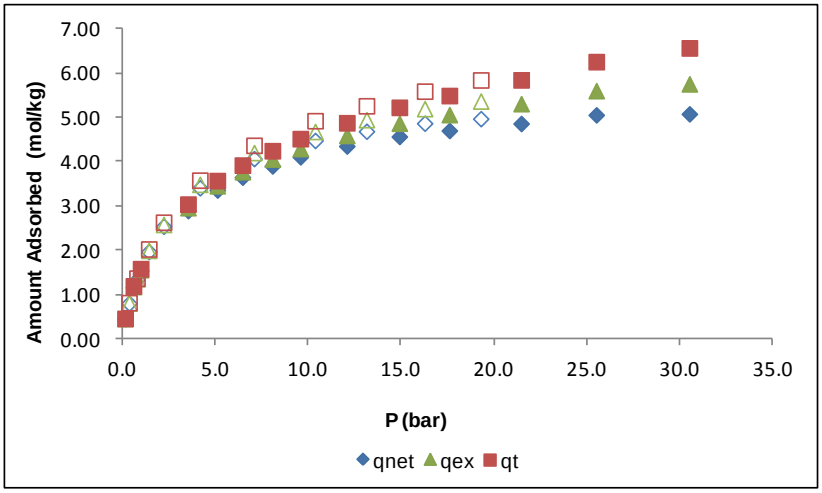

Figure C.6: Experimental single-component adsorption for CO_2 at 303.16K for MIL-53(Al). Filled symbols and open symbols denote adsorption and desorption data, respectively.

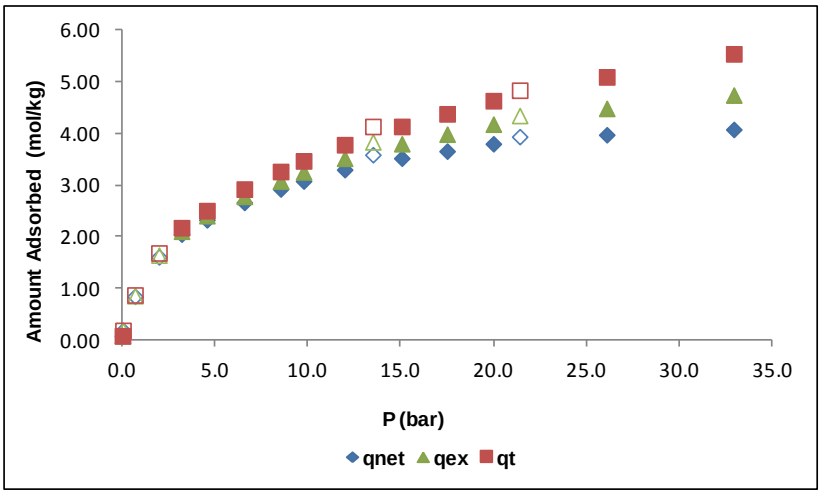

Figure C.7: Experimental single-component adsorption for CO_2 at 323.18K for MIL-53(Al). Filled symbols and open symbols denote adsorption and desorption data, respectively.

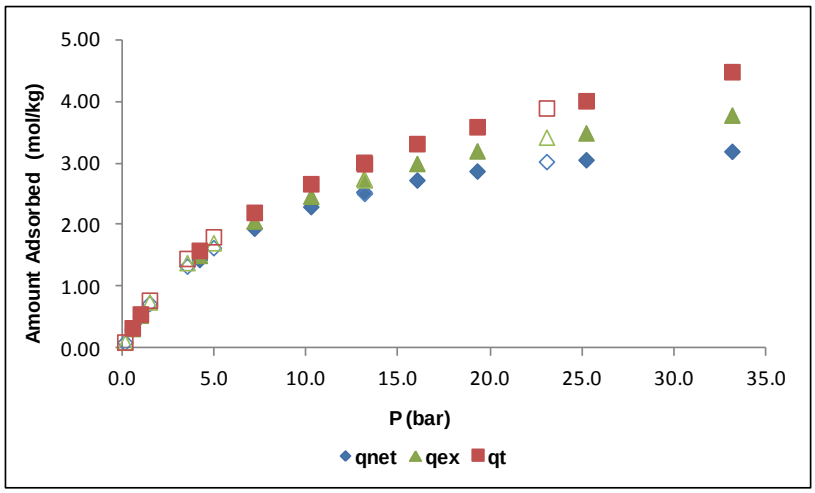

Figure C.8: Experimental single-component adsorption for CO_2 at 353.37K for MIL-53(Al). Filled symbols and open symbols denote adsorption and desorption data, respectively.

Table C.5: Isotherm data of ethane (C_2H_6) on sample of MIL-53(Al).

303.16K				323.08K			
P (bar)	q_{net} (mol/kg)	q_{ex} (mol/kg)	q_t (mol/kg)	P (bar)	q_{net} (mol/kg)	q_{ex} (mol/kg)	q_t (mol/kg)
0.440	1.861	1.869	1.879	0.369	1.209	1.215	1.223
0.952	2.498	2.516	2.537	0.703	1.741	1.754	1.769
4.002	3.507	3.584	3.676	0.973	1.990	2.007	2.027
8.975	4.002	4.181	4.395	3.307	2.861	2.920	2.990
14.661	4.186	4.494	4.863	6.983	3.285	3.412	3.564
22.095	4.237	4.739	5.340	12.164	3.542	3.772	4.047
29.834	4.162	4.913	5.812	20.729	3.628	4.046	4.545
34.853	4.055	5.013	6.159	27.599	3.570	4.160	4.865
11.931	4.241	4.485	4.778	37.330	3.326	4.212	5.271
6.863	3.996	4.130	4.291	43.343	3.126	4.232	5.555
2.362	3.325	3.370	3.423	33.020	3.504	4.248	5.138
0.248	1.623	1.627	1.633	16.158	3.694	4.008	4.385
0.087	0.849	0.850	0.852	2.036	2.634	2.670	2.713
				0.544	1.671	1.681	1.692
				0.254	1.097	1.102	1.107

353.21K				373.19K			
P (bar)	q_{net} (mol/kg)	q_{ex} (mol/kg)	q_t (mol/kg)	P (bar)	q_{net} (mol/kg)	q_{ex} (mol/kg)	q_t (mol/kg)
0.715	0.886	0.897	0.911	0.562	0.588	0.597	0.607
0.949	1.125	1.140	1.159	0.972	0.849	0.863	0.881
4.320	2.356	2.427	2.511	2.158	1.256	1.289	1.329
8.133	2.693	2.828	2.990	4.081	1.589	1.652	1.727
15.343	2.942	3.206	3.522	7.300	1.839	1.953	2.089
20.760	3.001	3.368	3.808	10.007	1.943	2.101	2.289
25.208	2.986	3.443	3.990	13.056	2.011	2.219	2.468
34.590	2.877	3.540	4.333	16.102	2.040	2.299	2.610
45.086	2.607	3.533	4.640	18.044	2.054	2.347	2.697
12.290	2.912	3.120	3.369	22.207	2.055	2.422	2.861
2.432	2.031	2.070	2.117	26.089	2.043	2.481	3.006
1.479	1.573	1.597	1.625	33.245	1.967	2.544	3.234
0.521	0.923	0.932	0.942	30.178	2.013	2.530	3.148
0.317	0.600	0.606	0.612	19.487	2.070	2.389	2.770
				12.346	2.014	2.210	2.445
				5.130	1.735	1.814	1.909
				2.969	1.487	1.533	1.587
				1.535	1.139	1.163	1.191
				0.597	0.669	0.678	0.689
				0.167	0.351	0.353	0.356

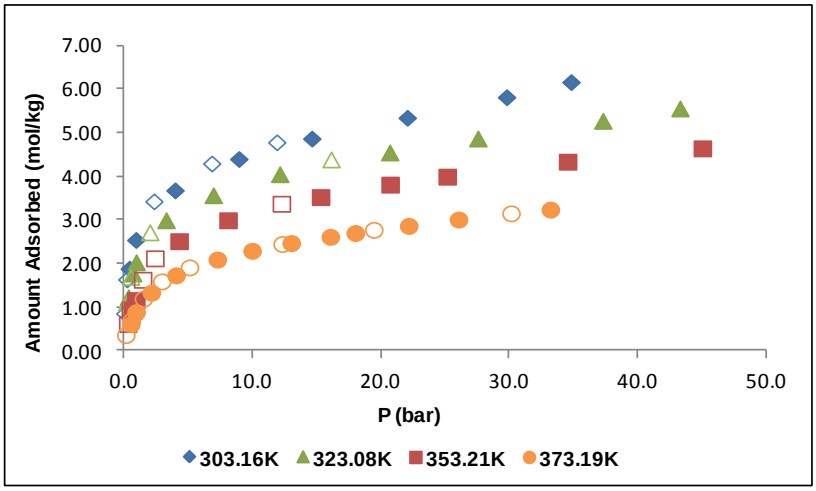

Figure C.9: Experimental single-component adsorption for C_2H_6 at 303.16K, 323.08K, 353.21K and 373.19K for MIL-53(Al). Filled symbols and open symbols denote adsorption and desorption data, respectively.

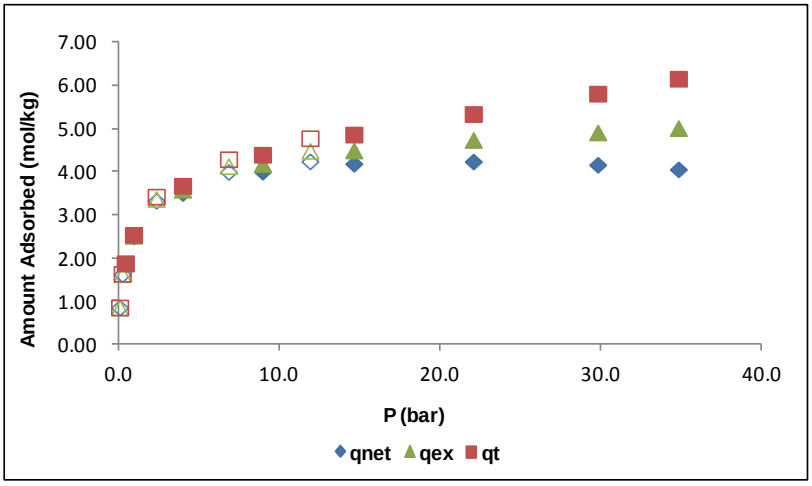

Figure C.10: Experimental single-component adsorption for C_2H_6 at 303.16K for MIL-53(Al). Filled symbols and open symbols denote adsorption and desorption data, respectively.

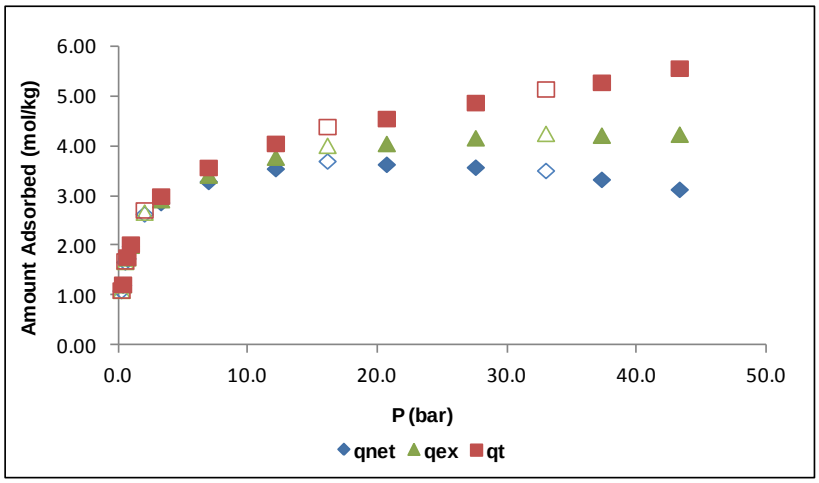

Figure C.11: Experimental single-component adsorption for C_2H_6 at 323.08K for MIL-53(Al). Filled symbols and open symbols denote adsorption and desorption data, respectively.

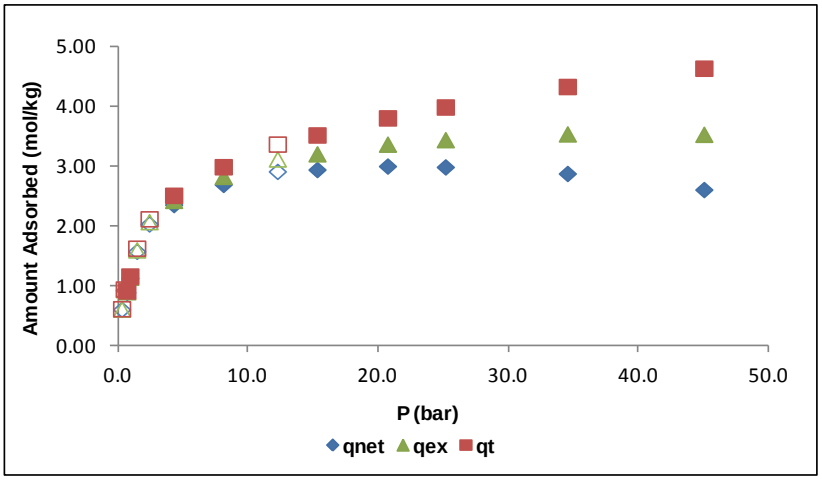

Figure C.12: Experimental single-component adsorption for C_2H_6 at 353.21K for MIL-53(Al). Filled symbols and open symbols denote adsorption and desorption data, respectively.

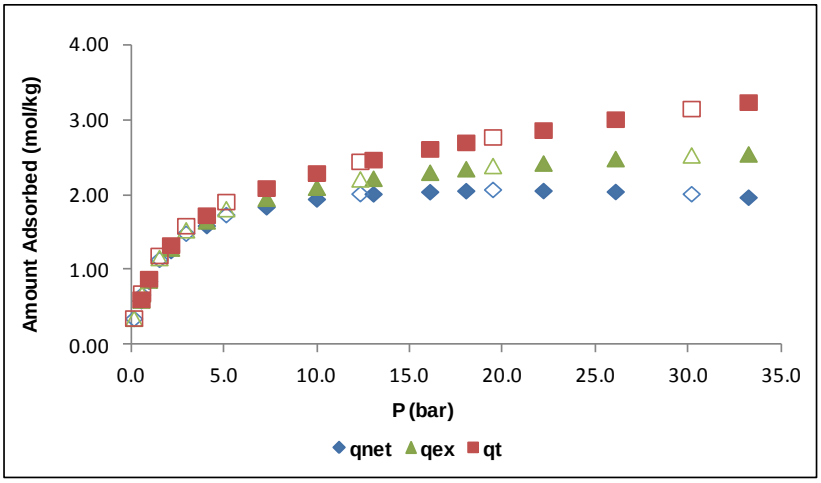

Figure C.13: Experimental single-component adsorption for C_2H_6 at 373.19K for MIL-53(Al). Filled symbols and open symbols denote adsorption and desorption data, respectively.

Figure C.6: Isotherm data of ethylene (C_2H_4) on sample of MIL-53(Al).

303.18K				323.21K			
P (bar)	q_{net} (mol/kg)	q_{ex} (mol/kg)	q_t (mol/kg)	P (bar)	q_{net} (mol/kg)	q_{ex} (mol/kg)	q_t (mol/kg)
0.552	1.526	1.528	1.530	0.149	0.465	0.468	0.471
0.970	1.856	1.858	1.860	0.513	1.094	1.103	1.113
1.638	2.255	2.286	2.323	3.533	2.240	2.302	2.377
3.346	2.662	2.725	2.801	5.527	2.467	2.566	2.684
6.055	2.978	3.095	3.234	10.255	2.745	2.934	3.159
9.987	3.206	3.403	3.639	12.140	2.806	3.030	3.299
14.011	3.318	3.601	3.940	14.112	2.855	3.118	3.434
17.980	3.389	3.762	4.209	16.118	2.883	3.188	3.551
21.420	3.328	3.774	4.307	21.048	2.907	3.315	3.803
25.865	3.348	3.918	4.599	30.242	2.864	3.481	4.220
33.328	3.273	4.053	4.988	33.811	2.879	3.584	4.428
30.446	3.402	4.097	4.929	29.211	2.957	3.549	4.258
22.768	3.517	4.006	4.592	23.595	3.013	3.476	4.031
15.911	3.514	3.840	4.230	17.849	3.006	3.345	3.752
12.687	3.463	3.718	4.023	7.450	2.731	2.866	3.027
7.132	3.237	3.375	3.541	2.563	2.155	2.200	2.254
4.335	2.976	3.058	3.157	1.481	1.836	1.863	1.894
1.953	2.511	2.548	2.592	0.953	1.559	1.575	1.595
0.431	1.550	1.558	1.568				
0.245	1.221	1.226	1.232				
0.111	0.801	0.803	0.805				
0.050	0.482	0.483	0.484				
0.012	0.160	0.160	0.160				
0.005	0.095	0.095	0.095				

353.16K				373.19K			
P (bar)	q_{net} (mol/kg)	q_{ex} (mol/kg)	q_t (mol/kg)	P (bar)	q_{net} (mol/kg)	q_{ex} (mol/kg)	q_t (mol/kg)
0.322	0.397	0.402	0.408	0.293	0.241	0.245	0.251
0.499	0.567	0.575	0.584	0.623	0.465	0.474	0.485
0.976	0.907	0.922	0.941	0.915	0.620	0.634	0.651
4.176	1.783	1.851	1.932	2.135	1.047	1.079	1.118
8.154	2.127	2.261	2.422	4.007	1.433	1.495	1.568
11.495	2.267	2.458	2.687	8.196	1.816	1.943	2.094
14.307	2.338	2.579	2.866	12.538	2.000	2.197	2.432
18.234	2.397	2.707	3.079	14.200	2.048	2.271	2.539
22.193	2.416	2.800	3.259	18.155	2.105	2.394	2.741
27.093	2.416	2.893	3.464	22.176	2.139	2.497	2.925
33.111	2.387	2.985	3.699	27.008	2.141	2.583	3.112
24.626	2.448	2.878	3.392	33.461	2.062	2.612	3.271
16.053	2.406	2.677	3.002	23.229	2.141	2.517	2.966
9.545	2.242	2.400	2.588	16.041	2.077	2.331	2.635
6.909	2.099	2.212	2.348	9.816	1.918	2.071	2.254
3.032	1.665	1.714	1.772	5.981	1.687	1.779	1.889
2.000	1.414	1.446	1.484	3.227	1.352	1.402	1.461
0.765	0.874	0.886	0.901	0.924	0.682	0.696	0.713
0.205	0.351	0.354	0.358	0.129	0.136	0.138	0.140
				0.080	0.089	0.090	0.092
				0.028	0.038	0.039	0.039

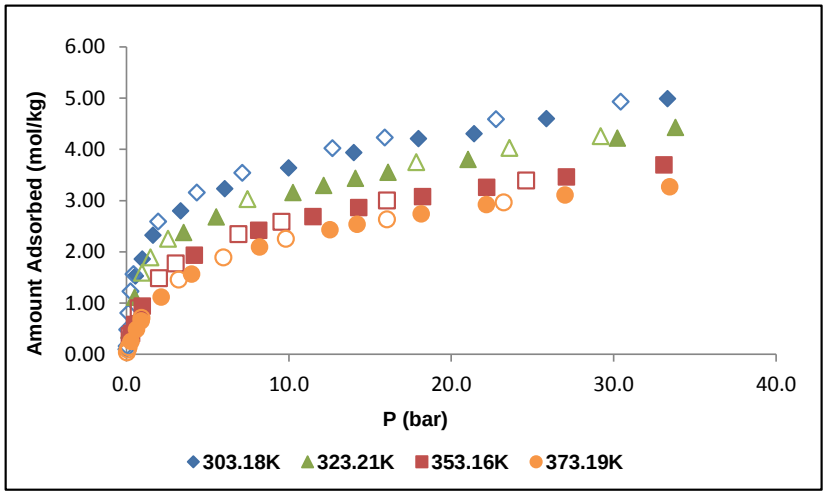

Figure C.14: Experimental single-component adsorption for C_2H_4 at 303.18K, 323.21K, 353.16K and 373.19K for MIL-53(Al). Filled symbols and open symbols denote adsorption and desorption data, respectively.

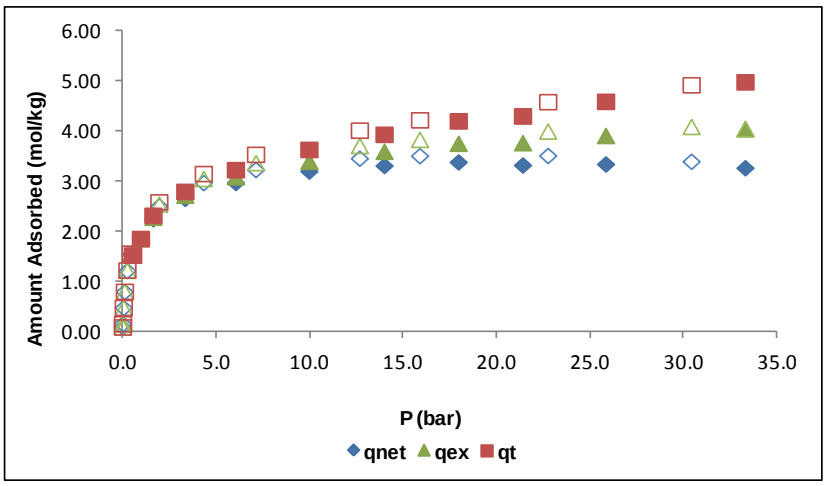

Figure C.15: Experimental single-component adsorption for C_2H_4 at 303.18K for MIL-53(Al). Filled symbols and open symbols denote adsorption and desorption data, respectively.

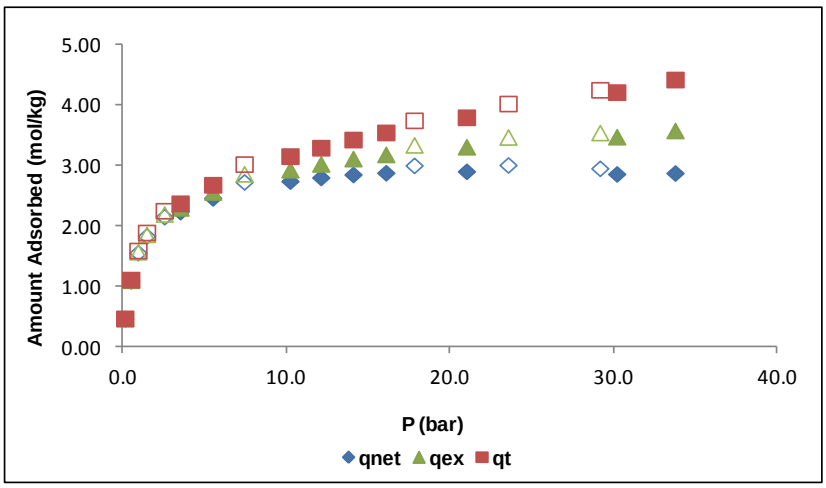

Figure C.16: Experimental single-component adsorption for C_2H_4 at 323.21K for MIL-53(Al). Filled symbols and open symbols denote adsorption and desorption data, respectively.

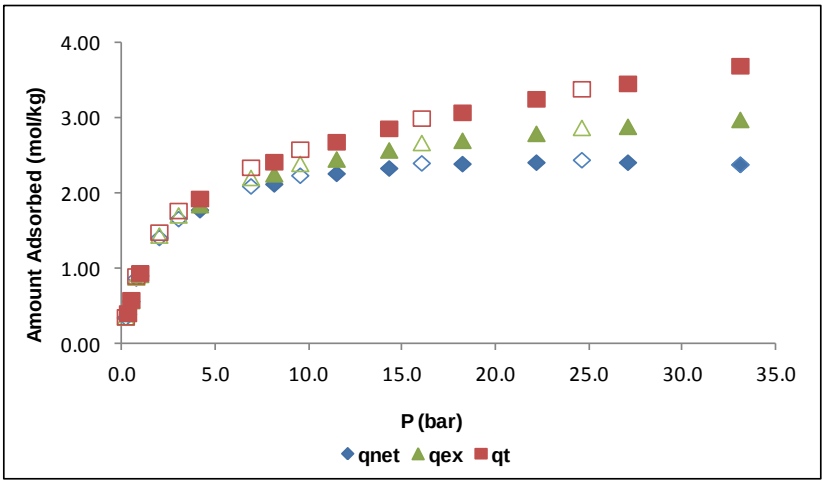

Figure C.17: Experimental single-component adsorption for C_2H_4 at 353.16K for MIL-53(Al). Filled symbols and open symbols denote adsorption and desorption data, respectively.

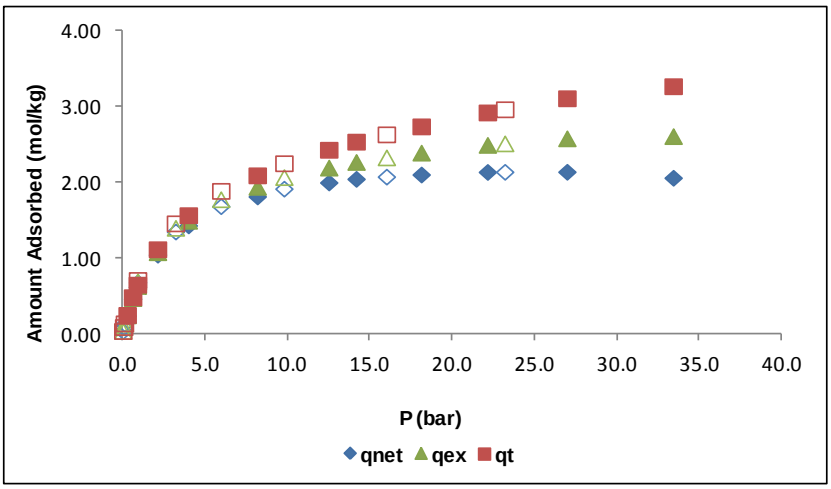

Figure C.18: Experimental single-component adsorption for C_2H_4 at 373.19K for MIL-53(Al). Filled symbols and open symbols denote adsorption and desorption data, respectively.

Table C.7: Isotherm data of propane (C_3H_8) on sample of MIL-53(Al).

303.18K				323.21K				353.47K			
P (bar)	q_{net} (mol/kg)	q_{ex} (mol/kg)	q_t (mol/kg)	P (bar)	q_{net} (mol/kg)	q_{ex} (mol/kg)	q_t (mol/kg)	P (bar)	q_{net} (mol/kg)	q_{ex} (mol/kg)	q_t (mol/kg)
0.005	0.327	0.328	0.328	0.002	0.002	0.002	0.002	0.003	0.030	0.030	0.030
0.069	1.050	1.051	1.052	0.010	0.003	0.003	0.004	0.028	0.292	0.293	0.293
0.156	1.448	1.451	1.454	0.078	0.028	0.029	0.031	0.178	1.032	1.035	1.038
0.985	1.864	1.882	1.905	0.098	0.053	0.055	0.057	0.623	1.452	1.462	1.474
1.772	2.174	2.208	2.248	0.231	0.253	0.257	0.261	0.973	1.583	1.599	1.618
3.248	2.365	2.429	2.505	0.475	0.950	0.958	0.968	2.011	1.753	1.786	1.825
6.076	2.614	2.740	2.890	0.945	1.620	1.636	1.655	5.656	1.950	2.046	2.160
9.122	3.031	3.233	3.475	1.571	1.920	1.948	1.982	8.016	2.019	2.159	2.325
7.565	2.784	2.946	3.139	4.970	2.413	2.506	2.617	12.228	2.068	2.292	2.559
4.477	2.561	2.651	2.758	7.582	2.545	2.692	2.869	17.719	2.088	2.438	2.857
2.388	2.378	2.424	2.479	9.331	2.627	2.814	3.038	26.259	2.099	2.718	3.459
1.385	2.196	2.222	2.254	12.691	2.769	3.041	3.366	23.025	2.083	2.585	3.186
0.802	2.043	2.058	2.076	14.122	2.859	3.171	3.544	10.957	2.085	2.282	2.518
0.540	1.960	1.970	1.982	11.150	2.707	2.938	3.215	4.007	1.947	2.014	2.093
0.282	1.839	1.844	1.850	8.637	2.612	2.783	2.987	1.491	1.760	1.784	1.813
0.097	1.660	1.662	1.664	6.475	2.534	2.657	2.805	0.415	1.472	1.479	1.487
0.046	1.480	1.481	1.482	3.575	2.358	2.423	2.501	0.105	1.062	1.064	1.066
0.012	1.191	1.191	1.191	1.222	2.081	2.103	2.129	0.025	0.520	0.520	0.520
0.002	0.768	0.768	0.769	0.702	1.957	1.970	1.984	0.007	0.280	0.280	0.280
				0.336	1.796	1.802	1.809				
				0.149	1.613	1.616	1.619				
				0.048	1.318	1.319	1.320				
				0.009	0.745	0.745	0.745				

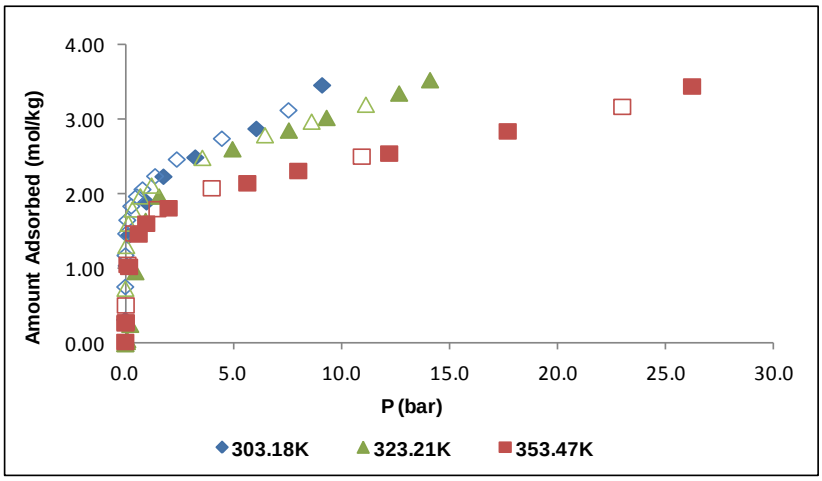

Figure C.19: Experimental single-component adsorption for C_3H_8 at 303.18K, 323.21K and 353.47K for MIL-53(Al). Filled symbols and open symbols denote adsorption and desorption data, respectively.

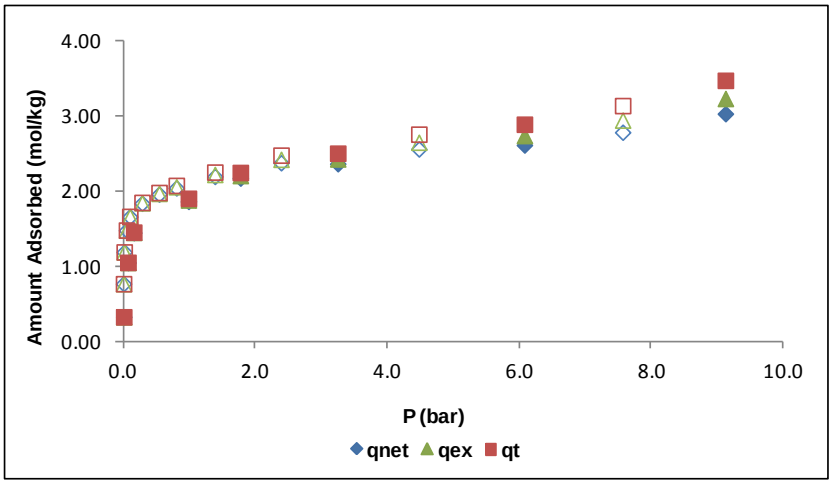

Figure C.20: Experimental single-component adsorption for C_3H_8 at 303.18K for MIL-53(Al). Filled symbols and open symbols denote adsorption and desorption data, respectively.

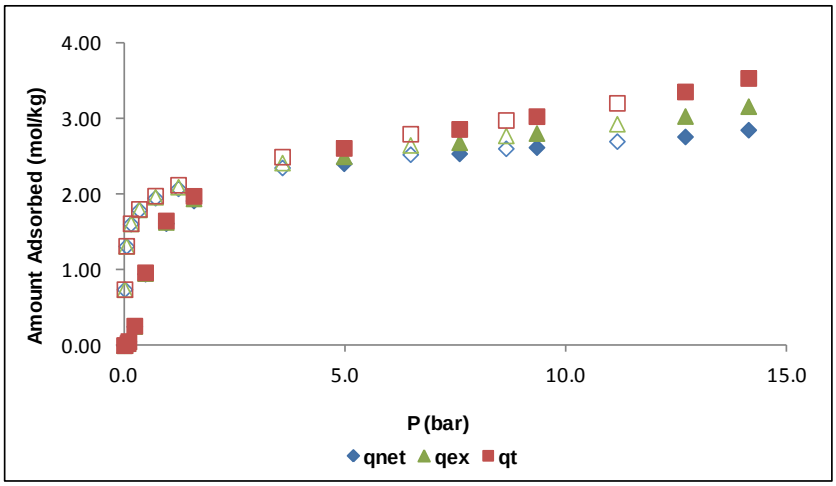

Figure C.21: Experimental single-component adsorption for C_3H_8 at 323.21K for MIL-53(Al). Filled symbols and open symbols denote adsorption and desorption data, respectively.

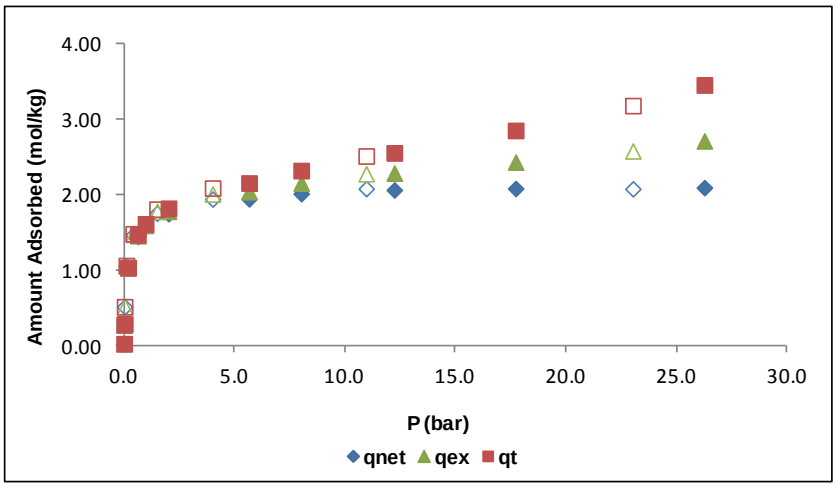

Figure C.22: Experimental single-component adsorption for C_3H_8 at 353.47K for MIL-53(Al). Filled symbols and open symbols denote adsorption and desorption data, respectively.

Table C.8: Isotherm data of butane (C_4H_{10}) on sample of MIL-53(Al).

303.20K				323.21K				353.12K			
P (bar)	q_{net} (mol/kg)	q_{ex} (mol/kg)	q_t (mol/kg)	P (bar)	q_{net} (mol/kg)	q_{ex} (mol/kg)	q_t (mol/kg)	P (bar)	q_{net} (mol/kg)	q_{ex} (mol/kg)	q_t (mol/kg)
0.002	0.407	0.407	0.407	0.002	0.102	0.102	0.102	0.003	0.045	0.045	0.046
0.006	0.589	0.589	0.589	0.007	0.514	0.514	0.514	0.008	0.276	0.276	0.276
0.010	0.682	0.682	0.683	0.011	0.632	0.632	0.632	0.036	0.772	0.772	0.773
0.045	0.871	0.872	0.873	0.034	1.034	1.034	1.035	0.082	0.908	0.909	0.911
0.083	0.978	0.979	0.981	0.089	1.122	1.124	1.126	0.391	1.164	1.170	1.178
0.592	1.474	1.485	1.498	0.288	1.365	1.370	1.376	0.867	1.312	1.327	1.343
1.074	1.811	1.832	1.856	0.773	1.595	1.608	1.625	2.142	1.466	1.501	1.544
2.095	2.202	2.244	2.293	1.005	1.679	1.697	1.718	4.431	1.618	1.695	1.787
1.518	1.994	2.024	2.059	2.248	1.960	2.001	2.051	8.620	1.943	2.109	2.307
0.843	1.737	1.753	1.773	3.086	2.206	2.265	2.334	5.860	1.719	1.824	1.950
0.372	1.436	1.443	1.451	3.980	2.461	2.538	2.630	3.109	1.521	1.574	1.637
0.156	1.296	1.299	1.302	1.656	1.845	1.875	1.911	1.620	1.458	1.485	1.517
0.069	1.203	1.204	1.206	0.550	1.574	1.583	1.595	0.613	1.285	1.295	1.307
0.024	1.149	1.149	1.150	0.171	1.401	1.404	1.407	0.243	1.144	1.148	1.152
0.004	0.864	0.864	0.864	0.028	1.093	1.093	1.094	0.017	0.696	0.697	0.697
				0.005	0.573	0.573	0.573				

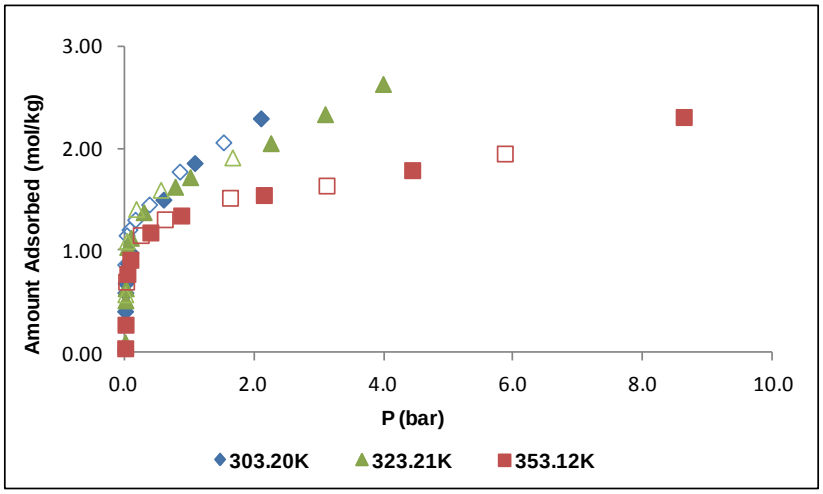

Figure C.23: Experimental single-component adsorption for C_4H_{10} at 303.20K, 323.21K and 353.12K for MIL-53(Al). Filled symbols and open symbols denote adsorption and desorption data, respectively.

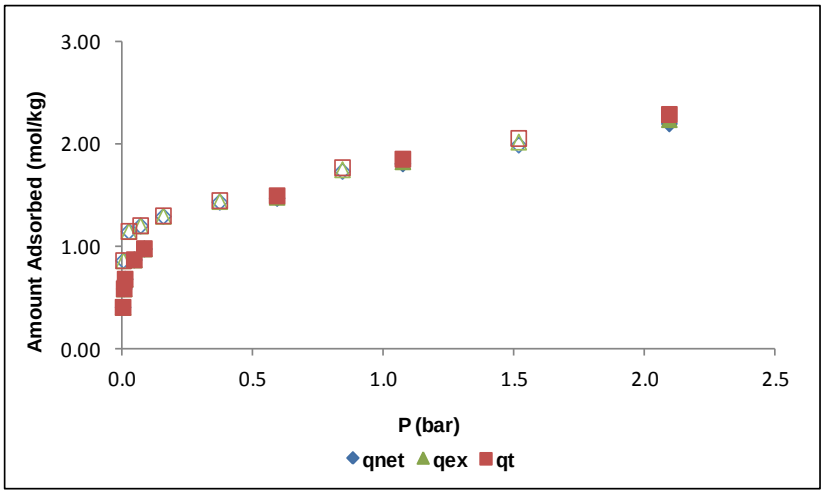

Figure C.24: Experimental single-component adsorption for C_4H_{10} at 303.20K for MIL-53(Al). Filled symbols and open symbols denote adsorption and desorption data, respectively.

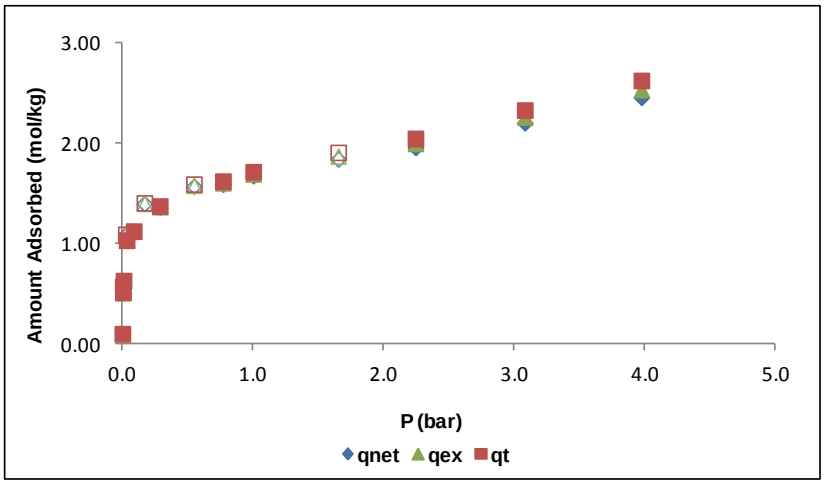

Figure C.25: Experimental single-component adsorption for C_4H_{10} at 323.21K for MIL-53(Al). Filled symbols and open symbols denote adsorption and desorption data, respectively.

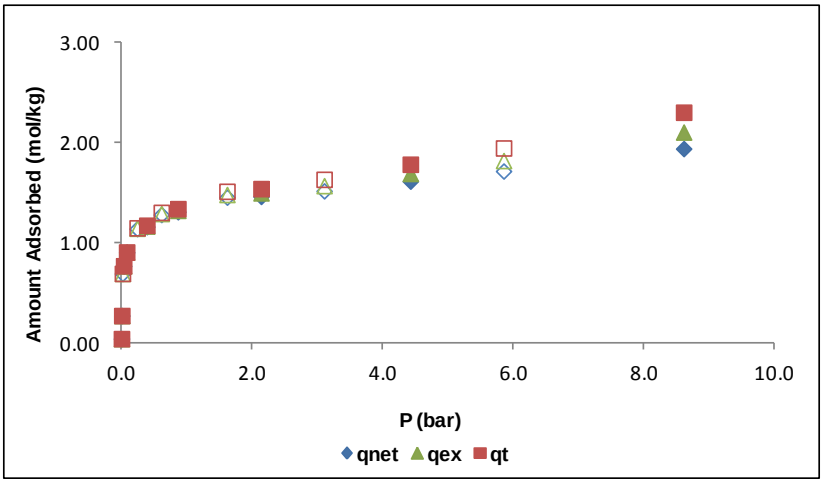

Figure C.26: Experimental single-component adsorption for C_4H_{10} at 353.12K for MIL-53(Al). Filled symbols and open symbols denote adsorption and desorption data, respectively.

➢ **Zeolite 5A**

Table C.9: Isotherm data of carbon dioxide (CO_2) on sample of zeolite 5A.

303.16K				323.18K				353.37K			
P (bar)	q_{net} (mol/kg)	q_{ex} (mol/kg)	q_t (mol/kg)	P (bar)	q_{net} (mol/kg)	q_{ex} (mol/kg)	q_t (mol/kg)	P (bar)	q_{net} (mol/kg)	q_{ex} (mol/kg)	q_t (mol/kg)
0.133	2.456	2.460	2.462	0.013	0.325	0.326	0.326	0.534	1.770	1.781	1.788
0.586	3.377	3.390	3.400	3.193	3.290	3.361	3.408	0.976	2.149	2.169	2.182
0.974	3.549	3.572	3.587	4.558	3.387	3.488	3.556	4.182	2.813	2.897	2.954
3.523	3.913	3.996	4.052	6.573	3.468	3.615	3.714	7.166	2.984	3.130	3.228
5.101	3.990	4.112	4.194	8.526	3.514	3.707	3.836	10.242	3.063	3.273	3.415
6.454	4.036	4.191	4.295	9.764	3.535	3.756	3.905	13.126	3.101	3.373	3.556
8.066	4.061	4.257	4.388	11.976	3.560	3.834	4.018	16.012	3.138	3.473	3.698
9.572	4.079	4.312	4.469	15.052	3.570	3.919	4.154	19.281	3.137	3.544	3.818
12.074	4.091	4.390	4.590	17.492	3.564	3.974	4.250	25.205	3.110	3.653	4.018
14.903	4.086	4.460	4.711	19.981	3.563	4.037	4.355	33.140	3.037	3.770	4.262
17.596	4.070	4.518	4.820	26.086	3.502	4.138	4.566	23.055	3.129	3.621	3.953
21.459	4.031	4.591	4.968	32.926	3.404	4.236	4.795	13.155	3.097	3.370	3.553
25.505	3.991	4.673	5.133	21.400	3.556	4.067	4.410	4.946	2.925	3.025	3.092
30.518	3.902	4.747	5.316	13.496	3.587	3.898	4.107	3.511	2.814	2.885	2.932
19.286	4.071	4.567	4.901	1.976	3.201	3.244	3.273	1.468	2.429	2.458	2.478
16.266	4.095	4.507	4.783	0.685	2.787	2.802	2.812	0.129	1.048	1.051	1.053
13.133	4.102	4.429	4.648	0.041	1.278	1.278	1.279				
10.365	4.099	4.352	4.523								
7.079	4.063	4.233	4.348								
4.162	3.980	4.079	4.145								
2.209	3.838	3.890	3.925								
1.412	3.721	3.754	3.776								
0.777	3.525	3.543	3.555								
0.348	3.247	3.255	3.261								

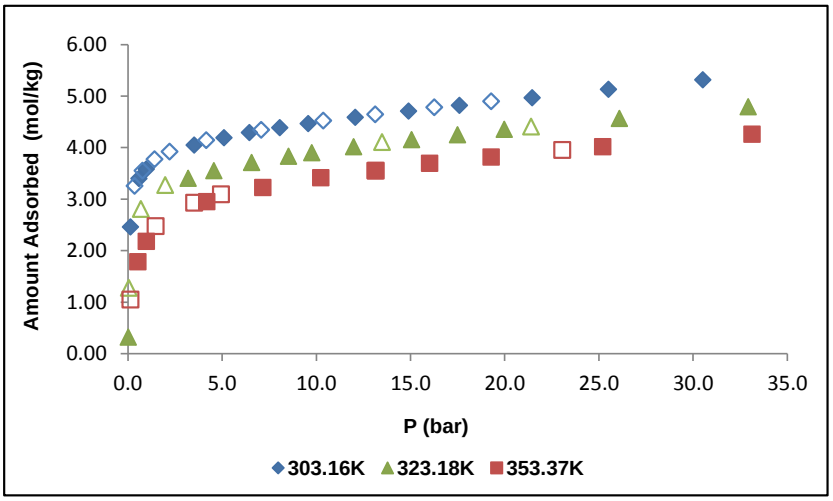

Figure C.27: Experimental single-component adsorption for CO_2 at 303.16K, 323.18K and 353.37K for Zeolite 5A. Filled symbols and open symbols denote adsorption and desorption data, respectively.

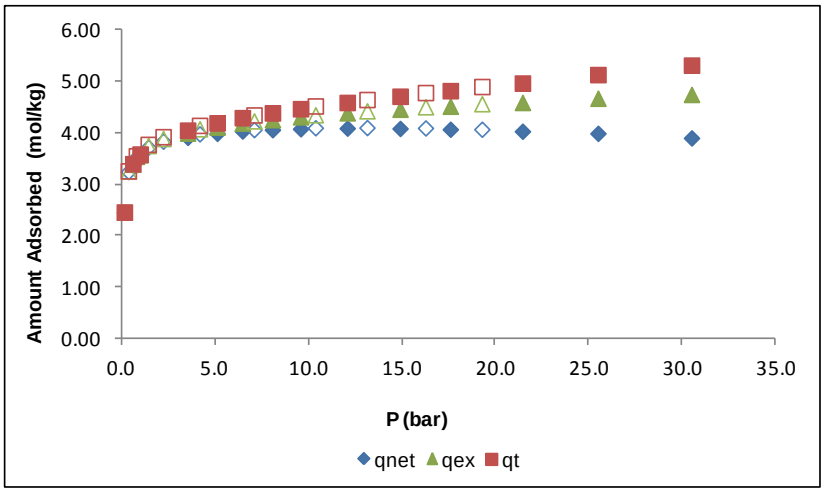

Figure C.28: Experimental single-component adsorption for CO_2 at 303.16K for zeolite 5A. Filled symbols and open symbols denote adsorption and desorption data, respectively.

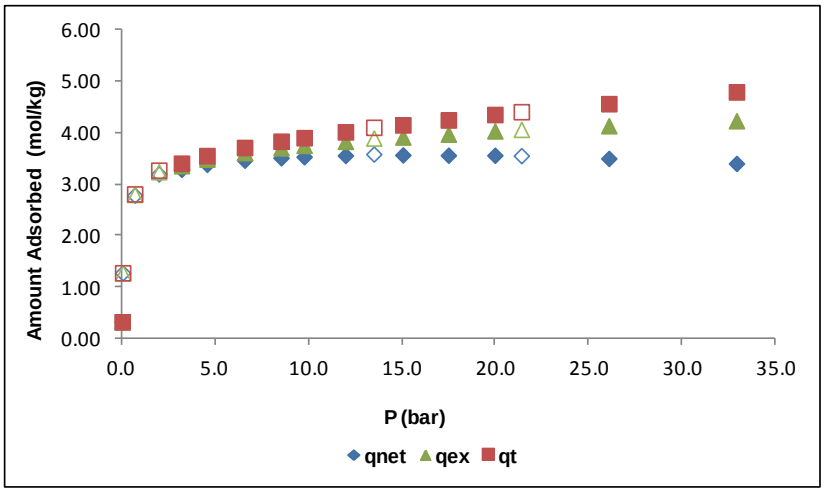

Figure C.29: Experimental single-component adsorption for CO_2 at 323.18K for zeolite 5A. Filled symbols and open symbols denote adsorption and desorption data, respectively.

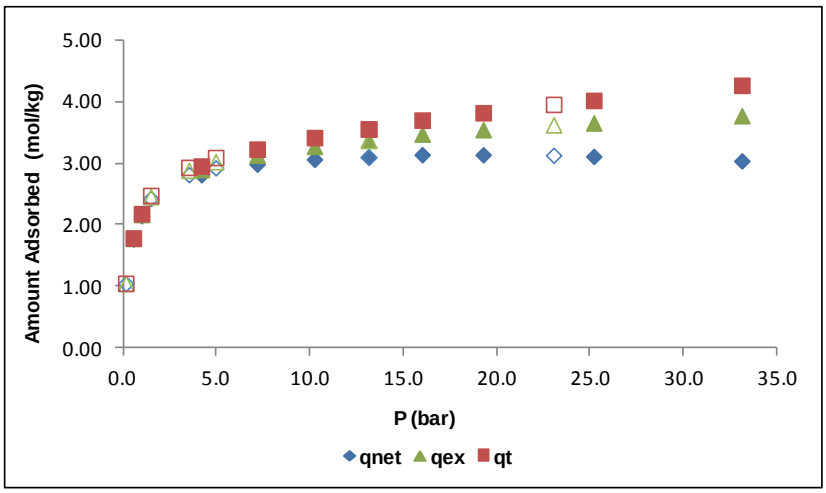

Figure C.30: Experimental single-component adsorption for CO_2 at 353.37K for zeolite 5A. Filled symbols and open symbols denote adsorption and desorption data, respectively.

Table C.10: Isotherm data of ethane (C_2H_6) on sample of zeolite 5A.

373.19K			
P (bar)	q_{net} (mol/kg)	q_{ex} (mol/kg)	q_t (mol/kg)
0.562	0.593	0.603	0.611
0.972	0.856	0.875	0.887
2.158	1.220	1.261	1.289
4.081	1.433	1.511	1.564
7.300	1.555	1.696	1.792
10.007	1.600	1.796	1.928
13.056	1.618	1.877	2.052
16.102	1.623	1.947	2.164
18.044	1.619	1.985	2.231
22.207	1.597	2.054	2.362
26.089	1.578	2.125	2.493
33.245	1.493	2.213	2.697
30.178	1.534	2.179	2.612
19.487	1.621	2.018	2.285
12.346	1.612	1.857	2.021
5.130	1.429	1.527	1.594
2.969	1.244	1.301	1.339
1.535	0.975	1.004	1.023
0.597	0.619	0.630	0.638
0.167	0.247	0.250	0.253

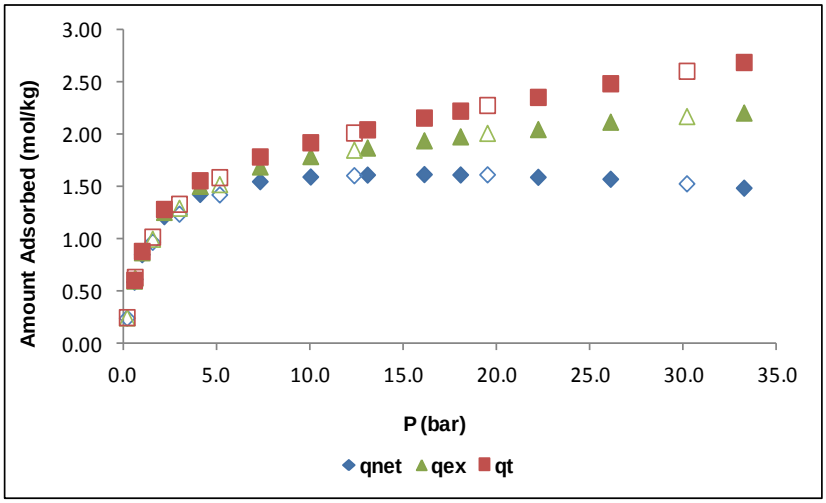

Figure C.31: Experimental single-component adsorption for C_2H_6 at 373.19K for zeolite 5A. Filled symbols and open symbols denote adsorption and desorption data, respectively.

Table C.11: Isotherm data of ethylene (C_2H_4) on sample of zeolite 5A.

323.21K				353.16K				373.19K			
P (bar)	q_{net} (mol/kg)	q_{ex} (mol/kg)	q_t (mol/kg)	P (bar)	q_{net} (mol/kg)	q_{ex} (mol/kg)	q_t (mol/kg)	P (bar)	q_{net} (mol/kg)	q_{ex} (mol/kg)	q_t (mol/kg)
0.149	1.495	1.498	1.500	0.322	1.211	1.218	1.222	0.293	0.866	0.872	0.876
0.513	1.968	1.979	1.987	0.499	1.391	1.401	1.408	0.623	1.185	1.196	1.204
3.533	2.468	2.547	2.599	0.976	1.663	1.682	1.695	0.915	1.333	1.350	1.362
5.527	2.535	2.658	2.741	4.176	2.133	2.217	2.274	2.135	1.636	1.677	1.704
10.255	2.587	2.822	2.980	8.154	2.249	2.416	2.528	4.007	1.840	1.916	1.968
12.140	2.591	2.871	3.059	11.495	2.281	2.519	2.680	8.196	1.999	2.158	2.264
14.112	2.585	2.914	3.135	14.307	2.286	2.586	2.787	12.538	2.059	2.304	2.469
16.118	2.572	2.951	3.207	18.234	2.270	2.657	2.918	14.200	2.066	2.345	2.533
21.048	2.525	3.033	3.375	22.193	2.241	2.720	3.042	18.155	2.064	2.425	2.668
30.242	2.377	3.146	3.664	27.093	2.190	2.786	3.186	22.176	2.041	2.487	2.787
33.811	2.318	3.198	3.790	33.111	2.119	2.864	3.365	27.008	2.005	2.556	2.927
29.211	2.412	3.151	3.648	24.626	2.235	2.771	3.131	33.461	1.911	2.597	3.058
23.595	2.507	3.085	3.474	16.053	2.301	2.640	2.867	23.229	2.048	2.516	2.832
17.849	2.580	3.003	3.289	9.545	2.293	2.490	2.622	16.041	2.082	2.399	2.612
7.450	2.600	2.769	2.882	6.909	2.255	2.396	2.491	9.816	2.058	2.248	2.376
2.563	2.445	2.502	2.540	3.032	2.093	2.154	2.195	5.981	1.976	2.091	2.169
1.481	2.324	2.357	2.379	2.000	1.979	2.019	2.046	3.227	1.822	1.884	1.925
0.953	2.211	2.232	2.246	0.765	1.664	1.679	1.690	0.924	1.398	1.416	1.428
				0.205	1.155	1.159	1.162	0.129	0.675	0.677	0.679
								0.080	0.532	0.534	0.535
								0.028	0.305	0.305	0.306

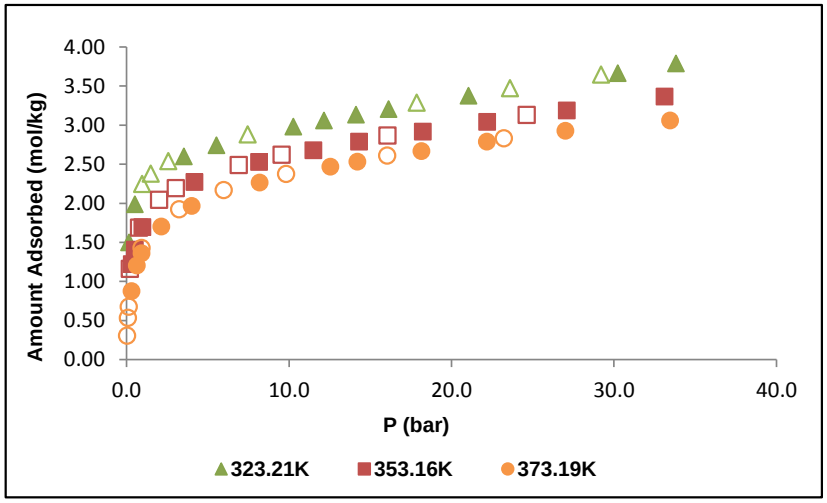

Figure C.32: Experimental single-component adsorption for C_2H_4 at 323.21K, 353.16K and 373.19K for Zeolite 5A. Filled symbols and open symbols denote adsorption and desorption data, respectively.

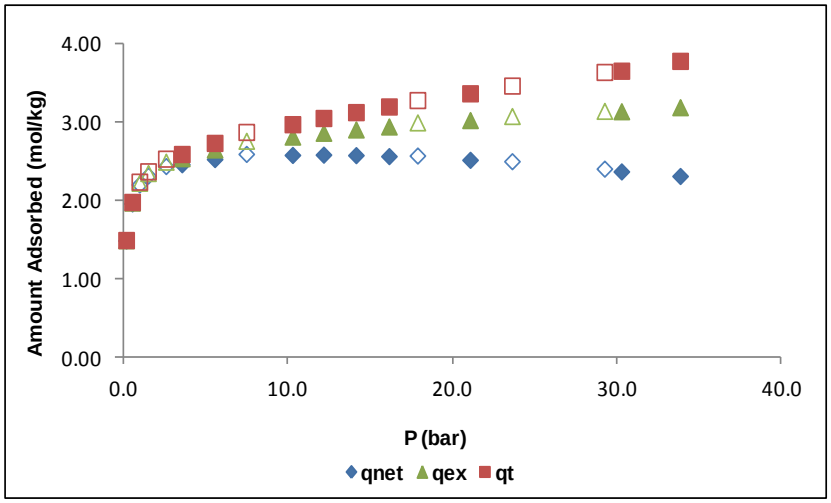

Figure C.33: Experimental single-component adsorption for C_2H_4 at 323.21K for zeolite 5A. Filled symbols and open symbols denote adsorption and desorption data, respectively.

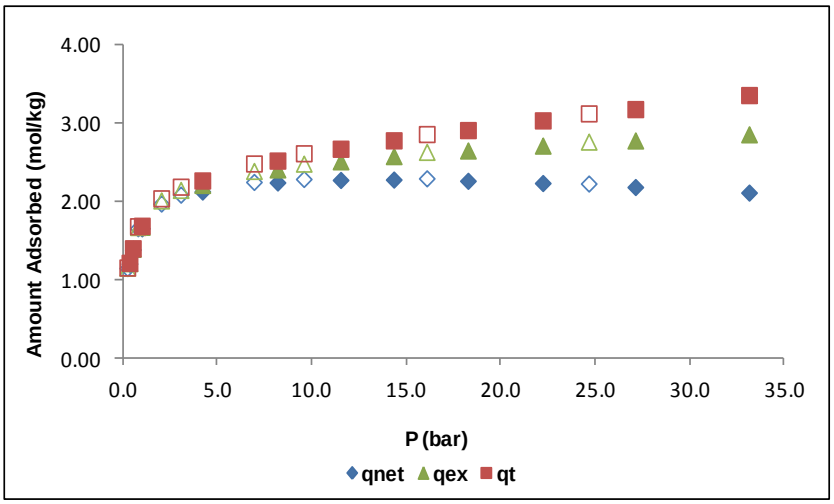

Figure C.34: Experimental single-component adsorption for C_2H_4 at 353.16K for zeolite 5A. Filled symbols and open symbols denote adsorption and desorption data, respectively.

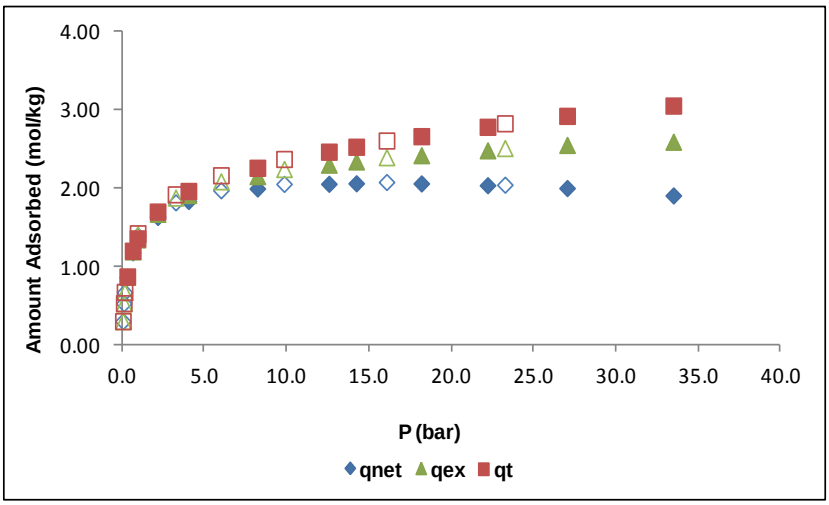

Figure C.35: Experimental single-component adsorption for C_2H_4 at 373.19K for zeolite 5A. Filled symbols and open symbols denote adsorption and desorption data, respectively.

Table C.12: Isotherm data of propane (C_3H_8) on sample of zeolite 5A.

303.18K				323.21K				353.47K			
P (bar)	q_{net} (mol/kg)	q_{ex} (mol/kg)	q_t (mol/kg)	P (bar)	q_{net} (mol/kg)	q_{ex} (mol/kg)	q_t (mol/kg)	P (bar)	q_{net} (mol/kg)	q_{ex} (mol/kg)	q_t (mol/kg)
0.005	0.651	0.651	0.651	0.002	0.003	0.003	0.003	0.003		0.039	0.039
0.069	1.530	1.531	1.532	0.010	0.004	0.004	0.005	0.028	0.336	0.337	0.337
0.156	1.660	1.664	1.666	0.078	0.036	0.038	0.039	0.178	1.054	1.058	1.060
0.985	1.932	1.955	1.971	0.098	0.056	0.058	0.060	0.623	1.442	1.455	1.463
1.772	2.014	2.057	2.085	0.231	0.254	0.259	0.263	0.973	1.558	1.577	1.591
3.248	2.092	2.171	2.225	0.475	0.925	0.935	0.942	2.011	1.675	1.716	1.743
6.076	2.155	2.312	2.417	0.945	1.464	1.484	1.497	5.656	1.775	1.894	1.975
9.122	2.266	2.517	2.687	1.571	1.656	1.691	1.714	8.016	1.799	1.973	2.090
7.565	2.195	2.397	2.532	4.970	1.884	2.000	2.078	12.228	1.788	2.067	2.254
4.477	2.131	2.243	2.319	7.582	1.912	2.096	2.219	17.719	1.731	2.167	2.461
2.388	2.066	2.123	2.162	9.331	1.924	2.158	2.314	26.259	1.582	2.355	2.874
1.385	2.002	2.035	2.057	12.691	1.937	2.275	2.503	23.025	1.647	2.274	2.695
0.802	1.927	1.946	1.958	14.122	1.945	2.334	2.596	10.957	1.806	2.051	2.216
0.540	1.871	1.884	1.892	11.150	1.935	2.223	2.417	4.007	1.781	1.864	1.920
0.282	1.781	1.788	1.793	8.637	1.930	2.143	2.287	1.491	1.677	1.707	1.727
0.097	1.625	1.627	1.628	6.475	1.923	2.078	2.181	0.415	1.464	1.472	1.478
0.046	1.500	1.501	1.501	3.575	1.894	1.975	2.030	0.105	1.116	1.118	1.120
0.012	1.118	1.118	1.118	1.222	1.786	1.813	1.831	0.025	0.703	0.704	0.704
0.002	0.441	0.441	0.441	0.702	1.717	1.732	1.742	0.007	0.505	0.506	0.506
				0.336	1.618	1.625	1.630				
				0.149	1.485	1.488	1.490				
				0.048	1.222	1.223	1.224				
				0.009	0.744	0.744	0.745				

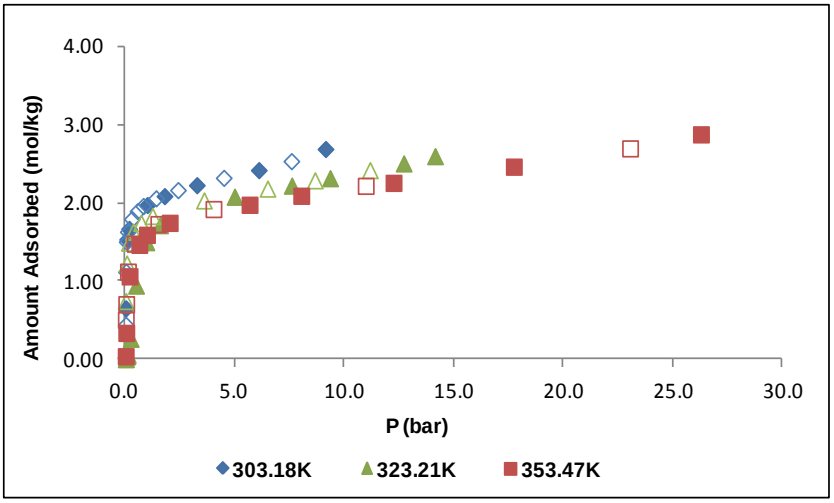

Figure C.36: Experimental single-component adsorption for C_3H_8 at 303.18K, 323.21K and 353.47K for Zeolite 5A. Filled symbols and open symbols denote adsorption and desorption data, respectively.

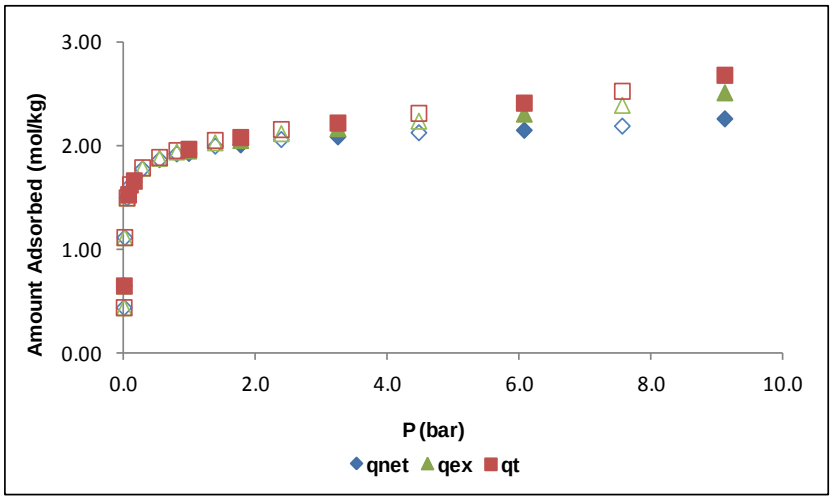

Figure C.37: Experimental single-component adsorption for C_3H_8 at 303.18K for zeolite 5A. Filled symbols and open symbols denote adsorption and desorption data, respectively.

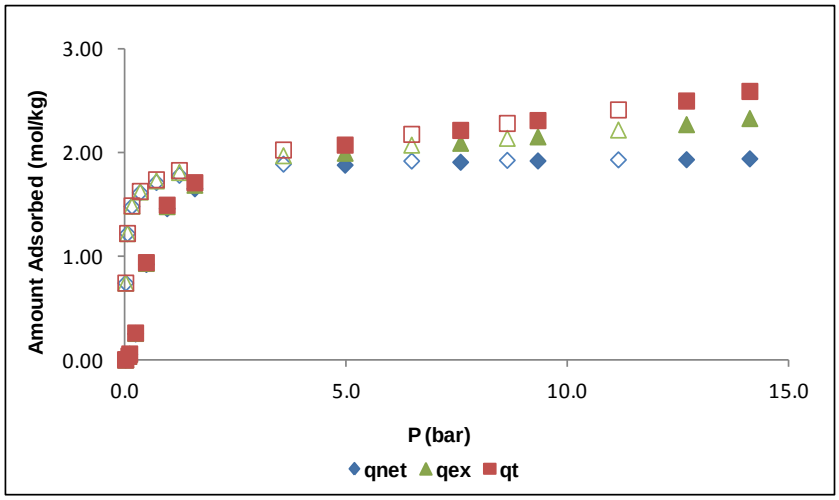

Figure C.38: Experimental single-component adsorption for C_3H_8 at 323.21K for zeolite 5A. Filled symbols and open symbols denote adsorption and desorption data, respectively.

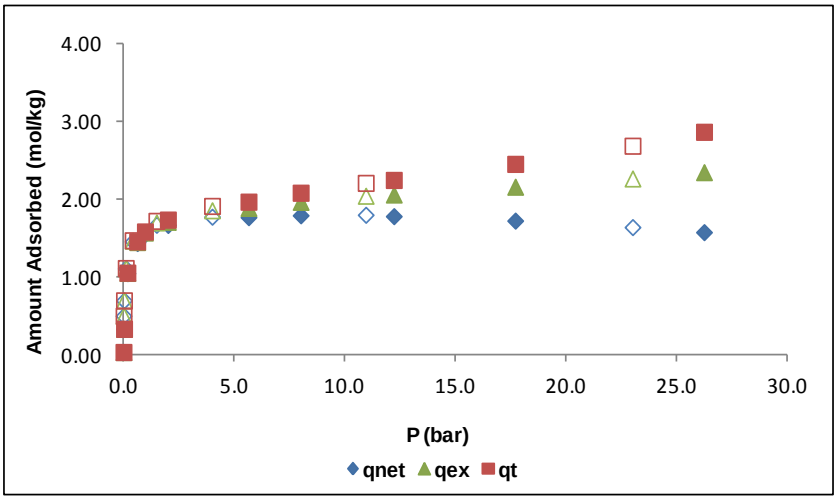

Figure C.39: Experimental single-component adsorption for C_3H_8 at 353.47K for zeolite 5A. Filled symbols and open symbols denote adsorption and desorption data, respectively.

Appendix D: Data Analysis

In this appendix, we can find all the supporting information, related to data analysis performed.

D.1: Adsorption Results using Sips and Toth approaches

At the Figures (D.1) to (D.12), are found the 3D images, taken directly from the *software* used to perform the global settings, *TableCurve, v.4.0.*.

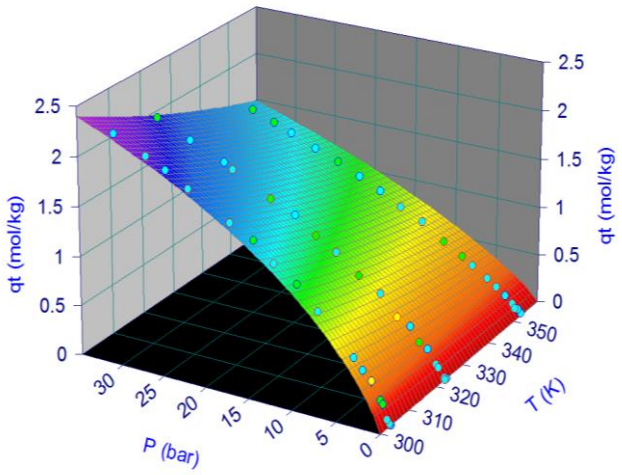

Figure D.1: Global fitting of the experimental N_2 adsorption data in MIL-53(Al) by the Sips isotherm, using the *software TableCurve 3D v.4.0.*

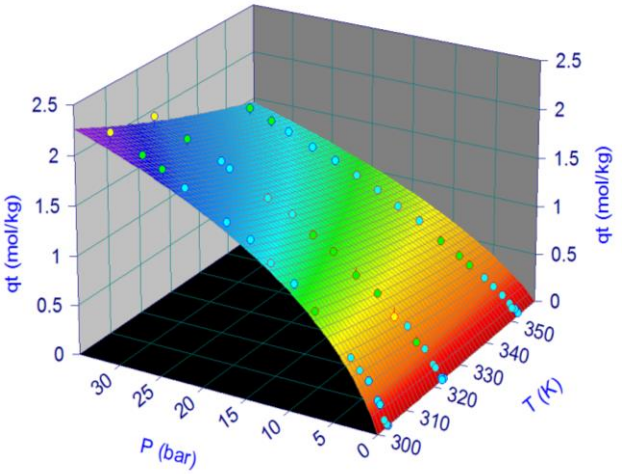

Figure D.2: Global fitting of the experimental N_2 adsorption data in MIL-53(Al) by the Toth isotherm, using the *software TableCurve 3D v.4.0.*

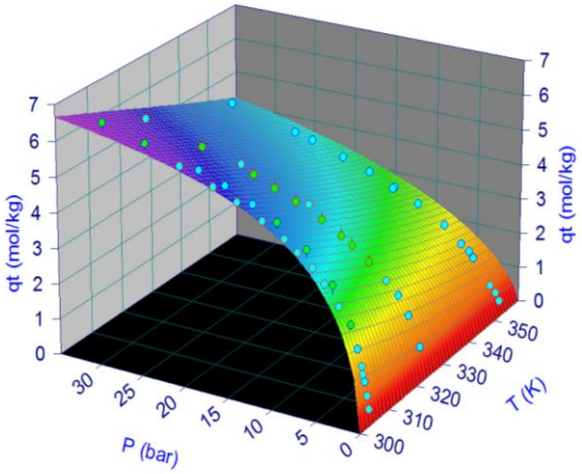

Figure D.3: Global fitting of the experimental CO_2 adsorption data in MIL-53(Al) by the Sips isotherm, using the *software TableCurve 3D v.4.0.*

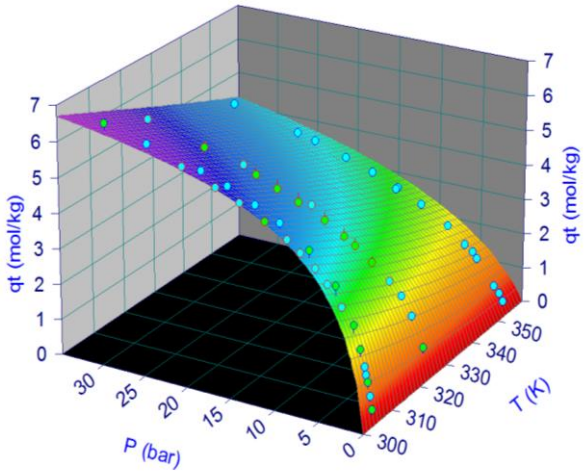

Figure D.4: Global fitting of the experimental CO_2 adsorption data in MIL-53(Al) by the Toth isotherm, using the *software TableCurve 3D v.4.0.*

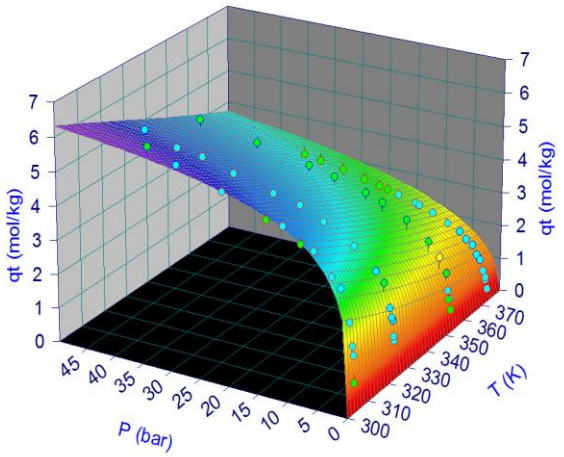

Figure D.5: Global fitting of the experimental C_2H_6 adsorption data in MIL-53(Al) by the Sips isotherm, using the *software TableCurve 3D v.4.0.*

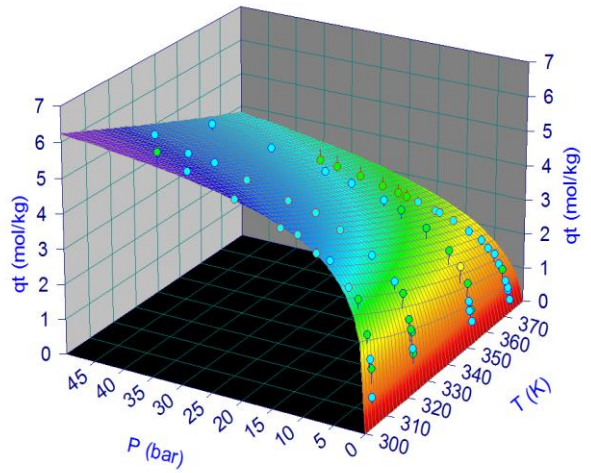

Figure D.6: Global fitting of the experimental C_2H_6 adsorption data in MIL-53(Al) by the Toth isotherm, using the *software TableCurve 3D v.4.0.*

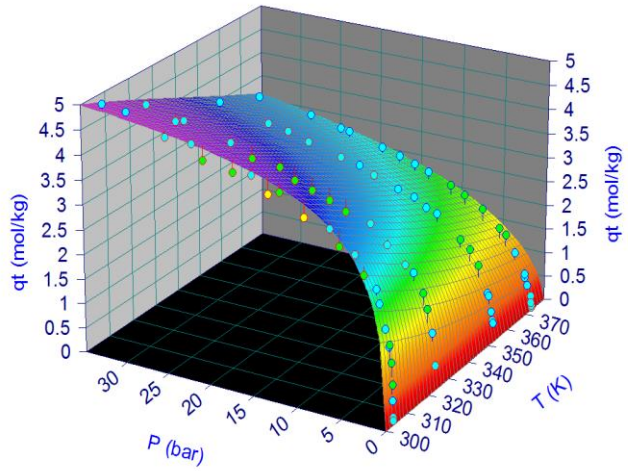

Figure D.7: Global fitting of the experimental C_2H_4 adsorption data in MIL-53(Al) by the Sips isotherm, using the *software TableCurve 3D v.4.0*

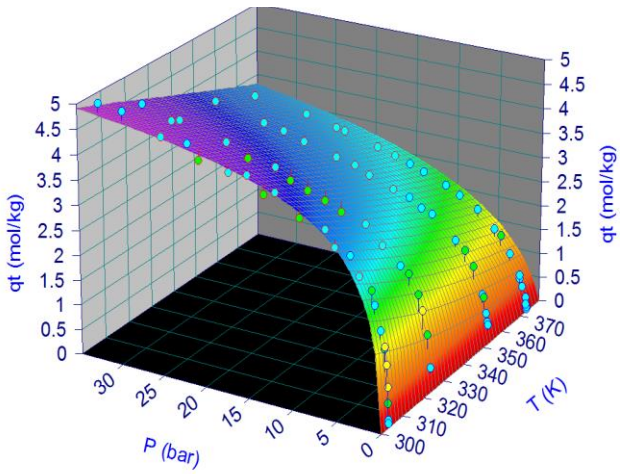

Figure D.8: Global fitting of the experimental C_2H_4 adsorption data in MIL-53(Al) by the Toth isotherm, using the *software TableCurve 3D v.4.0*

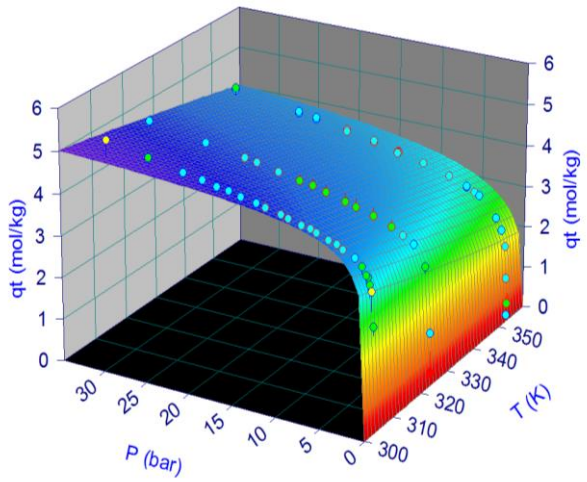

Figure D.9: Global fitting of the experimental CO_2 adsorption data in zeolite 5A by the Sips isotherm, using the *software TableCurve 3D v.4.0.*

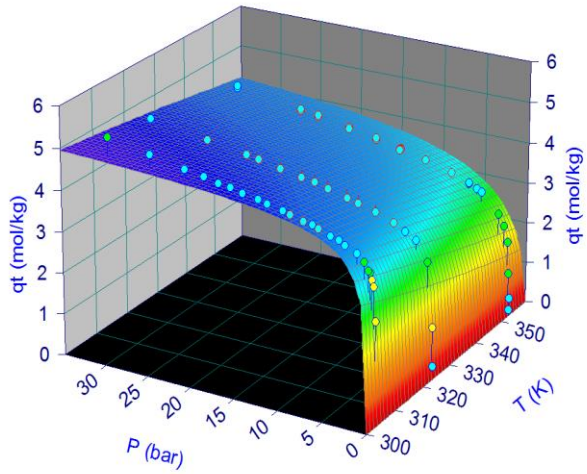

Figure D.10: Global fitting of the experimental CO_2 adsorption data in zeolite 5A by the Toth isotherm, using the *software TableCurve 3D v.4.0.*

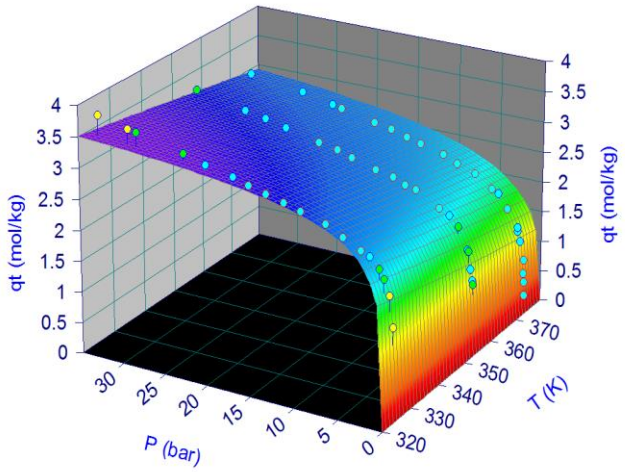

Figure D.11: Global fitting of the experimental C_2H_4 adsorption data in zeolite 5A by the Sips isotherm, using the *software TableCurve 3D v.4.0.*

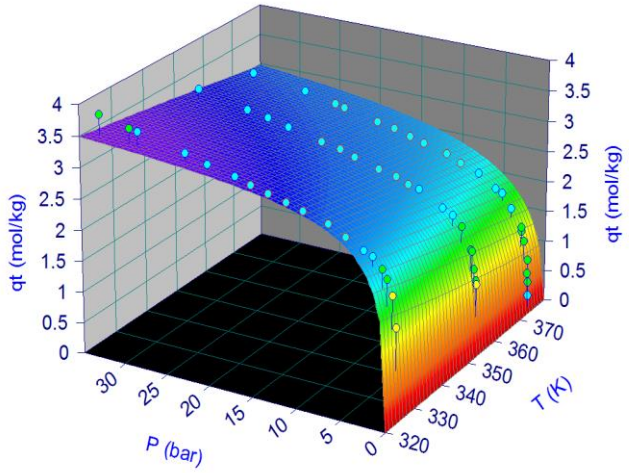

Figure D.12: Global fitting of the experimental C_2H_4 adsorption data in zeolite 5A by the Toth isotherm, using the *software TableCurve 3D v.4.0.*

D.2: Isosteric heat of Adsorption

The isosteric heats were determined using the two models studied here, Sips and Toth, taking into account the temperature dependence. In Figures (D.13) - (D.19) are shown the variation of the isosteric heats, in function of the fractional loading, (θ) for each gas, at the temperatures where adsorption equilibrium were measured. Each symbol corresponds to the value of Q_{st} calculated for the pressure and temperature of a point on the experimental adsorption isotherms.

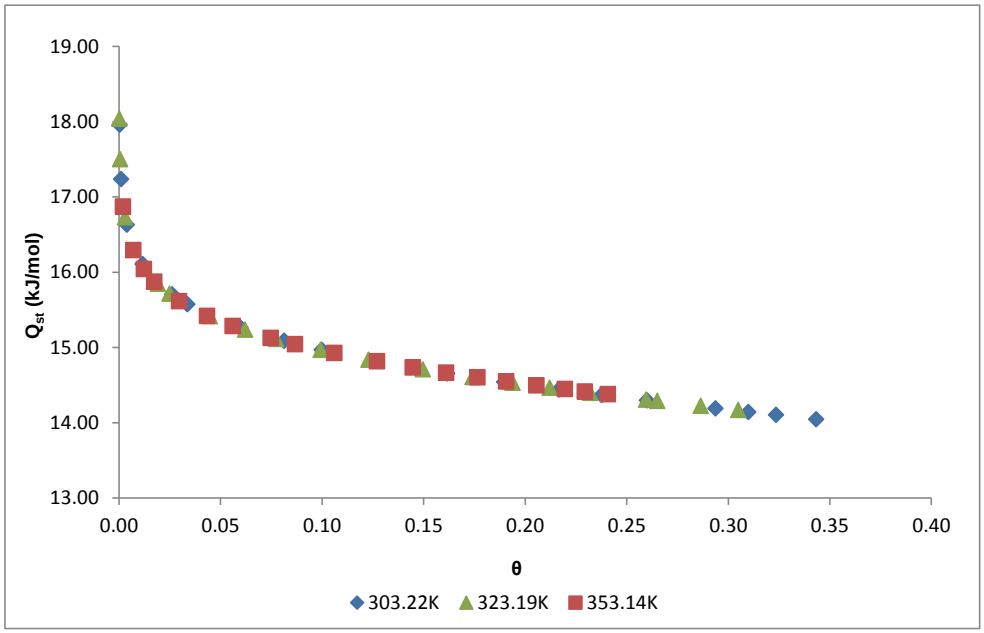

Figure D.13: Isosteric heats of adsorption for N_2 in MIL-53(Al), as a function of loading, determined from the temperature dependence of the Toth isotherm model.

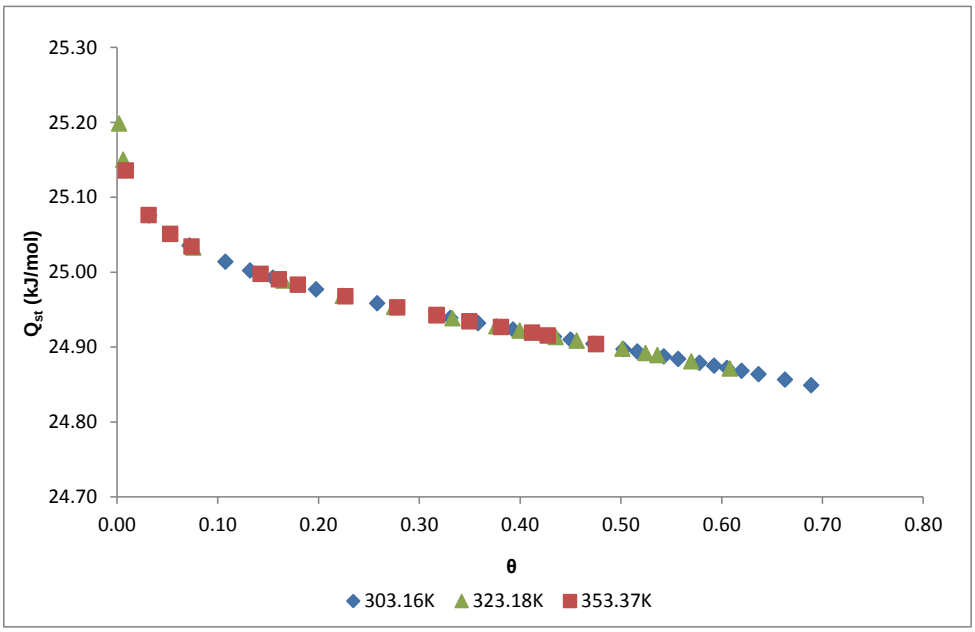

Figure D.14: Isosteric heats of adsorption for CO_2 in MIL-53(Al), as a function of loading, determined from the temperature dependence of the Toth isotherm model.

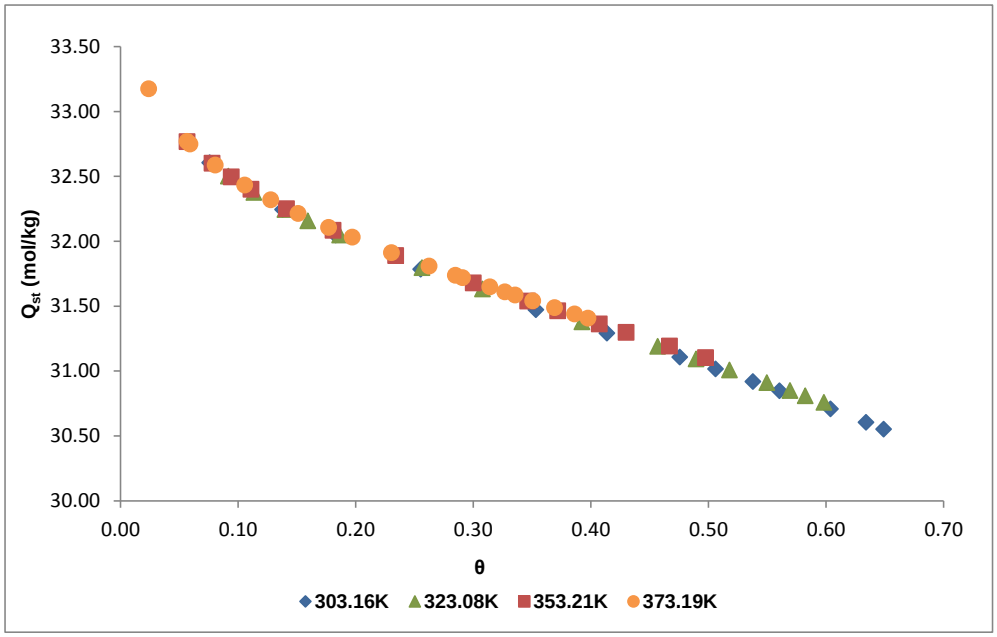

Figure D.15: Isosteric heats of adsorption for C_2H_6 in MIL-53(Al), as a function of loading, determined from the temperature dependence of the Toth isotherm model.

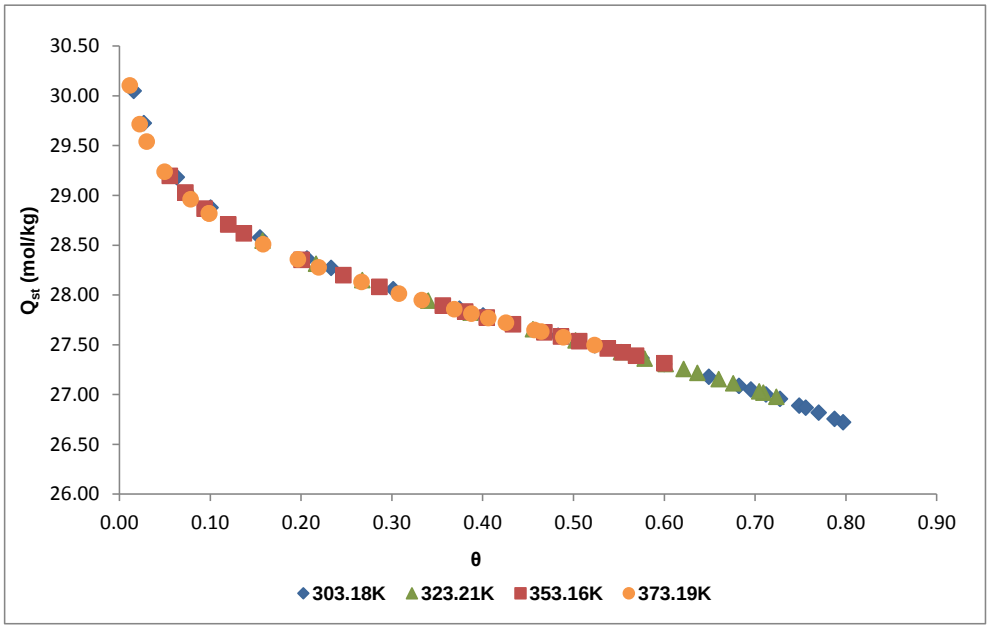

Figure D.16: Isosteric heats of adsorption for C_2H_4 in MIL-53(Al), as a function of loading, determined from the temperature dependence of the Toth isotherm model.

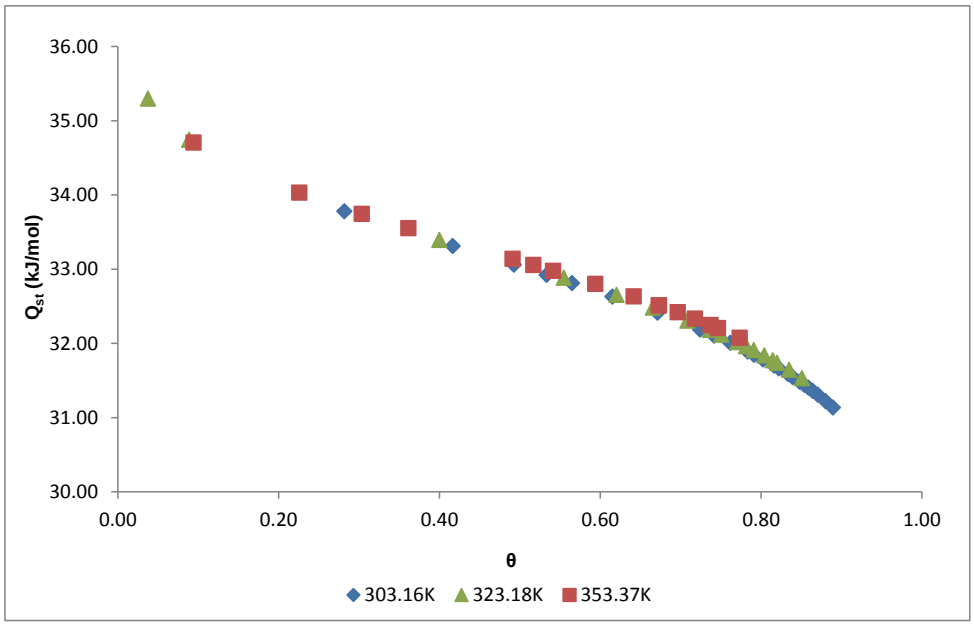

Figure D.17: Isosteric heats of adsorption for CO_2 in zeolite 5A, as a function of loading, determined from the temperature dependence of the Toth isotherm model.

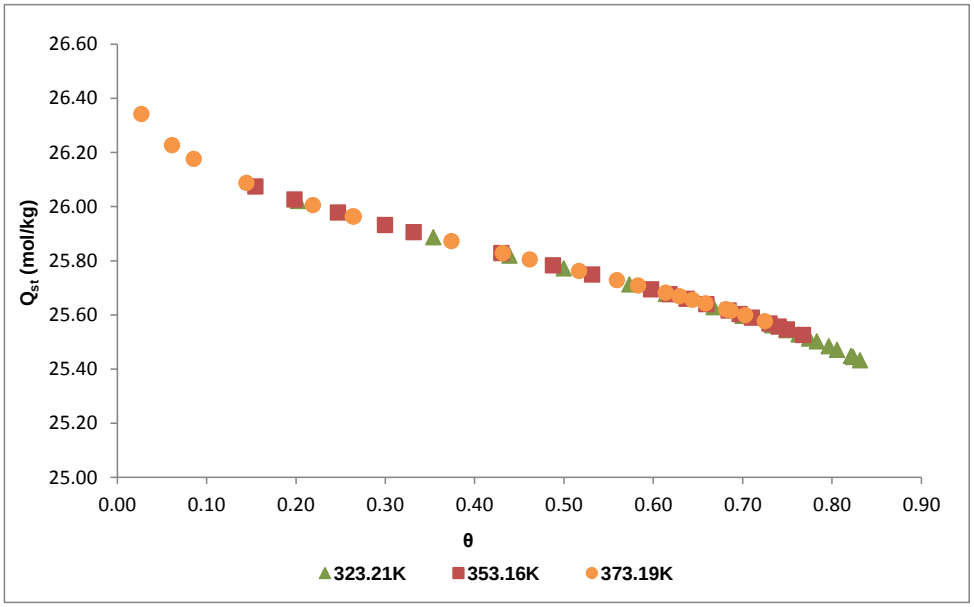

Figure D.18: Isosteric heats of adsorption for C_2H_4 in zeolite 5A, as a function of loading, determined from the temperature dependence of the Toth isotherm model.

References

[1] J.-R. Li, Y. Ma, M. C. McCarthy, J. Sculley, J. Yu, H.-K. Jeong, P. B. Balbuena and H.-C. Zhou, "Carbon dioxide capture-related gas adsorption and separation in metal-organic frameworks," *Coordination Chemistry Reviews,* vol. 255, pp. 1791-1823, 2011.

[2] R. P. Ribeiro, "Electric Swing Adsorption for Gas Separation and Purification," Ph.D. Thesis, Faculty of Engineering University of Porto, March, 2013.

[3] J. Jiang, "Metal-Organic Frameworks for CO2 Capture: What are Learned from Molecular Simulations," *Nova Science Publishers,* pp. 225-247, 2012.

[4] S. Xiang, Y. He, Z. Zhang, H. Wiu, W. Zhou, R. Krishna and B. Chen, "Microporous metal-organic framework with potential for carbon dioxide capture at ambient conditions," *Nature Communications,* pp. 1-9, 2012.

[5] S. Cavenati, C. A. Grande and A. E. Rodrigues, "Adsorption Equilibrium of Methane, Carbon Dioxide, and Nitrogen on Zeolite 13X at High Pressures," *J.Chem.Eng.,* vol. 49, pp. 1095-1101, 2004.

[6] I. A. Esteves, M. S. Lopes, P. M. Nunes and J. P. Mota, "Adsorption of natural gas and biogas components on activated carbon," *Separation and Purification Techonology,* vol. 62, pp. 281-296, 2008.

[7] C. A. Grande, "Biogas Upgrading by Pressure Swing Adsorption," in *Biofuel's Engineering Process Technology*, InTech, 2011, pp. 65-85.

[8] D. M. D'Alessandro, B. Smit and J. R. Long, "Carbon Dioxide Capture: Prospects for New Materials," *Angew. Chem. Int.,* vol. 49, pp. 6058-6082, 2010.

[9] V. Gomes and K. Yee, "Pressure Swing Adsorption for Carbon Dioxide Sequestration from Exhaust Gases," *Separation and Purification Technology,* Vols. 28, (2), pp. 161-171, 2002.

[10] J. Zhang and P. Webley, "Cycle Development and Design for CO2 Capture from Flue Gas by Vacuum Swing Adsorption," *Environmental Science & Technology,* Vols. 42, (2), pp. 563-569, 2008.

[11] A. Ribeiro, J. Santos and A. Rodrigues, "Pressure Swing Adsorption for CO2 Capture in Fischer-Tropsch Fuels Production from Biomass," *Adsorption-Journal of the International Adsorption Society,* Vols. 17, (3), pp. 443-452, 2011.

[12] C. A. Grande and A. E. Rodrigues, "Layered Vacuum Pressure Swing Adsorption for Biogas Upgrading," *Industrial & Engineering Chemistry Research,* vol. 46, pp. 7844-7848, 2007.

[13] Z. Zhou and B. Chu, "Light-scattering study on the association behavior of triblock polymers of ethylene oxide and propylene oxide in aqueous solution," *Journal of Colloid and Interface Science,* vol. 126, pp. 171-180, 1988.

[14] R. R. Davesac, "Separação propano/propileno e Reactores Adsorptivos com Modulação da Pressão," Ph.D. Thesis, Faculty of Engineering University of Porto, 2004.

[15] C. A. Grande, C. Gigola and A. E. Rodrigues, "Adsorption of Propane and Propylenein Pellets and Crystals of 5A Zeolite," *Industrial and Engineering Chemistry Research,* vol.

41, pp. 85-92, 2002.

[16] D. D. Duong, Adsorption Analysis: Equilibria and Kinetics, Series in Chem. Eng.: Imperial College Press, 1998.

[17] J. Keller and R. Staudt, Gas Adsorption Equilibria: Experimental Methods and Adsorptive Isotherms, Boston: Springer Science and Business Media, Inc., 2005.

[18] J. Humphrey and G. Keller, Separation Process Technology, New York: McGraw-Hill, 1997.

[19] D. M. Ruthven, Principles of Adsorption and Adsorption Processes, New York: Wiley-Intersciense Publication, 1984.

[20] A. W. Adamson, Physical Chemistryof Surfaces, New York: Wiley-Interscience Publication, 1997.

[21] S. Sircar, "Separation of Multicomponent Gas Mixtures". Patent US Patent 4,171,206, 1979.

[22] R. Wakasugi, A. Kodama, M. Goto and T. Hirose, "Dual Reflux PSA Process Applied to VOC Recovery as Liquid Condensate," *Adsorption-Journal of the International Adsorption Society,* vol. 11, pp. 561-566, 2005.

[23] A. D. Ebner and J. A. Ritter, "State-of-the-Art Adsorption and Membrane Separation Processes for Carbon Dioxide Production from Carbon Dioxide Emitting Industries," *Separation Science and Technology,* vol. 44, pp. 1273-1421, 2009.

[24] A. Ribeiro, C. Grande, F. Lopes, J. Loureiro and A. Rodrigues, "Four beds Pressure Swing Adsorption for Hydrogen Purification: Case of Humid Feed and Activated Carbon Beds," *Aiche Journal,* Vols. 55, (9), pp. 2292-2302, 2009.

[25] A. Ribeiro, C. Grande, F. Lopes and A. Rodrigues, "A Parametric Study of Layered Bed PSA for Hydrogen Purification," *Chemical Engineering Science,* Vols. 63, (21), pp. 5258-5273, 2008.

[26] F. Rouquerol, J. Rouquerol and K. Sing, Adsorption by Powders and Porous Solids, Academic Press, 1999.

[27] R. P. Ribeiro, T. P. Sauer, F. V. Lopes, R. F. Moreira, C. A. Grande and A. E. Rodrigues, "Adsorption of CO2, CH4, and N2 in Activated Carbon Honeycomb Monolith," *J. Chem. Eng. Data,* vol. 53, pp. 2311-2317, 2008.

[28] N. Casas, J. Schell, R. Blom and M. Mazzotti, "Adsorbents for Pre-Combustion CO2 capture by PSA: Breakthrough Experiments and Process Design," *Separation and Purification Technology,* vol. 112, pp. 34-38, 2013.

[29] G. Férey, "Hybrid Porous Solids: Past, Present, Future," *Chemical Society Reviews,* vol. 37, pp. 191-214, 2008.

[30] M. Khalfaoui, S. Knani, M. A. Hachicha and A. B. Lamine, "New theoretical expressions for the five adsorption type isotherms classified by BET based on statistical physics treatment," *Journal of Colloid and Interface Science,* vol. 263, pp. 350-356, 2003.

[31] K. S. Sing, D. H. Everett, R. A. Haul, L. Moscou, R. A. Pieroitti, J. Rouquerol and T. Siemieniewska, "Reporting Physisorption Data for Gas/Solid Systems with Special Reference to the Determination of Surface Area and Porosity," *Pure & App!. Chem.,* vol.

57, pp. 603-619, 1985.

[32] J. B. Condon, Surface Area and Porosity Determinations by Physisorptio. Measurements and Theory, Elsevier, 2006.

[33] R. T. Yang, Adsorbents: Fundamentals and Applications, New Jersey: John Wiley & Sons, Inc., 2003.

[34] S. Bourrelly, P. L. Llewellyn, C. Serre, F. Millange, T. Loiseau and G. Férey, "Different Adsorption Behaviors of Methane and Carbon Dioxide in the Isotypic Nanoporous Metal Terephthalates MIL-53 and MIL-47," *J.Am.Chem.Soc.,* vol. 127, pp. 13519-13521, 2005.

[35] H. Furukawa, K. Cordova, M. O'Keeffe and O. Yaghi, "The Chemistry and Applications of Metal-Organic Frameworks," *Science,* vol. 341, p. 6149, 2013.

[36] P. L. Llewellyn, S. Bourrelly, C. Serre, A. Vimont, M. Daturi, L. Hamon, G. D. Weireld, J.-S. Chang, D.-Y. Hong, Y. K. Hwang, S. H. Jhung and F. G., "High Uptakes of CO2 and CH4 is Mesoporous Metal-Organic Frameworks MIL-100 and MIL-101," *Langmuir,* vol. 24(14), pp. 7245-7250, 2008.

[37]

[38] U. Muller, S. Cavenati, C. Grande, A. Rodrigues, E. A., C. Kiener and U. Muller, "Metal Organic Framework Adsorbent for Biogas Upgrading.," *Industrial & Engineering Chemistry Research,* vol. 47 (16), pp. 6333-6335, 2008.

[39] N. Hedin, L. Andersson, L. Bergström and J. Yan, "Adsorbents for the post-combustion capture of CO2 using rapid temperature swing or vacuum swing adsorption," *Applied Energy,* vol. 104, pp. 418-433, 2013.

[40] S. Sircar and A. L. Myers, "Gas Separation by Zeolites," Pennsylvania, U.S.A., Marcel Dekker, Inc., 2003.

[41] Z. Liu, A. C. Grande, P. Li, J. Yu and A. E. Rodrigues, "Adsorption and Desorption of Carbon Dioxide and Nitrogen on Zeolite 5A," *Separation Science and Technology,* vol. 46, pp. 434-451, 2011.

[42] G. Arun, L. Ma and G. Changyou, "Zeolite molecular sieve 5A acts as a reinforcing filler, altering the morphological, mechanical, and thermal properties of chitosan," *Journal of Materials Science,* vol. 48, p. 3926–3935, 2013.

[43] A. D. Wiersum, J.-S. Chang, C. Serre and P. L. Liewellyn, "An adsorbent performance indicator as a first step evaluation of novel sorbents for gas separations: application to Metal-Organic Frameworks," *Langmuir, American Chemical Society Publications,* pp. 1-35, 2013.

[44] A. Ribeiro, M. Campo, G. Narin, J. Santos, A. Ferreira, J.-S. Chang, Y. Hwang, U. Lee and J. Loureiro, "Pressure Swing Adsorption Process for the Separation of Nitrogen and Propylene with a MOF Adsorbent MIL-100(Fe)," *Separation and Purification Technology,* Vols. 110, (0), pp. 101-111, 2013.

[45] G. Férey, C. Mellot-Draznieks, C. Serre and F. Millange, "Crystallized Frameworks with Giant Pores: Are There Limits to the Possible?," *Accounts of Chemical Research,* vol. 38, pp. 217-225, 2005.

[46] J. Jiang, "Metal-Organic Frameworks for CO2 Capture: What are Learned from Molecular Simulations," in *Coordination Polymers and Metal Organic Frameworks*, Nova Science

Publishers, Inc., 2012, pp. 225-247.

[47] A. Lyubchyk, I. A. Esteves, F. J. Cruz and J. P. Mota, "Experimental and Theoretical Studies of Supercritical Methane Adsorption in the MIL-53(Al) Metal Organic Framework," *The Journal of Physical Chemistry,* vol. 115, pp. 20628-20638, 2011.

[48] S. Bourrelly, B. Moulin, A. Rivera, G. Maurin, S. Devautour-Vinot, C. Serre, T. Devic, P. Horcajada, A. Vimont, G. Clet, M. Daturi, J.-C. Lavalley, S. Loera-Serna, R. Denoyet, P. L. Llewellyn and G. Férey, "Explanation of the Adsorption of Polar Vapors in the Highly Flexible Metal Organic Framework MIL-53(Cr)," *Journal of the American Chemical Society,* vol. 132, pp. 9488-9498, 2010.

[49] J. Liu, P. K. Thallapally, B. McGrail, D. R. Brown and J. Liu, "Progress in adsorption-based CO2 capture by metal–organic frameworks," *Chemical Society Reviews,* vol. 41, pp. 2308-2322, 2012.

[50] N. Ramsahye, G. Maurin, S. Bourrelly, P. L. Llewellyn, T. Devic, C. Serre, T. Loiseau and G. Férey, "Adsorption of CO2 in metal organic frameworks of different metal centres: Grand Canonical Monte Carlo simulations compared to experiments," *Adsorption,* vol. 13, pp. 461-467, 2007.

[51] N. A. Ramsahye, G. Maurin, S. Bourrelly, P. L. Llewellyn, C. Serre, T. Loiseau, T. Devic and G. Férey, "Probing the Adsorption Sites for CO2 in Metal Organic Frameworks Materials MIL-53 (Al, Cr) and MIL-47 (V) by Density Functional Theory," *The Journal of Physical Chemistry C,* vol. 112, pp. 514-520, 2008.

[52] Y. Liu, Z. U. Wang and H.-C. Zhou, "Recent advances in carbon dioxide capture with metal-organic frameworks," *GreenHouse Gases - Science and Technology,* vol. 2, pp. 239-259, 2012.

[53] A. Boutin, F.-X. Coudert, M.-A. Springuel-Huet, A. V. Neimark, G. Férey and A. H. Fuchs, "The Behavior of Flexible MIL-53(Al) upon CH4 and CO2 Adsorption," *The Journal of Physical Chemistry C,* vol. 114, pp. 22237-22244, 2010.

[54] F. Ullmann, Ullmann's Encyclopedia of Industrial Chemistry, New York: John Wiley & Sons, 2003.

[55] I. A. A. C. Esteves, "Gas Separation Processes by Integrated Adsorption and Permeation Technologies," Ph.D.Thesis, Faculty of Science and Technology of Lisbon, May 2005.

[56] Micromeritics, "Porosimetry," One Micromeritics Drive, 1st January 2001. [Online]. Available: http://www.micromeritics.com/. [Accessed 21th February 2014].

[57] A. Lyubchyk, "Gas Adsorption in the MIL-53(Al) Metal Organic Framework. Experiments and Molecular Simulation," Ph.D.Thesis, Faculty of Science and Technology of Lisbon, July 2013.

[58] Rubotherm, "Rubotherm - Magnetic Suspension Balances," Rubotherm (GmbH), [Online]. Available: http://www.rubotherm.com/. [Accessed 15th December 2013].

[59] G. Rubotherm Präzionsmesstechkin, "Sorption - ISOSORP - The New Sorption Suspension Balance".

[60] JULABO - The Temperatura Control Company, "Refrigerated/Heating Circulators - Operating Manual - F32 HL," 77960 Seelbach / Germany, 2010.

[61] NIST, "National Institute of Standards and Technology," Material Measurement

Laboratory, 2011. [Online]. Available: http://webbook.nist.gov/. [Accessed 12th February 2014].

[62] O. Talu and S. Gumma, "Gibbs Dividing Surface and Helium Adsorption," *Kluwer Academic Publishers,* vol. Adsorption 9, pp. 17-28, 2003.

[63] S. Gumma and O. Talu, "Net Adsorption: A Thermodynamic Framework for Supercritical Gas Adsorption and Storage in Porous Solids," *Langmuir Article,* vol. 26, pp. 17013 - 17023, 2010.

[64] Langmuir, "The adsorption of gases on plane surfaces of glass, mica and platinum," *J. Chem. Soc.,* vol. 40, pp. 1361-1928, 1928.

[65] M. Dubinin, "The potential theory of adsorption of gases and vapors for adsorbents with energetically non-uniform surfaces.," *Chem. Rev.,* vol. 60, p. 235, 1960.

[66] S. Ozawa, S. Kusumi and Y. Ogino, "Physical Adsorption of Gases at High-Pressure .4. Improvement of Dubinin-Astakhov Adsorption Equation," *Journal of Colloid and Interface Science,* Vols. 56, (1), pp. 83-91, 1976.

[67] M. Dubinin, "Adsorption in Micropores.," *Journal of Colloid and Interface Science,* Vols. 23, (4), pp. 487-&, 1967.

[68] Do. D. D., Adsorption Analysis: Equilibria and Kinetics, vol. 2, Queenslan: Imperial College Press, 1998.

[69] S. A. Al-Muhtaseb and J. A. Ritter, "New Virial-Type Model for Predicting Single- and Multicomponent Isosteric Heats of Adsorption," *Ind. Eng. Chem. Res.,* vol. 37, pp. 684-696, 1998.

[70] J. P. Mota and A. J. Rodrigo, "Calculations of Multicomponent Adsorption-Column Dynamics Combining the Potential and Ideal Adsorbed Solution Theories," *Ind. Eng. Chem. Res,* Vols. 39, (7), pp. 2459-2467, 2000.

[71] P. Rallapalli, K. Prasanth, D. Patil, R. S. Somani, R. Jasra and H. Bajaj, "Sorption studies of CO2, CH4, N2, CO, O2 and Ar on nanoporous aluminum terephthalate [MIL-53(Al)]," *J. Porous Mater,* 2010.

[72] J. Möllmer, M. Lange, A. Möller, C. Patzschke, S. Karolin, D. Lässig, L. Jörg, R. Gläse, H. Krautscheid and R. Staudt, "Pure and mixed gas adsorption of CH4 and N2 on the metal–organic framework Basolite A100 and a novel copper-based 1,2,4-triazolyl isophthalate MOF†," *Journal of Materials Chemistry,* vol. 22, pp. 10274-10286, 2012.

[73] Z. R. Herm, B. Eric D. and J. R. Long, "Hydrocarbon Separations in Metal−Organic Frameworks," *Chemistry of Materials,* vol. 26, pp. 323-338, 2013.

[74] P. L. Llewellyn, G. Maurin, T. Devic, S. Loera-Serna, N. Rosenbach, C. Serre, S. Bourrelly, P. Horcajada, Y. Filinchuk and G. Férey, "Prediction of the Conditions for Breathing of Metal Organic Framework Materials Using a Combination of X-ray Powder Diffraction, Microcalorimetry, and Molecular Simulation," *J.AM.CHEM.SOC.,* vol. 130, pp. 12808-12814, 2008.

[75] T. K. Trung, P. Trens, N. Tanchoux, S. Bourrelly, P. L. Llewellyn, S. Loera-Serna, C. Serre, T. Loiseau, F. Fajula and G. Férey, "Hydrocarbon Adsorption in the Flexible Metal Organic Frameworks MIL-53(Al, Cr)," *J.AM.CHEM.SOC.,* vol. 130, pp. 16926-16932, 2008.

[76] G.-M. Nam, B.-M. Jeong, S.-H. Kang, B.-K. Lee and D.-K. Choi, "Equilibrium Isotherms of CH4, C2H6, C2H4, N2, and H2 on Zeolite 5A Using a Static Volumetric Method," *J.Chem.Eng.,* vol. 50, pp. 72-76, 2005.

[77] M. Polanyi, "Basics of the potential theory of adsorption," *Zeitschrift Fur Elektrochemie Und Angewandte Physikalische Chemie,* vol. 35, pp. 431-432, 1929.

[78] R. Yang, Gas Separation by Adsorption Processes, USA: Butterworth Publishers, 1987.

[79] C. Holland, S. Al-Muhtaseb and J. Ritter, "Adsorption of C-1-C-7 normal alkanes on BAX activated carbon. 1. Potential theory correlation and adsorbent characterization," *Industrial & Engineering Chemistry Research,* vol. 40(1), pp. 338-346, 2001.

[80] X. Du and E. Wu, "Application of the Adsorption Potential Theory to Hydrogen Adsorption on Zeolites above Critical Temperature," *Acta Physico-Chimica Sinica,* Vols. 23, (6), pp. 813-819, 2007.

[81] S. Mehta and R. Danner, "Improved Potential-Theory Method for Predicting Gas-Mixture Adsorption Equilibria," *Industrial & Engineering Chemistry Fundamentals,* Vols. 24, (3), pp. 325-330, 1985.

[82] G. Wood, "Affinity coefficients of the Polanyi/Dubinin adsorption isotherm equations - A review with compilations and correlations," *Carbon,* Vols. 39, (3), pp. 343-356, 2001.

[83] G. Wood, "Activated Carbon Adsorption Capacities for Vapors," *Carbon,* Vols. 30, (4), pp. 593-599, 1992.

[84] C. Spencer and R. Danner, "mproved Equation for Prediction of Saturated Liquid Density," *Journal of Chemical and Engineering Data,* Vols. 17, (2), pp. 236-&, 1972.

[85] R. Reid, J. Prausnitz and B. Poling, The Properties of Gases and Liquids, Singapore: McGraw-Hill, 4th Edition ed..

[86] R. Agarwal and J. Schwarz, "Analysis of High-Pressure Adsorption of Gases on Activated Carbon by Potential-Theory," *Carbon,* Vols. 26, (6), pp. 873-887, 1988.

[87] T. Loiseau, C. Serre, C. Huguenard, G. Fink, F. Taulelle, M. Henry, T. Bataille and G. Férey, "A Rationale for the Large Breathing of the Porous Aluminum Terephthalate (MIL-53) Upon Hydration," *FULL PAPER,* vol. 10, pp. 1373-1382, 2004.

[88] H. M. Magee, "Nitrogen Gas Adsorption in Zeolites 13X and 5A," Walla Walla University, 204 S. College Ave.,College Place, WA 99324, 2010.

[89] M. F. J. Eusébio, *Development of an universal interface for monotoring and control of chemical and biochemical processes, Ph. D. Thesis,* Faculdade de Ciências e Tecnologia da Universidade Nova de Lisboa (FCT/UNL), Lisbon, 2006.

[90] L. Xinyuan Technology Co., "Xinyuan Molecular Sieve," 2011. [Online]. Available: http://www.molecularsieve.org/. [Accessed 03rd March 2014].

[91] S. Al-Muhtaseb, C. Holland and J. Ritter, "Adsorption of C-1-C-7 normal alkanes on BAX-activated carbon. 2. Statistically optimized approach for deriving thermodynamic properties from the adsorption isotherm.," *Industrial & Engineering Chemistry Research,* vol. 40(1), pp. 319-337, 2001.